# Hydrological Modelling of the Quilcayhuanca Valley, Peru

Gavin McNamara

Department of Earth and Planetary Sciences

McGill University, Montreal

April 2023

A thesis submitted to McGill University in partial fulfilment of the requirements of the degree of

Master of Science

# Table of Contents

# List of Figures

# List of Tables

# Abstract

The glaciated valleys of the Andes provide vital freshwater to the arid west coast of South America. The Cordillera Blanca, Peru, is the largest glacierized region in the tropics, containing 25% of the world's tropical glaciers with a total glaciated area of 431 $km^2$. Climate change is causing major hydrologic alteration to the Cordillera Blanca as regional glacial coverage decreased by 40% since the 1970s.

Physically based models are useful to comprehend the hydrological processes of remote regions with sparse meteorological data. The Cold Regions Hydrological Model (CRHM) is a flexible, physically based numerical model developed for improving the understanding of cold regions hydrological processes in poorly gauged or ungauged basins. The model includes processes specific to mountain environments, including snow and glacier accumulation and ablation, interception, infiltration through frozen soils, and surface and subsurface hydrology.

CRHM is used to simulate the hydrology of the Quilcayhuanca Valley, a pampa valley on the western side of the Cordillera Blanca from June 2014 to August 2018. The model uses a variety of data sources, including satellite imagery, digital elevation models, and weather stations (precipitation, temperature, solar radiation, relative humidity, and wind speed) from the valley floor (Casa de Agua, 3905 m.a.s.l.) and at Cuchillacocha Lake (4625 m.a.s.l.). Due to the high level of confidence in the process representations of the modules, calibration was limited to only varying runoff routing and subsurface parameters.

The model, divided into 19 hydrologic response units, accurately simulates the discharge recorded at the catchment outflow. The model is validated with respect to streamflow, groundwater levels, glacier melt rates, and evapotranspiration rates. The results show that 31% of the total water exiting the basin is groundwater and increases during the dry season. As glaciers recede, relative groundwater contributions are further increased. A basin-wide glacier mass balance was calculated at -2.51 m water equivalent per year. Despite lower ablation rates in the dry season, the glacier contribution to streamflow is much higher (60% dry season versus 31% wet season). The proportional quantity of evapotranspiration in Quilcayhuanca Valley is significant, comprising 20% of total hydrological outflows.

A parameter sensitivity analysis was conducted for key hydrological uncertainties including lapse rates, groundwater routing, and ice albedo. To better understand how ongoing climate

change will affect the hydrology of the valley, parameters such as temperature and precipitation, as well as the degree of glaciation, are modified to evaluate their impact on model outcomes. The results of these virtual experiments show that basin-wide mass balances for air temperature increases of 2 °C and 4 °C were -7.03 m and -11.74 m water equivalent per year, respectively. All glaciers within the catchment have annual negative mass balances at a warming of 0.9 °C. In a scenario with complete deglaciation, basin streamflow is reduced by 60% in the dry season and 42% on an annual basis. The results from the research are important for conceptualizing and quantifying the socio-hydrology risks for water security in the Andes and in directing future research questions.

# Résumé

Les vallées glaciaires des Andes fournissent un approvisionnement vital en eau douce à la côte ouest aride de l'Amérique du Sud. La Cordillera Blanca, au Pérou, est la plus importante région englacée des Tropiques, renfermant 25% des glaciers tropicaux de la planète, d'une superficie totale de 431 $km^2$. Les changements climatiques modifient considérablement l'hydrologie de la Cordillera Blanca, la superficie des glaciers ayant diminué de 40% dans la région depuis les années 1970.

Les modèles reposant sur des processus physiques sont utiles pour comprendre les processus hydrologiques de régions éloignées pour lesquelles peu de données météorologiques existent. Le *Cold Regions Hydrological Model* (CRHM, modèle hydrologique pour les régions froides) est un modèle numérique physique mis au point afin de comprendre les processus hydrologiques des régions froides dans des bassins pour lesquels il existe peu ou pas de données de mesure. Le modèle intègre des processus propres aux milieux montagneux, dont l'accumulation et l'ablation de neige et de glace, l'interception, l'infiltration à travers des sols gelés et l'hydrologie de surface et de subsurface.

CRHM est utilisé pour simuler l'hydrologie de la vallée de Quilcayhuanca, une vallée de pampas située du côté ouest de la Cordillera Blanca, de juin 2014 à août 2018. Le modèle emploie différentes sources de données, dont l'imagerie satellite, des modèles altimétriques numériques et des données de stations météorologiques (précipitation, température, rayonnement solaire, humidité relative et vitesse des vents) situées au fond de la vallée (Casa de Agua, 3905 m.a.s.l.) et au lac Cuchillacocha (4625 m.a.s.l.). Étant donné le degré de confiance élevé dans les représentations de processus des modules, l'étalonnage s'est limité à ne changer que des paramètres associés à la trajectoire des eaux de ruissellement et à la subsurface.

Le modèle, divisé en 19 unités de réaction hydrologique, simule avec exactitude le débit enregistré à l'exutoire du bassin. Il est validé par rapport au débit des cours d'eau, aux niveaux d'eau souterraine, aux rythmes de fonte des glaciers et aux taux d'évapotranspiration. Les résultats montrent que 31% de toute l'eau quittant le bassin est de l'eau souterraine et qu'elle augmente durant la saison sèche. Au fil du retrait des glaciers, les proportions de l'eau souterraine continuent d'augmenter. Le bilan massique des glaciers à l'échelle du bassin obtenu est de -2,51 m équivalents en eau par année. En dépit de taux d'ablation plus faibles durant la saison sèche, la

contribution des glaciers au débit des cours d'eau est beaucoup plus grande (60% durant la saison sèche contre 31% durant la saison humide). La proportion de l'évapotranspiration dans la vallée de Quilcayhuanca est importante, représentant 20% du total des débits hydrologiques sortants.

Une analyse de sensibilité des paramètres a été effectuée pour des sources d'incertitude hydrologiques clés, dont les gradients thermiques verticaux, la trajectoire de l'eau souterraine et l'albédo de la glace. Pour mieux comprendre l'incidence des changements climatiques en cours sur l'hydrologie de la vallée, des paramètres comme la température et les précipitations, ainsi que le degré de glaciation, sont modifiés afin d'évaluer leur incidence sur les extrants du modèle. Les résultats de ces expériences virtuelles montrent que les bilans massiques à l'échelle du bassin pour des hausses des températures de 2 °C et 4 °C sont de -7,03 m et -11,74 m équivalents en eau par année, respectivement. Tous les glaciers dans le bassin ont des bilans massiques annuels négatifs pour un réchauffement de 0,9 °C. Dans un scénario de déglaciation complète, le débit des cours d'eau dans le bassin chute de 60% durant la saison sèche et de 42% sur une base annuelle. Les résultats de ces travaux sont importants pour la conceptualisation et la quantification des risques socio-hydrologiques associés à la sécurité hydrique dans les Andes et pour orienter des travaux de recherche futurs.

# Acknowledgments

I am deeply grateful to have had the opportunity to have worked with, and mostly been aided by, many kind, generous, and welcoming people. I could not have asked for a better supervisor in Jeffrey McKenzie. I learned a great deal from Jeff, including the power of genuine and compassionate personal interactions. Thank you, Barret Kurylyk, for your mentorship and for guiding me towards mountain hydrology research. I was honoured to spend a few weeks in the company of Jeff, Bryan Mark, and Robert Hellstrom in Peru, and their knowledge was crucial in directing this project (and in knowing where the best pizza in Huaraz is). The hospitality extended by Patty during my time in Huaraz was unparalleled, and the many interesting conversations with Peruvian hydrologists and glaciologists inspired me greatly.

My thesis would not have been possible without the support extended to me through John Pomeroy and the Coldwater Laboratory group in Canmore. I am indebted to the expertise of Logan Fang, Caroline Aubry-Wake and John Pomeroy. Their patience for my elementary CRHM questions was extremely useful. Caroline was an invaluable resource regarding Cordillera Blanca science, computer modelling, and anything research related. Lauren Somers was always shockingly responsive and helpful.

At McGill, the support of the 'Laboratory of Advanced Hydrogeological Modeling and Stuff' group and the Department of Earth and Planetary Sciences (namely Kristy Thornton and Anne Kosowski), was fantastic.

This project was partially funded by a NSERC CGSM scholarship.

# 1 Introduction

Globally, mountain regions are referred to as natural water towers for downstream communities. On an annual basis, these elevated regions capture and store freshwater as snow and ice in the winter or wet season (depending on location) and release this important resource in the dry season or summer, when there is higher water demand. Mountains cover approximately one quarter of the world's land surface and contain approximately 12% of the world's population (Toledo et al., 2021). Water storage and delivery is arguably one of the most critical services provided by mountains, with approximately 40% of the world's population relying on this mountain-derived water for drinking purposes, hydroelectricity, and agriculture (Toledo et al., 2021). Globally, glaciers are retreating at an accelerated pace with tropical alpine glaciers having undergone the most rapid decrease in areal coverage (Bradley et al., 2006).

In South America, the glaciated valleys of the Andes provide vital freshwater to the arid west coast. While tropical Andes contain more than 99% of all tropical glaciers (Kaser, 1999), climate change and rapid glacier recession threaten the fate of water resources for more than 10 million people in the Andean highlands (Buytaert et al., 2006). Andean countries depend heavily upon the water supplied from glaciated basins when it is most needed during the dry season (Vuille et al., 2008). The Cordillera Blanca, Peru, is the largest glacierized region in the tropics, containing 41% of Peru's tropical glaciers, and spanning a total glaciated area of 431 $km^2$ (ANA, 2021). Climate change is causing major changes to the mountain range as glacial coverage in this region has decreased by over 40% since 1975 (ANA, 2021). Aside from water resources, melting glaciers in the Cordillera Blanca pose significant geological hazards, such as glacial lake outburst floods (GLOFs), avalanches, landslides, etc. (Carey, 2010).

Numerical hydrologic models are an important tool for integrating field data and addressing research questions (Aubry-Wake et al., 2022b) in remote, data-sparse regions. For example, the Cold Regions Hydrological Modelling (CRHM) platform is designed for use in mountainous regions with a physical basis, flexible modular structure, and robust component algorithms (Pomeroy et al., 2022).

CRHM has never been applied to glacierized catchments in the tropics. It has been used twice in southern Chile, first by Gonthier (2011) to analyze three high mountain basins in the

semiarid Andes, and then on a much larger scale, with a catchment area of 15 904 km$^2$, in Baker River Basin in Chile (Krogh et al., 2015). In these Andean settings, the model was successful in representing multiple processes of hydrology in this basin and in illustrating potential future research questions.

Broadly, my research objective is to understand the current catchment hydrological processes and controls within a Cordillera Blanca glacierized, and to understand how the system will change in the future due to climate change. The sub-objectives of the research are to: (1) improve the comprehension of basin scale hydrology in the Cordillera Blanca, (2) identify major unknown parameters that influence the hydrology through sensitivity analysis, and (3) to provide potential estimates of how the system will respond to glacial and meteorological changes.

To achieve the proposed objectives, I will use CRHM to simulate the Quilcayhuanca Valley, Cordillera Blanca. The valley is one of the most intensively studied sub-catchment for both glaciology, groundwater and runoff generation and has area of 67.3 km$^2$. The model is appropriate based on the available observation data and the degree of detail available for glacio-hydrologic modelling. There have been numerous in-depth studies within the Quilcayhuanca Valley that have reported on specific hydrologic components, providing the necessary data (e.g., Glas et al., 2018 and references within) for a modeling approach. Model validity will be assessed based on comparisons with observed data and published literature results. The results from the modeling will include improved hydrologic understanding, parameter sensitivity analysis, and testing how future climate scenarios will impact the valley.

# 2 Literature Review

## 2.1 Glacier Melt

Following is an introductory overview of the role of glaciers in basin scale mountain hydrology and how glacier melt is measured, quantified, and modelled. Understanding the physical processes of glacier melt and meltwaters' effects on downstream hydrology is crucial to inform water policy and management. Glacial meltwater provides numerous services and benefits to society, such as drinking water, hydropower, irrigation, tourism, and recreation.

Of the available freshwater on Earth, 75% is frozen and locked as glacier ice (IPCC, 1996). Glaciers have been monitored for centuries through various methods (Clason et al., 2021). The Little Ice Age inspired European artists and naturalists to draw, paint, and record glacial changes from the 13th to early 20th century (Nussbaumer and Zumbühl, 2012). People in mountain towns and villages witness changes firsthand through damage caused by glacier advance, or glacier lake outburst floods (Hoinkes, 1975). More scientific methods of observation commenced in 1894, under the establishment of the International Glacier Commission at the Council of the Sixth International Geological Congress in Zurich. Recent methodological advances in paleoclimate reconstructions through ice cores, dendrochronology, geochemistry, sedimentary records, and other methods have provided a broad understanding into global glacier responses to past climate change. The past few decades have seen improvements in remotely sensed data via satellite and aircraft imagery (Clason et al., 2021). The use of this imagery has allowed for a more consistent global monitoring and surveillance of glacier mass changes. However, manual field work is still integral to glacier monitoring research projects (Clason et al., 2021).

Glaciology has a clear focus on the linkages between glaciers and the climate (Hock, 2005). Walcher (1773) was one of the earliest pioneers in this field, suggesting that climate influenced glacier fluctuations. Over a century later Finsterwalder and Schunk (1887) proposed the link between air temperature and glacier melt. Hess (1904) claimed that the most important factor for glacier ablation was radiation, and Angstrom (1933) emphasized temperature, radiation, and wind as the primary factors controlling melt rates (Hock, 2005). Sverdrup (1935) was the first to apply a complete energy balance for a glacier surface, with a focus on the turbulent fluxes to obtain ablation rates (Sverdrup, 1935, 1936). Early glaciological surveys were started in the Alps in the 1930s, focused on water balance and glacial response to seasonal and climate fluctuations (Hock, 2005). Due to the remote nature of most glaciers, hydrometeorological data is often sparse and lacking. Computer modelling has aided in understanding knowledge gaps, but these models are often applied with numerous untestable assumptions. The first computer simulation models for glacier mass balance were developed in the 1960s (Anderson, 1972). Over the past century, modelling glacier melt has advanced from simple temperature-index models to spatially distributed energy-balance models with hourly time steps (Hock, 2005). Remote sensing and better constraints on physically based processes have further aided in the evolution of these sophisticated models.

### 2.1.1 Mass Balance

The quantity of glacier melt generation is partially controlled by whether a glacier is advancing or retreating. This state, called the mass balance, is the difference between the amount of mass loss (ablation) and mass gained (accumulation) over a given time. It is typically expressed in units of metre water equivalent (m w.e.). The line between a net positive (accumulation) part of a glacier and a net negative (ablation) part of a glacier is called the equilibrium line of altitude (ELA). In the current warming climate scenario, the ELA of the majority of the planets' glaciers is rising in altitude, leading to negative mass balance as there is more ablation than accumulation.

For *in situ* assessment, the mass balance of a glacier is determined by the glaciological method, in which numerous points of accumulation and ablation are measured at various points over one or more annual cycles (Hock et al., 1999). These points represent the change in glacier mass measured relative to a previous measurement, typically the previous year's summer surface. The balance (b) can be positive or negative and symbolizes the change in mass measured at a point at any time (Equation 1; Ostrem et al., 1991). One balance year is represented by the time between two summer surfaces (ss). The local net balance ($b_n$) is the change in mass over one balance year, expressed as:

$$b_n = b_w + b_s = c_t + a_t \quad (1)$$

where $b_w$ is the winter balance (maximum balance value), $b_s$ is the summer value (minimum balance value), $c_t$ is the total accumulation, $a_t$ is the total ablation, and with all values are given in metres water equivalent (Ostrem et al., 1991). Typically, the winter balance ($b_w$) and the summer balance ($b_s$) are measured at each stake (point measurement) and extrapolated over the entire glacier.

Modern advances in remote sensing technologies have led to new methods for remote sensing of glacier mass balance estimates. For regional assessments, airborne and satellite remote sensing is the only practical method to estimate mass balances (Bamber, 2006). There are a variety of approaches to calculate glacier mass balances from remote sensing data, but these will not be discussed further. However, there are substantive improvements being made in this line of research and there is continued progress as remote sensing technology and data resolution improves.

### 2.1.2 Glaciers as Storage

Glaciers act as water storage on a variety of time scales (Figure 1). For long-term storage (years to centuries), ice quantities effect the global sea level and water balance for glacierized catchments (Jansson et al., 2003), and is governed by regional climate. Alpine glaciers and ice caps contain a small amount of frozen freshwater compared to the Greenland and Antarctic Ice Sheets, but this portion of ice storage is well monitored and comprises 0.5 m of potential sea level rise (IPCC, 2001; Jansson et al., 2003). Hydrologically, catchments with glaciers differ from unglaciated catchments in that they have a decreased annual variability of streamflow (Baraer et al., 2012). In mid- to high-latitude settings, a glacierized catchment will provide the highest proportions of glacier melt during hot, dry months, thus buffering the variations in annual precipitation and temperature patterns (Jansson et al., 2003). Hopkinson and Young (1998) found that for the Bow River, Alberta, the annual glacier runoff averaged 2% of basin yield, but for the driest month of a low flow year glacier melt contributed up to 54% of basin runoff. Therefore, glacier melt contributions to streamflow are generally greatest when it is in highest demand from downstream communities. Fountain and Tangborn (1985) suggest that a minimum in year-to-year streamflow variation occurs for basins that are approximately 36% glacierized.

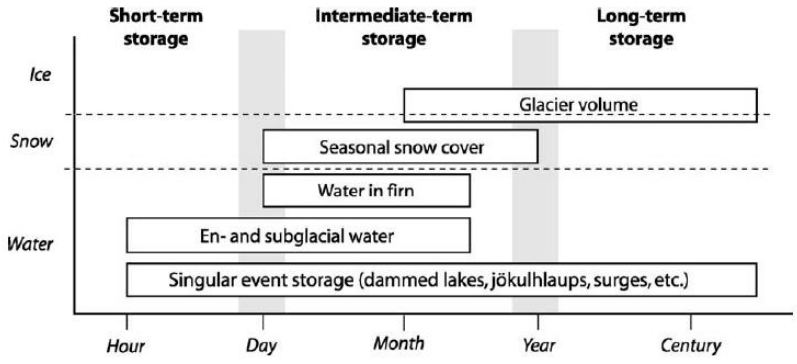


*Figure 1- Various forms of glacier storage and their corresponding timescales (Figure from Hock, et al., 2003)*

On a seasonal scale, water is released from snow and glacial ice, affecting the runoff patterns and downstream river flow regimes. A large proportion of precipitation is stored on glaciers as snow during winter, and released in summer as meltwater (Jansson et al., 2003). Glacier free catchments have earlier spring/ summer discharge peaks when compared with glacierized valleys (Figure 2).

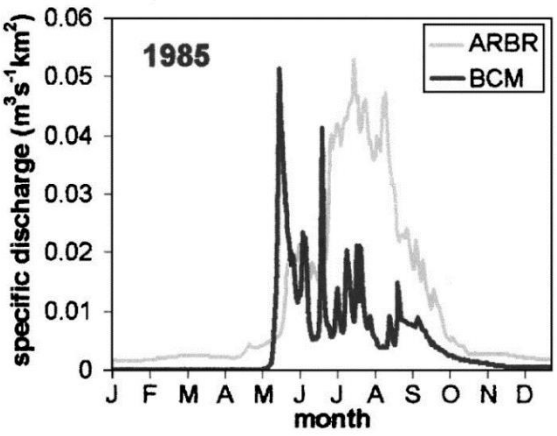


*Figure 2- Example hydrograph displaying seasonal variations for glacial (ARBR) and nival (BCM) catchments (Figure from Fleming et al., 2005.)*

The delay in melt is partially due to the elevation differences in glacierized versus glacier-free basins, but there are also insulation effects of snowmelt from underlying material. If a snowpack is overlying a glacier rather than soil or rock, there would be reduced longwave radiation and ground heat flux components. Fountain and Tangborn (1985) discovered that maximum variation for month-to-month runoff flow occurs for basins with less than 10% glacial cover but is a minimum for basins with more that 30% glacier coverage. Small differences in glaciation within low glacier coverage basins has a larger effect on runoff measurements than larger differences in glacier coverage within highly glaciated basins. Fountain and Tangborn (1985) found that the delay of seasonal runoff is only 2 weeks if glacier cover increases from 50 to 100%, but it is only about a month if glacier cover changes from 0 to 7%. These results suggest that the presence of even small glaciers may have a significant effect on downstream flow patterns. Therefore, there are large implications when considering different emission scenarios and the effect of glacier melt on downstream communities.

On short timescales, there are diurnal patterns of water flow through a glacier. This is triggered by diurnal melt water input and corresponding water pressure variations and has been inferred based on dye-tracer experiments and other investigations (Jansson et al., 2003). There are also singular storage releases which encompass unique events such as glacier surges or drainage of glacier-dammed water (Jansson et al., 2003).

Glaciers' effect on the hydrology of a catchment can be numerically modelled using different approaches. Stochastic models use multiple regression techniques to relate glacier melt

and meteorological data. Air temperature, precipitation, and wind speed are the three meteorological variables required to provide an accurate estimate of runoff (Hock et al., 2006). These stochastic models require site specific calibration, and thus lack a processes basis. The calibration is based on observational records and therefore the stochastic models do not prove to be effective in estimating accurate future runoff scenarios in a changing climate (Hock et al., 2006). Conceptual models are often favoured due to their moderate data requirements. These models typically consist of a series of numerical steps simplifying physical processes and involve reservoirs that have storage constants relating flows to stored water volumes (e.g., Baraer et al., 2012).

The most sophisticated glacier hydrology models are physically based. There are many processes that vary with time and space that are unique to each glacierized catchment, and this can result in over-parameterized models (Beven, 2009). Physically based models include surficial, englacial, and subglacial components (Hock et al., 2006). These are often the best predictive models as they most accurately describe the processes involved in a catchment. However, they are limited by the availability and accuracy of input data (Beven, 2009).

### 2.1.3 Snow and Ice Properties

The energy balance at the glacier-atmosphere interface controls melt rates (Hock, 2005), and is largely controlled by the characteristics of snow and ice. The contribution of radiation, turbulent, and mass fluxes to the energy balance is influenced by the presence of snow, firn, and ice (King et al., 2008). Snow and ice have fixed surface temperatures during melting (0 °C), high thermal emissivity, variable albedo, and variable surface roughness (Hock, 2005). Strong temperature gradients can develop because of the temperature limit for melting snow and ice. This temperature stratification, overlying typical mountain glaciers, leads to atmospheric gravity flows and wind generation. Turbulent fluxes can then become independent of radiation due to the fixed surface temperature during a melt period (Hock, 2005).

Condensation and evaporation can be an important energy source and/or sink for a glacier surface. The latent heat of evaporation ($2.501 \times 10^6$ J kg$^{-1}$ at 0 °C) is 7.5 times the latent heat of fusion required for melting snow and ice ($0.334 \times 10^6$ J kg$^{-1}$). Therefore, condensation can be a large energy source for a glacier surface. It has been found that the vapour pressure of a melting surface is relatively low, 0.611 kPa, creating a vapour gradient and favouring conditions for

condensation. When vapour gradients are reversed, evaporation occurs, and a large amount of energy is absorbed in the transition of liquid to gas. Even more energy is absorbed in the phase transition from solid to gas if sublimation occurs (2.838 x 106 J kg-1 at 0 °C).

Shortwave radiation can penetrate up to 10 m in ice and 1 m in snow (Warren, 1982). The process of radiation absorption is important for pre-melt periods and for internal melting. It was found to account for 20% of the internal snow melt on Peyto Glacier (Föhn, 1973). Albedo also varies between snow and ice, with values typically between 0.3-0.5 for ice and 0.7-0.9 for snow (Patterson, 1994).

## 2.2 Glacio-hydrologic modelling

### 2.2.1 Modelling glacier melt

Modelling snow and ice melt in glaciated environments is crucial for understanding mountain hydrology as glaciers often exist in remote, hard to access mountainous areas where *in situ* data is lacking. The success of a model depends upon the correct implementation and parameterization of the underlying physical processes governing glacier melt. Mountainous regions have unique seasonal and diurnal discharge patterns due to high elevation snow and ice. Models of meltwater production are typically based on either air temperature (temperature-index models) or surface energy fluxes (energy-balance models) (Hock, 2005). Temperature-index models have historically been favoured for a few key reasons: the availability of temperature data, the relative ease of temperature interpolation and forecasting, and their computational simplicity (Hock, 2003). However, physically based energy balance models with high temporal resolution have become more popular with increased computational power and digital terrain models. High spatial resolution is required for accurate glacial melt estimates, especially in mountainous areas where elevation, slope, and aspect play major roles in melt rates (Hock, 2003).

### 2.2.2 Temperature index and degree-day models

Temperature index or degree-day models are often used for glacier melt estimates. These models are contingent upon the empirical relationship between air temperature and snow and ice melt (Hock, 2003). Due to the availability of air temperature data, simplicity, and generally good performance, these models have been widely used and continue to be popular (Hock, 2005). The temperature index model is:

$$M = M_f(T_i - T_b)$$

(2)

where M is the depth of meltwater produced in a selected interval of time, $M_f$ is the melt factor, $T_i$ is the index air temperature, and $T_b$ is the base temperature. Due to the lack of physical basis for the temperature index model, the calibrations vary by an order of magnitude. This inexactness leads to a wide range of melt factor values. The classical degree-day model is expressed as (Hock, 2005):

$$\sum_{i=1}^{n} M = DDF \sum_{i=1}^{n} T^{+} \times \Delta t$$

(3)

relating the ice or snow melt, M (mm), during a period of *n* time intervals, Δt, to the sum of positive air temperatures of each time interval, $T^+$, during the same period. The degree-day factor, DDF, is the factor of proportionality, expressed in mm $d^{-1}$ $K^{-1}$. The degree-day factor, like the melt factor, $M_f$, varies considerably because it accounts for multiple terms of the energy balance equation (Singh and Kumar, 1996). Typically, degree-day values based on melt measurements range from 2.5 to 11.6 mm $d^{-1}$ $K^{-1}$ for snow and 6.6 to 20.0 mm $d^{-1}$ $K^{-1}$ for ice (Hock, 2005).

The relationship between air temperature and glacier melt can be an effective assumption, however, there are many potential errors for these models in mountainous environments. Glaciers exist in these complex environments where topographic effects such as aspect, slope, and shading can greatly impact melt rates. Also, it has been shown that the temperature index or degree-day models' accuracy declines with increasing temporal resolution (Hock, 2003). The reason for these shortcomings may be due to the underlying assumption and simplification that air temperature controls snow and ice melt rates. There may be a false causality between snowmelt and the temperature of the air, as the underlying processes dictating snow melt are more complex. In Equations 2 and 3, the melt factor and the degree-day factor represent the spatial and temporal variations of shortwave and longwave radiation, as well as the turbulent heat fluxes. The reason for the generally good performance of temperature-index models on large temporal and spatial scales is the correlation with air temperature and the components of the energy balance equation

(Hock, 2005). Longwave incoming radiation and the turbulent heat fluxes are dependent upon air temperature, which in turn is affected by solar irradiance (Hock, 2005). These relationships are highly variable and complex, but models should strive to represent reality as best as possible. Snowmelt should be understood and calculated using physical processes rather than a generalized relationship.

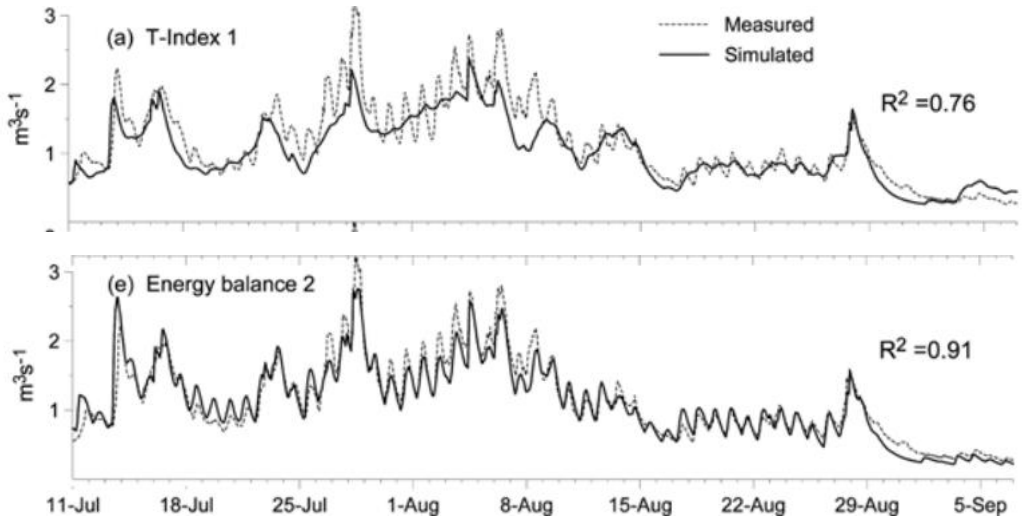


*Figure 3- Simulated and measured hourly discharge ($m^3 s^{-1}$) of Storglaciären Glacier, Sweden, using temperature-index and energy balance models for simulating glacial melt production (Figure from Hock, 2005). Melt calculations are based on the classical degree-day model (a), and a more sophisticated energy-balance model (e).*

The nuances of melt variability depend upon many factors, including humidity, sensible and latent heat fluxes, albedo, shortwave and longwave radiation fluxes (Sicart et al., 2008). However, despite the simplification of complex processes, the temperature-index and degree day models (Figures 3) provide a reasonable estimate for long term catchment scale hydrology (Hock, 2005).

### 2.2.3 Energy balance models

The energy balance model is often described as "physically-based" because the balance is based on the conservation of energy and each component of the energy balance is represented by a process described by physics (Figure 4). The physically based approach to model glacier melt requires data for each energy flux to and from the glacier surface (Hock, 2005). These energy fluxes are represented as:

$$Q_m = SW_{in}\,(1- a) + LW + Q_E + Q_H + Q_D + Q_G \qquad (4)$$

where $Q_m$ is the energy available for melt (W $m^{-2}$), $SW_{in}$ is the incoming shortwave radiation (W $m^{-2}$), α is albedo, LW is net longwave radiation (W $m^{-2}$), $Q_E$ is the latent heat flux (W $m^{-2}$), $Q_H$ is the sensible heat flux (W $m^{-2}$), $Q_D$ is the energy advected from rain, and $Q_G$ is the ground heat flux (W $m^{-2}$).

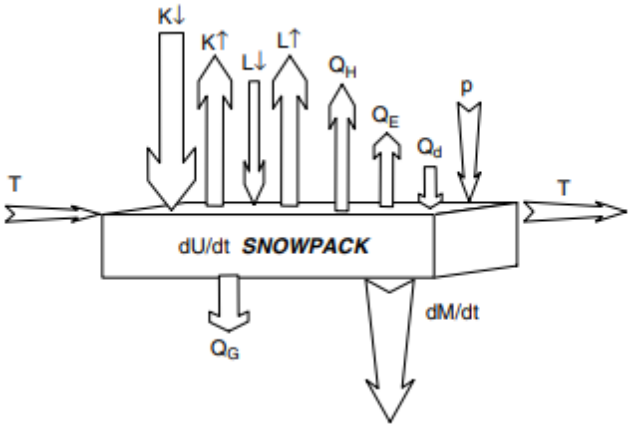


*Figure 4- Conceptual diagram with energy balance terms. Note that this control volume represents a snowpack, though the fluxes would be the same for a glacier's ice surface. T represents horizontal transfer of snow mass, dU/dt is the rate of internal energy in the volume per unit surface area per unit time, and dM/dt represents the change in melt per unit area per unit time. (Figure from Pomeroy et al., 2007)*

For glaciology, a positive $Q_m$ value indicates energy gain and therefore melt may occur on the glacier surface.

Net shortwave radiation is represented by $SW_{in}$ (1- α) in Equation 4. Almost all shortwave radiation originates from the sun and has a wavelength range of approximately 0.15-4 μm, while longwave radiation is predominantly thermal radiation of terrestrial and atmospheric origin with a wavelength range of 4-120 μm (Hock, 2005). Therefore, shortwave radiation is largely affected by terrain variations such as slope, aspect, albedo, and shading in mountainous environments.

A primary variable governing net shortwave radiation is albedo (α). In an alpine environment, albedo can range from 0.1 for dirt covered ice to 0.9 for fresh snow (Hock, 2005). Snow albedo affects melt rates, and albedo can change in a matter of days based upon snow metamorphism. Fresh snow can decrease in albedo from 0.9 to 0.6 in a few days due to changing grain size, water content, surface roughness, sediment content and debris cover (Hock, 2005). Snow albedo drops over time as snow metamorphism occurs, and there have been numerous empirical attempts to describe this process. An accurate albedo value is crucial for the energy

balance model, so it is important to consider the snow albedo-time relationship (Equation 5; Corps of Engineers, 1956):

$$a = a_0 + be^{-ndk} \quad (5)$$

where $\alpha_0$ is the minimum snow albedo, $n_d$ is the number of days since the last significant snowfall, and b and k are empirical coefficients. The physically based Cold Regions Hydrologic Model utilizes work done by Gray and Landine (1987) for modules involving snowmelt (Equation 6 and 7). Gray and Landine (1987) examined albedo depletion curves and discovered that albedo at any time A(t) could be approximated by the expression:

$$A(t) = A_i - 0.071t \quad (6)$$

for melt periods and,

$$A(t) = A_i - 0.196t \quad (7)$$

for post melt periods, where $A_i$ is the albedo of the snow cover at the start of melt and *t* is the number of days following the start of continuous depletion (Gray, 1987).

Longwave radiation (LW, or L↓↑) is primarily emitted by atmospheric water vapour, carbon dioxide and ozone (Hock, 2005). The main variables controlling the amount of longwave radiation are cloudiness and the amount and temperature of water vapour (Equation 8 and 9). Incoming longwave radiation (L↓) is:

$$L\downarrow = \varepsilon_c \sigma T_a^4 F(n) \quad (8)$$

where $\varepsilon_c$ is the full-spectrum clear-sky emissivity, σ is the Stefan-Boltzman constant ($5.67 \times 10^{-8}$ W $m^{-2}$ $K^{-4}$), $T_a$ is the air temperature (K), and F(n) is a cloud factor relating the increase in radiation to the cloud amount (n). Outgoing longwave radiation (L↑) is calculated using the following equation:

$$L\uparrow = \varepsilon_s \sigma T_s^4 + (1- \varepsilon_s)L\downarrow$$

*( 9 )*

where $\varepsilon_s$ is the emissivity of the glacier surface, and $T_s$ is the temperature of the glacier surface (K). The flux of longwave irradiance describes how greenhouse gases drive climate change. King et al. (2007) describe how cloud cover has the opposite effect on S↓ and L↓ (King et al., 2007). Therefore, the relationship between cloud cover and net short and longwave radiation is complex and varies with the landscape. Over a high albedo surface, such as a glacier, melt can increase with increased cloudiness, as the increase in L↓ can outweigh the decrease in shortwave radiation (King et al., 2007).

The turbulent heat fluxes of sensible ($Q_H$) and latent ($Q_E$) are driven by turbulent eddies in the surface boundary layer (Morris, 1989). These eddies are caused by a temperature and moisture gradient between the air and snow or ice surface (Hock, 2005). Over weeks or months these turbulent fluxes are small when compared to the net radiation flux. However, over short time intervals (hours or days), or in certain environments, they can exceed radiation fluxes (Hock, 2005). The bulk aerodynamic method is often used for calculating sensible ($Q_H$) and latent ($Q_E$) heat fluxes:

$$Q_H = \rho_a c_p C_H u \, (\theta_z - \theta_s)$$

*( 10 )*

$$Q_E = \rho_a L_v C_E u \, (q_z - q_s)$$

*( 11 )*

where $\rho_a$ is the air density, $c_p$ is the specific heat capacity of air, $L_v$ is the latent heat of vaporization, $C_H$ and $C_E$ are the respective exchange coefficients for heat and vapour pressure, u is the mean wind speed, $\theta_z$ and $\theta_s$ are mean potential temperatures, $q_z$ and $q_s$ are mean specific humidity at height z and the surface, respectively (Hock, 2005). The number of coefficients and measurements required to accurately represent the turbulent heat fluxes displays some of the uncertainty built into energy balance models (Equation 10 and 11).

The ground heat flux ($Q_G$) describes the energy transfer between the glacier and the underlying earth material. The temperature of the snow/ ice must be raised to 0 °C before any surface melting can occur (Hock, 2005). For cold glaciers the amount of heat flux absorbed by the

ice before melting can occur may be significant. Temperature-depth profiles down to the base of the seasonally affected layer (generally 10-15 m below the surface) can help estimate this flux value (Patterson, 1994). There are several equations and models that attempt to constrain this value, but these will not be discussed in this paper.

The energy advected from rain ($Q_D$) is typically negligible and is often ignored in surface energy balance budgets (Hock, 2005). The unique occasion where this value may have a significant impact on surface melt is when there is prolonged warmth (Hock, 2005). Most energy used for melt is supplied by radiation, followed by the sensible and latent heat fluxes (Hock, 2005). The fraction of melt energy supplied by net radiation tends to increase with altitude, as the vertical lapse rates of temperature and vapour pressure lead to smaller turbulent fluxes (Hock, 2005).

Once $Q_M$ is calculated from the surface energy balance (Equation 4), the rate of melting, M, is then calculated (Equation 12; Hock, 2005):

$$M = \frac{Q_M}{\rho_w L_f} \qquad (12)$$

where $\rho_w$ is the density of water and $L_f$ is the latent heat of fusion. Energy-budget models are typically either point studies or spatially distributed models.

There are unique relationships between temperature, energy fluxes, and total melt energy in various climate settings, particularly in the tropics which behave differently than higher latitudes (Sicart et al., 2008). For example, for the Zongo Glacier in Bolivia net shortwave radiation drives the variability of the energy balance and is poorly correlated to air temperature. The glacier surface typically gains energy via the sensible heat flux, whereas the latent heat flux is a sink. During the melt season these turbulent fluxes tend to cancel out. In the climate of the tropical Andes, air temperature is a poor index of melt because of low and steady temperatures during the melt season, as well as low air temperatures at very high elevations (Sicart et al., 2008). Also, air temperature is not highly correlated with melt on daily time scales due to albedo changes caused by frequent snowfalls (Sicart et al., 2008).

## 2.3 Climate change and Cordillera Blanca hydrology

As described in the Introduction and Study Area Sections, the research is focused on the Cordillera Blanca, Peru. Following is a literature review of our current understanding of the hydrology of the mountain range.

### 2.3.1 Climate change

It is now widely documented that glaciers are retreating globally due to increased temperatures and shifting precipitation regimes (Clason et al., 2021), and conversely glaciers can also act as sensitive indicators for climate and environmental change. Globally, temperatures are increasing more rapidly in mountainous regions (0.3 °C decade$^{-1}$) than the global average (0.2 °C decade$^{-1}$, IPCC, 2019). Over the past 70 years in the Cordillera Blanca, Peru, temperature has increased at a rate of 0.10 °C decade$^{-1}$ (Rabatel et al., 2013). Other results indicate a sharper temperature increase; between 1951 and 1999, Mark (2002) and Mark and Seltzer (2005) observed a temperature increase of 0.35-0.39 °C decade $^{-1}$ in central Peru (9–11°S).

In the 20$^{th}$ century the altitude of the zero-degree isotherm (freezing level height) has risen by an average of ~45 m across the Tropical Andes (Schoolmeester et al. 2018). The primary drivers for this rise are the shifting patterns and higher frequency of El Niño events, as well as a warming troposphere (Rabatel et al., 2013). El Niño - Southern Oscillation (ENSO) events, which are associated with a band of warm water, develop in the equatorial Pacific, and influence the Andean climate (Schoolmeester et al. 2018). Areas above 2,000 m receive less rain and experience higher temperatures than normal during El Niño events, and vice versa during La Niña years (Garreaud, 2009). This results in variations of ELA and glacier mass balance (Veettil et al., 2017).

Following the SRES A2 emission scenario, results from Vuille et al. (2008) indicate that by the end of the 21$^{st}$ century the tropical Andes may undergo a warming of 4.5-5 °C. Future predictions of precipitation are less certain, but many model results point to an increase in precipitation in the wet season and a decrease in the dry season (Vera et al., 2006). There are also many predictions for altitude amplification, or elevation dependent warming. This means the rate of warming is more rapid at higher elevations (Pepin et al., 2015; Urrutia and Vuille, 2009).

### 2.3.2 Cordillera Blanca glacier melt effect on streamflow

Of Peru's 18 snow-capped mountain ranges, the Cordillera Blanca has the greatest glacier area coverage (40.8% of Peruvian total) and glacial ice volume (42.2% of Peruvian total). The Cordillera Blanca has 493 glaciers of the 2025 across Peru studied by Peru's National Water Authority (Autoridad Nacional del Agua, ANA, 2021). The Cordillera Blanca has decreased 40.5% in glacial areal coverage from 1975 to 2019; from 729.41 $km^2$ to 431.43 $km^2$ (ANA, 2021). Prior to this, the total glaciated area in the Cordillera Blanca was between 800-850 $km^2$ in 1930 (Georges, 2004). In the tropical Andes the mean annual mass balance has decreased from -0.2 m w.e. in the period 1964-1975 to -0.76 m w.e. in the period 1976- 2010 (Rabatel et al., 2013). Peruvian glaciers are highly susceptible to the effects of climate change as 86% have an area less than 1 $km^2$ (ANA, 2021). Low lying and small glaciers are generally retreating at the highest rates in this region (Rabatel et al., 2013).

A physically based, energy balance melt model was applied by Fyffe et al. (2021) within the Peruvian Cordilleras Blanca and Vilcanota. Warmer temperatures led to a higher percentage of precipitation falling as rainfall instead of snow, resulting in ablation increases from decreased albedo and an increase in net shortwave radiation (Fyffe et al., 2021). Despite the higher shortwave radiation in the dry season, the energy available for glacier melt was found to be lower because of the low humidity and cloudless skies causing a strongly negative latent heat flux and net longwave radiation. The dynamics and phase of wet season precipitation were found to be the primary drivers of Peruvian glaciers mass and energy balance (Fyffe et al., 2021).

Glacier melt provides buffering capacity for seasonal variability in streamflow, as glacier melt occurs throughout the dry season. The disappearance of glaciers will affect water use for agriculture and hydropower generation, as well as the availability of drinking water in Peru. Hydropower is the primary source of energy for electricity generation in Peru, and many other Andean countries (Bradley et al., 2006). Downstream populations are highly dependent on the availability of water resources all year (Bury et al., 2011). As glaciers retreat, the Rio Santa streamflow has declined noticeably in the dry season (Baraer et al., 2015). Tropical glaciers' contribution to dry season streamflow is approximately 50% in glacierized valleys of the Cordillera Blanca (Gordon et al., 2015). An estimate of the monthly maximum contribution of glacial melt water to available water supply in a typical year in Huaraz is 67%, while the monthly maximum

contribution in a drought year is 91% (Buytaert et al., 2017). Model results from various studies indicate that "glacier peak water" has already been passed for almost all basins in the Cordillera Blanca (Huss and Hock, 2018; Huss et al., 2017; Baraer et al., 2012). In other words, the decrease in glacial ice mass outweighs the effect of temperature increase when considering overall glacier melt contributions to streamflow; seasonal runoff will steadily decrease. This reduction in glacier meltwater is most noticeable during the dry season, when its relative contribution is highest (Baraer et al., 2012).

### 2.3.3 Groundwater in the Cordillera Blanca

Groundwater in high mountain basins is poorly understood and receives little scientific attention despite its' major influence on the timing and quantity of downstream water supplies (Baraer et al., 2015). Approximately half the discharge of the Cordillera Blanca proglacial streams originates from groundwater in the dry season (Somers et al., 2016). Baraer et al. (2015) found that in the Cordillera Blanca, the contribution of groundwater was between 24% and 80% of study areas outflow for the 2008 dry season. Findings from Glas et al. (2018) also show that groundwater may contribute up to 80% of the dry season streamflow for some valleys. The relative groundwater contribution is inversely proportional to the glacierized area percentage within a basin, and basins with less than 8% glacierized area have more groundwater than meltwater in their outflows in the dry season of 2008 in the Cordillera Blanca (Baraer et al., 2015). With 17% glacial coverage within the Quilcayhuanca basin (the research site), the relative groundwater contribution was found to be over 40% for the dry season (Baraer et al., 2015).

The talus slopes in the steep Cordillera Blanca valleys have a key role in the hydrologic systems, collecting water from precipitation at high elevations, storing it for months or years, and releasing it as springs on the valley floor (Glas et al., 2019, Somers et al., 2020). Talus aquifers of the Cordillera Blanca formed via gravitational slope deposits and are covered by glaciofluvial sediments (Glas et al., 2019). These deposits act as a confining layer over the saturated buried talus aquifers (Glas et al., 2019). Gordon et al. (2015) found that valley-crossing moraines play a major role in groundwater contribution to streamflow. In one site, stream discharge increased by 200 L $s^{-1}$ (18% of average discharge) over a valley-crossing moraine (1.2 km reach) (Gordon et al., 2015). Generally, losses of stream water were observed near the upper ends of meadows, while gaining stream reaches were observed at the lower ends of the meadows (Gordon et al., 2015).

A variety of groundwater investigation methods have been used for Quilcayhuanca, including:

• Detailed geochemical analysis (Chavez, 2013)

• Tracer dilution gaging (Gordon et al., 2015)

• Electrical and seismic geophysical methods (Glas, 2018)

• Ground penetrating radar (Maharaj, 2011)

• Heat tracing and energy balance modeling (Maharaj, 2011; Somers et al., 2016)

• Hydrochemical mixing model (Baraer et al., 2015)

• Piezometer installation and time series analysis (Chavez, 2013)

• Shallow boreholes (Baraer et al., 2015; Chavez, 2013)

• Vertical streambed temperature tracing (Maharaj, 2011)

As glaciers recede, groundwater will become a more dominant contributor to streamflow, particularly in the dry season (Somers et al., 2016). Groundwater receives minor recharge (~2%) from glaciers and thus may prove to be an important buffer to streamflow declines as glaciers melt in the short term (30 years) (Somers et al., 2019). However, in the long-term groundwater storage and discharge will decrease as evapotranspiration rates increase and precipitation decreases (Somers et al., 2019).

### 2.3.4 Cordillera Blanca hydro-social components

The effect on downstream communities from shifting Cordillera Blanca glaciers and hydrology is more complex and nuanced than simply quantifying physical water quantity changes. Carey (2010) laments the simplistic narrative of glaciers as vanishing water towers in his comprehensive book titled *In the Shadow of Melting Glaciers*. He documents that this story of loss and doom do not consider two factors: studies do not claim precise estimates of glacier loss and resulting runoff quantities, and water availability is not equivalent to water use. Water availability is often conflated with water use, yet despite a decline in glacial area coverage, hydroelectricity output at Cañón del Pato in the Cordillera Blanca has risen steadily from 50 megawatts in 1958 to 256 megawatts in 2002 (Carey, 2010). In a setting such as the Cordillera Blanca, water use is less about the environment, hydrology, and climate of a region than it is about the economy, politics, and culture (Mark et al., 2017). The shifting hydrological patterns induce significant risks and vulnerabilities of downstream water users; however, the analysis of these impacts is much more complex than the physical quantities of hydrological components

outlined in this study (e.g., Bury et al., 2013; Mark et al., 2017; Drenkhan et al., 2022). Water access rights and hydro-social risks are multifaceted, heterogeneous, and intersectional across diverse water users and sectors (Mark et al., 2017).

Glaciers are often represented as "the world's water towers" (Vivoroli et al., 2020) due to their importance for downstream communities. They are also scientific laboratories, recreational zones, tourist attractions, natural hazards, and spiritual centers (Carey et al., 2017). As to natural hazards, Peruvians have suffered more than any other society on earth from melting glaciers; since 1941 there have been ~25,000 deaths from Cordillera Blanca glacier disasters (e.g., Evans et al., 2009). Historically, there has been a silver lining with reference to melting ice in Peru, as it has in part led to the commodification of glaciers, increased consumption of Andean resources, tourism, and the modernization of Peru (Carey, 2010).

# 3 Study Site and Observations

## 3.1 Location and Climate

The research study site is the Quilcayhuanca Valley within the greater Cordillera Blanca, Peru. The Cordillera Blanca is in the northern Peruvian Andes and has the highest concentration of tropical glaciers in the world (Autoridad Nacional del Agua, 2014). The Cordillera Blanca range is oriented NNW-SSE, and is approximately 180 km long, and 21 km wide (Chavez, 2013). There are several peaks above 6000 m elevation, including Peru's highest peak, Huascaran, at 6,768 metres above sea level (m a.s.l.). The Cordillera Blanca is located between 8°40' to 10° south of the equator, and experiences a pronounced wet and dry season, with over 80% of the 800-1200 mm $yr^{-1}$ precipitation falling between October and May (Baraer et al., 2009). In the region (between 8°S and 27°S), Andean rivers typically have a discharge peak in February and March resulting from the mature phase of the South American Monsoon System (Arias et al., 2021). The temperature range is typical of the tropics, with the daily temperature range being greater than the annual monthly variability (Kaser et al., 1990).

The Quilcay River drains to the Rio Santa, which flows northward and then west to the Pacific Ocean. The Rio Santa captures runoff from the eastern side of the non-glacierized Cordillera Negra and the western side of the glacierized Cordillera Blanca. The Rio Santa flows

over 300 km northwest from its headwaters of Laguna Conococha, at 4100 m above sea level (Mateo et al., 2021). The Rio Santa discharge experiences a strong seasonal variation, with the wet season peak in March typically being 20 times greater than the dry season July-September discharge (Mateo et al., 2021). Rio Santa streamflow is maintained in the dry season via glacial melt water and stored groundwater (Bury et al., 2011). At La Balsa station, glacial meltwater contributions are 10-20% of the total annual discharge and may exceed 40% in the dry season (Mark et al., 2005). Results from Mark and McKenzie (2007) show that 66% of dry season Rio Santa discharge originates from the glacierized tributaries.

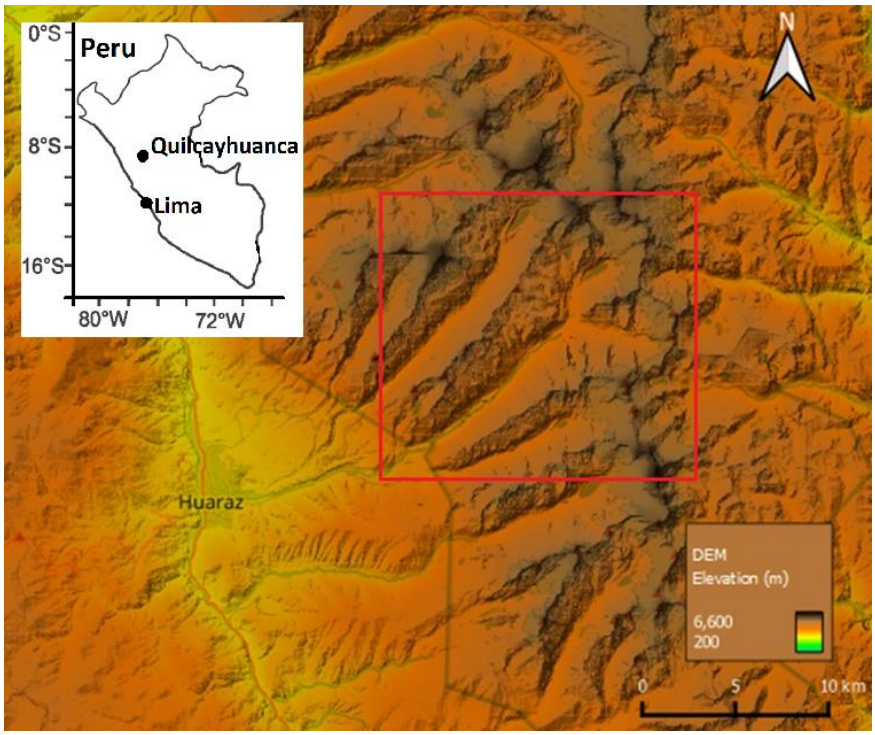


*Figure 5- Shaded DEM of Y-shaped Quilcayhuanca drainage basin (red box), with Huaraz on left side of map. The elevation data and underlying hillshade are from SRTM (plugin; CRS: ESPG:3857-WGS 84/ Pseudo-Mercator) within QGIS 3.18.*

The Quilcayhuanca Valley (Figure 5) bottom is a long, topographically flat, high elevation valley classified as pampa (Maharaj, 2011). Pampas are a subset of a neotropical alpine ecosystem known as a pàramo, which covers more than 75,000 km$^2$ of the northern Andes of Peru, Ecuador, Colombia, Venezuala, and Costa Rica (Buytaert et al., 2006). Pàramos are characterized by a relative humidity greater than 80%, low temperatures, and high assemblages of clay and organic

material, which allows the valley floor to act as large water storage in the Andean highlands (Maharaj, 2011).

*Figure 6- Looking northeast towards Y-shaped confluence of the Quilcayhuanca Valley. Mount Pucaranra on left, and Chinchey on right. The highest peak in the Quilcayhuanca Valley is Mount Chinchey at 6,309 m a.s.l.. The photo location is at upper end of the flat pampa valley floor.*

Four geologically distinct depositional layers are found filling the Quilcayhuanca Valley floor (Figure 6). Based on ground penetrating radar surveys during the dry season (Maharaj, 2011), at the surface is dry, organic rich soils underlain by water saturated sandy, organic rich soils. These were underlain by an effectively impermeable ~3 m thick water-saturated clay layer, which hydrologically isolates the upper organic layers from the higher permeability layers below. Under the clay layer are coarse grained gravels from colluvial deposits, intermixed with glacial outwash till and diamicton (Maharaj, 2011). A conservative estimate for the minimum thickness of these talus deposits was placed at 15 m (Maharaj, 2011), and the geometric mean for the hydraulic conductivity of these talus layers was found to be $2.1 \times 10^{-5}$ m/s (Chavez, 2013). These buried talus layers were classified as confined aquifers based on their relatively high hydraulic conductivities and lateral extent (Chavez, 2013). Artesian conditions were observed for these

buried talus deposits, indicating their hydraulic connectivity to the exposed valley wall talus deposits (Chavez, 2013).

## 3.2 Observation site descriptions

There are automated weather and stream gauging stations at two locations within the Quilcayhuanca Valley, providing hourly hydrometeorological observations at an upper station and a lower station (Figure 7).

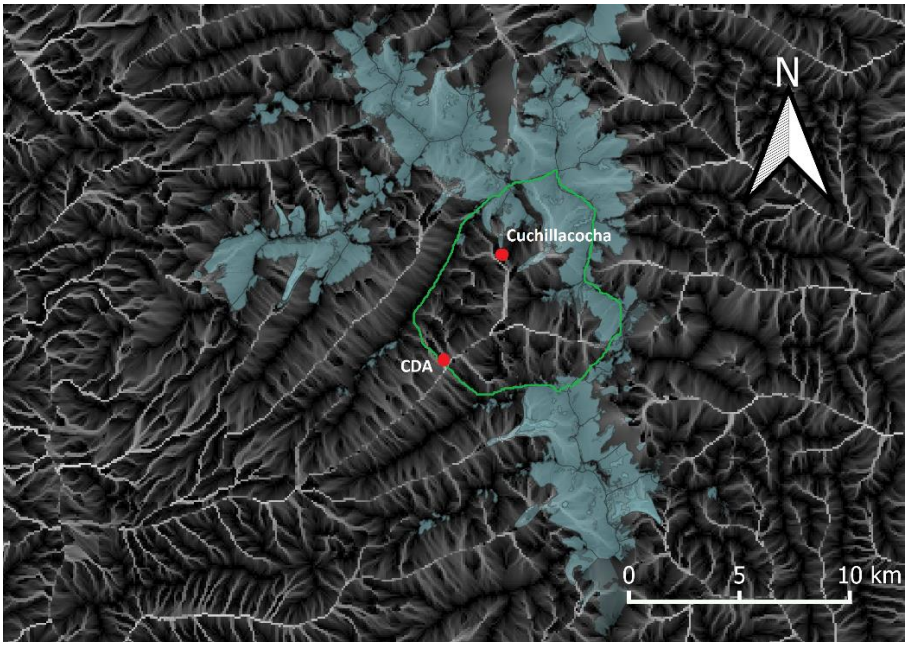


*Figure 7- Catchment area with delineation (green) of the Quilcayhuanca Valley basin. The drainage basin is deliberately smaller than natural catchment area so that model output will match the area with observed data. The map displays glaciers (shaded blue), and both observation stations, Cuchillacocha and Casa De Agua (CDA). Glaciers are delineated using global land ice measurements from space (GLIMS) database (Racoviteanu et al., 2009). Map generated by QGIS 3.18.*

The higher elevation station, beside Laguna (Lake) Cuchillacocha (9°25’ S, 77°20’ W), is at an elevation of 4642 m a.s.l. and is at the headwaters of the northern arm of the Quilcayhuanca Valley. The Cuchillacocha station represents a high elevation sub-basin (5.066 $km^2$) within the greater Quilcayhuanca basin. The lower elevation station, Casa De Agua (9°27’ S, 77°22’ W), is at an elevation of 3924 m a.s.l., and is located on the valley floor beside the Quilcay River. The catchment area above Casa De Agua totals 67.34 $km^2$, and is the area focused on in this study.

Both stations measure hourly streamflow (kPa; °C), air temperature (°C), precipitation (mm), relative humidity (%), wind speed (m $s^{-1}$), and incoming solar radiation (W $m^{-2}$, Figure 8).

Discharge is measured at both stations using a Model 3001 Solinst Levelogger Edge and a stage-discharge relationship (rating curves, Figure A1). The Casa de Agua rating curve has an $R^2$ of 0.91 and the Cuchillacocha rating curve has an $R^2$ of 0.71. The variability and sources of error are discussed in greater detail by Mateo et al. (2021). The sensors (HOBO loggers) collecting meteorological data are from Onset Computer Corporation (Mateo et al., 2021). As is typical in high mountainous areas, observational data are prone to errors and the density of stations could be improved. However, two hydrometeorological stations is relatively good data coverage for a remote high mountain basin in the Andes (van Tiel et al., 2020).

*Figure 8- Dr. Hellstrom providing updates for the automated weather station sensors at upper Laguna Cuchillacocha station (Elevation of 4642 m). Photo taken on May 2nd, 2022, by Bryan Mark.*

# 4 Methods

## 4.1 Model selection and workflow

The Cold Regions Hydrological Modelling platform (CRHM; Pomeroy et al., 2007; Pradhananga and Pomeroy, 2022) is selected to investigate the hydrological processes and inter-annual variability of the Quilcayhuanca basin. CRHM is a flexible, physically based model developed at the Centre for Hydrology, University of Saskatchewan (CRHM; Pomeroy et al., 2007). It

originated with the aim of improving the understanding of cold regions hydrological processes in poorly gauged or ungauged basins (Pomeroy et al., 2007). Physically based models can prove to be useful in comprehending the hydrological processes of remote regions with sparse meteorological data (Krogh et al., 2015). The model includes phenomena specific to cold environments, including snow and ice accumulation, interception, transport and melt, and infiltration through frozen soils (Krogh et al., 2015). CRHM is not a calibration-based model, and instead relies on parameters deduced or measured from rigorous field or modelling studies (Krogh et al., 2015). The parameterization of the CRHM module characteristics is based on a variety of sources including observed data from weather stations, previous literature, satellite imaging, and digital elevation models. In combination with the open structure and flexible modular framework, CRHM is a good numerical tool for testing hydrological comprehension in remote regions with minimal field data (Krogh et al., 2015). CRHM has not previously been applied to a glaciated catchment in the tropics.

Model validity is evaluated with observed streamflow and water table levels, and then with literature values for glacial melt and evapotranspiration. Given the availability of data coverage and overlap, the model is validated using various time frames (depending on which data is available) within the period from June 27, 2014, to August 12, 2018. Following validation, parameters such as the degree of glaciation, ice albedo, or temperature and precipitation trends are then easily modified to inspect how the catchments may respond to a changing climate.

## 4.2 Model framework and setup

There are 4 components to the CRHM Model (Figure 9): (1) the meteorological data that forces the model are input as observation files, (2) hydrological response units (HRUs) are used to divide the catchment into discrete areas of similar response, (3) modules represent hydrological processes that affect the basin hydrology, and (4) parameters represent the physical characteristics and details within each module and HRU.

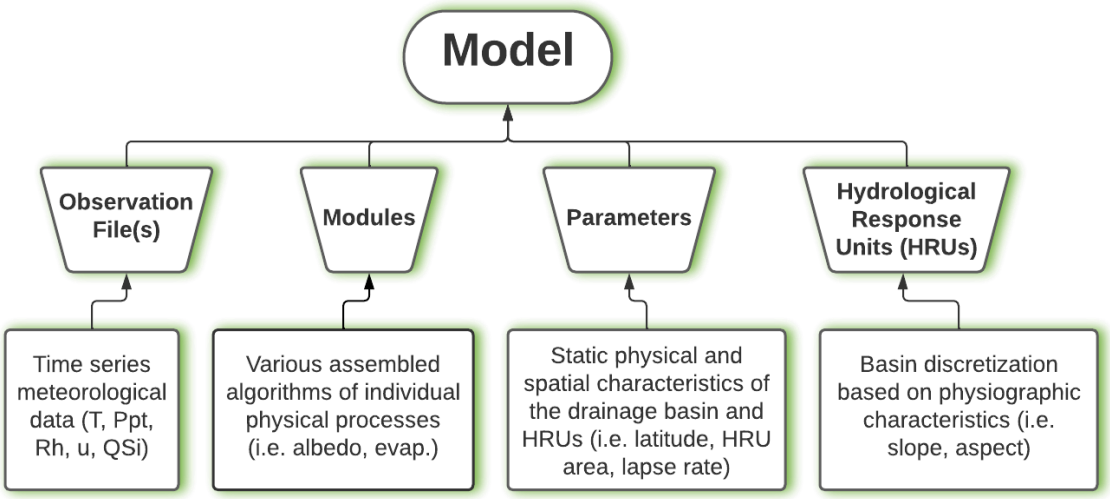


*Figure 9- Conceptual CRHM framework with user-defined input components.*

### 4.2.1 Observation files and data processing

CRHM requires observation files with hourly meteorological data with no data gaps. To have continuous meteorological observation data from June 27, 2014, to August 13, 2018, a linear regression was used to impute missing data. The regress and impute functions were used from the CRHMr package developed by Kevin Shook (https://github.com/CentreForHydrology/CRHMr/blob/master/CRHMr.pdf, last access: November 23, 2022). The regress function generates the regression slopes (multipliers) and intercepts (offset values) required by the impute function. A linear (least-squares) regression of the primary dataset against the secondary dataset is performed. Missing (NA) values in the data frame are then filled in using the impute function from the CRHMr package. Secondary values are adjusted using the regression slopes and intercepts to fill in the gaps (NA values). Figures A2 and A3 (from Mateo et al., 2021) in the Appendix display the gaps in hydrometeorological data.

Continuous discharge observation data was available for August 4, 2016, to August 13$^{th}$, 2018, for the basin outflow point (Casa de Agua). Streamflow comparisons were all made with the Casa de Agua discharge station.

### 4.2.2 HRU Delineation

The CRHM structure requires the basin to be subdivided into areas with similar biophysical landscape characteristics; theoretically, they respond identically to hydrological events. These areas are termed hydrological response units (HRUs, Figure 10).

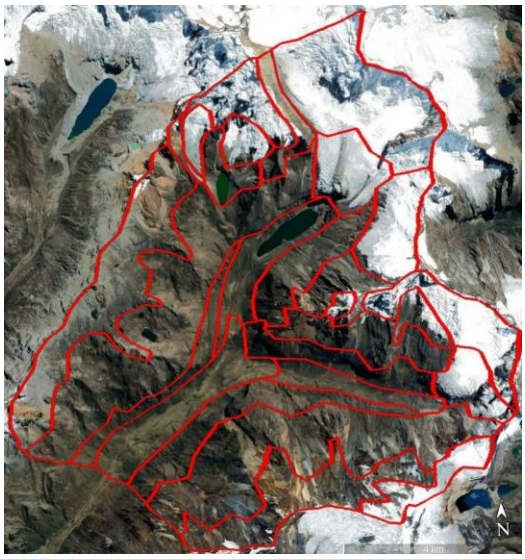

*Figure 10- Google earth image of Quilcayhuanca basin with HRU divisions.*

One benefit of CRHM is the ability to select a suitable spatial scale based on the available data, landscape types, and the purposes of the simulations. Within each HRU, processes and states are calculated based on single sets of parameters, state variables, and fluxes (Pomeroy et al., 2022). Snow and hydrologic flow pathways are directed between HRUs based on routing selection, and/or landscape characteristics (e.g., vegetation height for blowing snow). In the Quilcayhuanca Valley, based on the scale of the basin and the amount of data and observations available, 19 HRUs were selected to best capture the hydrologic system. The HRUs were selected based on similar slope, aspect, elevation, landcover type, and measurement station locations (Figure 11).

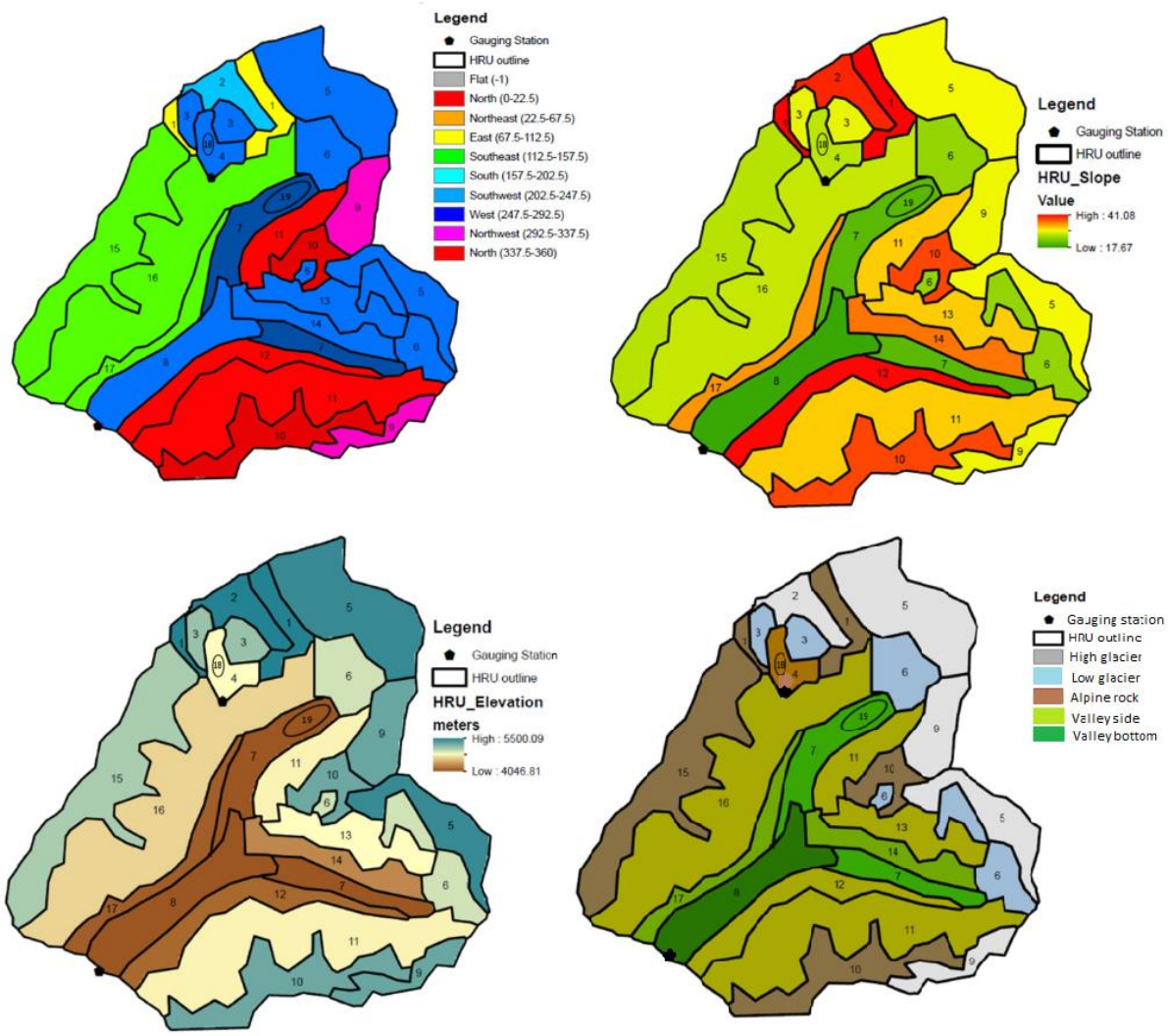


*Figure 11- Basin discretization established through intersections of aspect (top right), slope (top left), elevation (bottom left), and landcover type (bottom right).*

The identifications of the HRUs, along with their respective area, and mean aspect, slope, and elevation, are listed in Table 1. There are two lake HRUs, Cuchillacocha (with a volume of 2 x $10^6$ $m^3$) and Tullpacocha (12 x $10^6$ $m^3$, Frey et al., 2018). The lake module in CRHM was not updated at the time of this writing, so lakes are treated as depression storage and the Priestley-Taylor evaporation method was used for the lake HRUs.

*Table 1- Area and mean aspect, slope, and elevations of 19 Quilcayhuanca HRUs*

| HRU # | HRU Name | Area ($km^2$) | Mean Aspect (°) | Mean Slope (°) | Mean Elevation (m a.s.l.) |
|---|---|---|---|---|---|
| 1 | Cuchillacocha Alpine Rock | 1.53 | 104 | 41 | 5276 |
| 2 | Cuchillacocha High Glacier | 1.32 | 203 | 39 | 5495 |
| 3 | Cuchillacocha Low Glacier | 1.24 | 204 | 28 | 5021 |
| 4 | Cuchillacocha Outlet (alpine rock) | 0.84 | 205 | 26 | 4793 |
| 5 | Quilcay High Glacier (Southwest) | 7.37 | 210 | 29 | 5251 |
| 6 | Quilcay Low Glacier | 4.06 | 220 | 24 | 4893 |
| 7 | Upper Valley | 3.49 | 269 | 20 | 4290 |
| 8 | Lower Valley (Quilcay Outlet) | 3.66 | 219 | 18 | 4045 |
| 9 | Quilcay High Glacier (West) | 3.20 | 310 | 28 | 5152 |
| 10 | Quilcay Alpine Rock (North) | 4.63 | 339 | 38 | 5138 |
| 11 | Sub-Alpine (North) | 9.49 | 330 | 32 | 4762 |
| 12 | Steep Valley Side (North) | 2.72 | 339 | 41 | 4358 |
| 13 | Sub-Alpine (South) | 2.42 | 207 | 32 | 4778 |
| 14 | Steep Valley Side (South) | 2.01 | 207 | 36 | 4450 |
| 15 | Quilcay Alpine Rock (Southeast) | 6.25 | 123 | 26 | 4976 |
| 16 | Sub-Alpine (Southeast) | 10.62 | 137 | 27 | 4666 |
| 17 | Steep Valley Side (Southeast) | 1.90 | 131 | 34 | 4299 |
| 18 | Lake (Cuchillacocha) | 0.14 | 205 | 1 | 4621 |
| 19 | Lake (Tullpacocha) | 0.45 | 270 | 1 | 4288 |

### 4.2.3 Module selection

Following is a brief description of modules used for the Quilcayhuanca Basin (Fang et al., 2013):

1) Observation module: reads the measured meteorological data file into the model. This includes precipitation, temperature, relative humidity, wind speed, and shortwave solar radiation. Selected corrections are made, such as temperature lapse rates or precipitation height adjustments, and these are directed as inputs to the other modules.
2) Albedo module (Verseghy, 1991): estimates snow albedo and indicates beginning of melt period for the energy balance module.
3) Soil infiltration module (Ayers, 1959): Handles unfrozen soil infiltration based on groundcover and soil texture types. Output is used in the soil module.
4) Basin module: Declares general parameters for the model, including HRU areas, slopes, aspect, latitudes, and elevations).
5) Canopy module (Ellis et al., 2010): calculates net all wave radiation and precipitation intercepted by canopy to update under canopy values. Output values required by the energy balance snowmelt module (SNOBAL).

6) Evaporation module (Granger and Gray, 1989; Granger and Pomeroy, 1997): calculates hourly evapotranspiration based on Penman-Monteith and Priestley-Taylor equations.
7) Glacier module (Gray and Landine, 1987): Energy budget of firn and ice melt model. Glacier storage and melt calculated using parameters, including albedo and ice thickness. Katabatic wind parameterization was used to calculate turbulent fluxes (Equation 10 and 11) based on previous field work and literature (Aubry-Wake et al., 2015; Munro 2004; Oerlemans and Grisogono, 2002; Pradhananga and Pomeroy, 2022).
8) Global module (Garnier and Ohmura, 1970): Calculate theoretical short-wave direct and diffuse solar radiation. Module handles slope, aspect, and the elevation and transmissivity applicable to the region. The maximum number of daily sunshine hours is also calculated. Output is sent to other modules for radiation input.
9) Hydraulic conductivity module: Flow rates in soil and groundwater layers are calculated. Vertical flow of excess soil water to groundwater is also controlled by this module. These drainage factors are calculated using Darcy's Law for unsaturated flow.
10) Longwave radiation module (Sicart et al., 2006): Measured shortwave radiation is used to calculate longwave radiation, which is used by the energy balance snowmelt module.
11) Routing module: The Muskingum method is used to handle the routing of surface runoff, subsurface runoff and HRU routing. Surface, subsurface, and ground water storage values are input into this module as well as flow directions for each storage unit. Manning's Equation (Chow, 1959) is used for surface flow velocity, and Clark's lag and route algorithm (Clark, 1945) is used for subsurface and ground water flows. More details are provided in Table A2 (Appendix).
12) Blowing snow module (Pomeroy and Li, 2000): Snow transport and sublimation of blowing snow is calculated using hourly wind speed, air temperature and relative humidity observations. Module handles transport of snow between HRUs.
13) Energy balance snowmelt module (Marks et al., 1998): Snowmelt and melt runoff is calculated using the energy balance model and input data on measurement heights and depths, energy exchanges, and snow properties. Fluxes of sensible heat, latent heat, ground heat, advection from rainfall, radiation, and the change in internal energy for the top active snowpack layer and the underlying layer are calculated for the energy balance model.

14) Soil moisture module: Soil moisture is estimated throughout the year. Soil is divided into an upper recharge layer and a lower layer. Infiltration will fill the recharge layer storage requirements before passing into the lower layer. Once both storage layers are filled, the excess water will contribute to groundwater flow, depressional storage, and subsurface flow. After infiltration, evaporation and subsurface runoff are handled.
15) Avalanching module: calculates SWE slope transport (Bernhardt and Schulz, 2010) based on snow holding depth parameter.
16) Wind speed module: Estimates wind speed variations due to topography. Walmsley et al. (1989) derived a simple parametric version of the Mason and Sykes (1979) wind flow model for estimating wind speed variation induced by 2D and 3D topographic features.

### 4.2.4 Model parameterization

CRHM is not designed to be entirely based on calibration, where parameters are iteratively modified across a range of potential values to achieve a best fit between model outcomes and observation data. Instead, the model is primarily parameterized with robust field data and related modelling studies (Krogh et al., 2015). For this research, the parameterization of the CRHM module characteristics is based on a variety of sources including observed data from the two weather stations, previous literature from the Cordillera Blanca, satellite imaging, and digital elevation models. Some parameters are established through field observations and previous site-based literature include surface water routing, hydraulic conductivity, glacier ice thickness, soil thickness, lapse rates, and vegetation height. All parameter values for the 19 HRUs and 17 modules are in Tables 1 and 2 in Appendix A. Note that the shared module does not represent a hydrological process and performs no calculations; it simply lists parameters that are shared between modules. Due to the high level of confidence in the process representations of the modules and the appropriate model structure, calibration was limited to runoff routing and subsurface aspects (Pomeroy et al., 2022). Subsurface parameters were estimated through a combination of manual calibration and conceptual models developed in previous literature. Groundwater is routed directly to the groundwater storage of downslope HRUs or as overland flow to downslope HRUs.

Due to COVID-19, I was not able to undertake an extensive, systematic field campaign in the Quilcayhuanca Valley. However, I was able to visit the region for one week in May 2022.

During the visit I was able to make visual observations of the HRUs delineated for the model and interact with local researchers who provided additional detail and context about the Cordillera Blanca.

## 4.3 Model evaluation

In this section, several comparisons are made to check the validity of simulations. Evaluating multiple hydrological processes to assess model performance is crucial to reducing internal consistencies and improve simulation fidelity (van Tiel et al., 2020; Aubry-Wake et al., 2022b). The model was assessed using observation data and literature relating streamflow, groundwater flow, evapotranspiration, and glacier melt. Reliable, relatively continuous observation data between the years 2014 to 2018 is used for comparison. Groundwater, evapotranspiration, and glacier melt comparisons are made from 2014 to 2018, and streamflow from 2016 to 2018. Comparisons are made with a range of metrics as appropriate for each hydrological process and available data. If model results cannot be directly compared to observation data, values from literature describing the Quilcayhuanca Valley or other Cordillera Blanca valleys are used. Therefore, model validity will be tested in conjunction with other model results, as these comparisons often yield improved hydrological understanding.

To assess model performance of streamflow and groundwater level, five statistical indices are used for evaluating performance: coefficient of determination ($R^2$), Nash-Sutcliffe efficiency (NSE, Nash and Sutcliffe, 1970), percent bias ($P_{BIAS}$), Pearson-moment correlation coefficient (r), and Kling-Gupta Efficiency (KGE, Gupta et al., 2009) were calculated as follows:

$$NSE = 1 - \left( \frac{\sum (T_t^{obs} - T_t^{sim})^2}{\sum (T_t^{obs} - \bar{T}_t^{obs})^2} \right) \quad (13)$$

$$P_{BIAS} = \left( \frac{\sum T_t^{obs} - T_t^{sim}}{\sum T_t^{obs}} \right) \times 100 \quad (14)$$

$$R^2 = \frac{(\sum[T_t^{obs} - \bar{T}_t^{obs}][T_t^{sim} - \bar{T}_t^{sim}])^2}{\sum(T_t^{obs} - \bar{T}_t^{obs})^2 \sum(T_t^{sim} - \bar{T}_t^{sim})^2}$$

*( 15 )*

$$r = \frac{\sum(T_t^{obs} - \bar{T}_t^{obs})(T_t^{sim} - \bar{T}_t^{sim})}{\sqrt{\sum(T_t^{obs} - \bar{T}_t^{obs})^2 \sum(T_t^{sim} - \bar{T}_t^{sim})^2}}$$

*( 16 )*

where $T_t^{obs}$, $T_t^{sim}$, $\bar{T}_t^{obs}$, $\bar{T}_t^{sim}$ are the observed, simulated, mean of the observed, and mean of the simulated values, respectively, and:

$$KGE = 1 - \sqrt{(r-1)^2 + (\alpha - 1)^2 + (\beta - 1)^2}$$

*( 17 )*

where r is the linear correlation between observations and simulations, $\alpha$ is a measure of flow variability error, and $\beta$ relates to the bias.

The NSE (Equation 13) calculates model efficiency to reproduce the time evolution of hydrological variables; it is useful for evaluating streamflow hydrograph prediction (Nash and Sutcliffe, 1970). An NSE value of 0 indicates that the model simulations are no better predictors than the average of observed values, and an NSE value of 1 indicates perfect agreement between simulations and observations. The percent bias ($P_{BIAS}$, Equation 14) quantifies the average difference between the observed and simulated values over the entire simulated period. A value close to 0% indicates a small deviation of the simulated results to the observed values. The coefficient of determination ($R^2$, Equation 15) is a numerical descriptor for the proportion of the measured data variance that can be predicted by the model results. The coefficient varies from 0 to 1, with higher values displaying a better model fit. The Pearson- moment correlation coefficient (r, Equation 16) ranges from -1 to 1 and calculated the correlation between two variables (Fang et al. 2013). Positive values indicate a positive correlation and vice versa. A Kling-Gupta Efficiency (KGE, Gupta et al., 2009, Equation 17) value of KGE > -0.41 indicates that the model results are better than the average of the observations, while a KGE < -0.41 denotes poor model performance (Knoben et al., 2019).

# 5 Results and Discussion

## 5.1 Streamflow

For each model simulation, an initial two-year spin-up period was used to establish dynamic equilibrium. Streamflow comparisons are based on daily average values of hourly discharge. Comparisons between simulated and observed streamflow were made for the period of August 4, 2016, to August 12, 2018 (Figure 12).

The simulation results closely capture the rise and fall of the wet season and dry season transitions, and the timing of major peak flows. However, the model underestimates wet season flows in 2016 and overestimates wet season flows in 2017. The model produces similar dry season discharges as the observed values.

Results from Moriasi et al. (2007) show that the performance of streamflow simulations using a monthly time step are satisfactory if NSE > 0.5 and $R^2$ > 0.5, but that shorter time steps typically lead to poorer performance (Dos Santos et al. 2020). Therefore, due to the higher flow variability at daily time steps, certain studies have labelled NSE values in the range of 0.15 to 0.5 as “near satisfactory” (Dos Santos et al. 2020; Chou et al. 2022). Therefore, for the daily time step simulation of this study, an NSE value of 0.51 indicates “satisfactory” model performance for streamflow hydrograph prediction (Chou et al. 2022). A $P_{BIAS}$ value of 6.8% was found for this study, indicating a close match for simulated streamflow prediction, and observed values. The coefficient of determination results for streamflow prediction were “satisfactory” (R2= 0.63, Dos Santos et al. 2020) and good for the Pearson-moment correlation coefficient (r=0.79). The KGE value of 0.76 for the streamflow simulation in this study indicate good predictive power of the model.

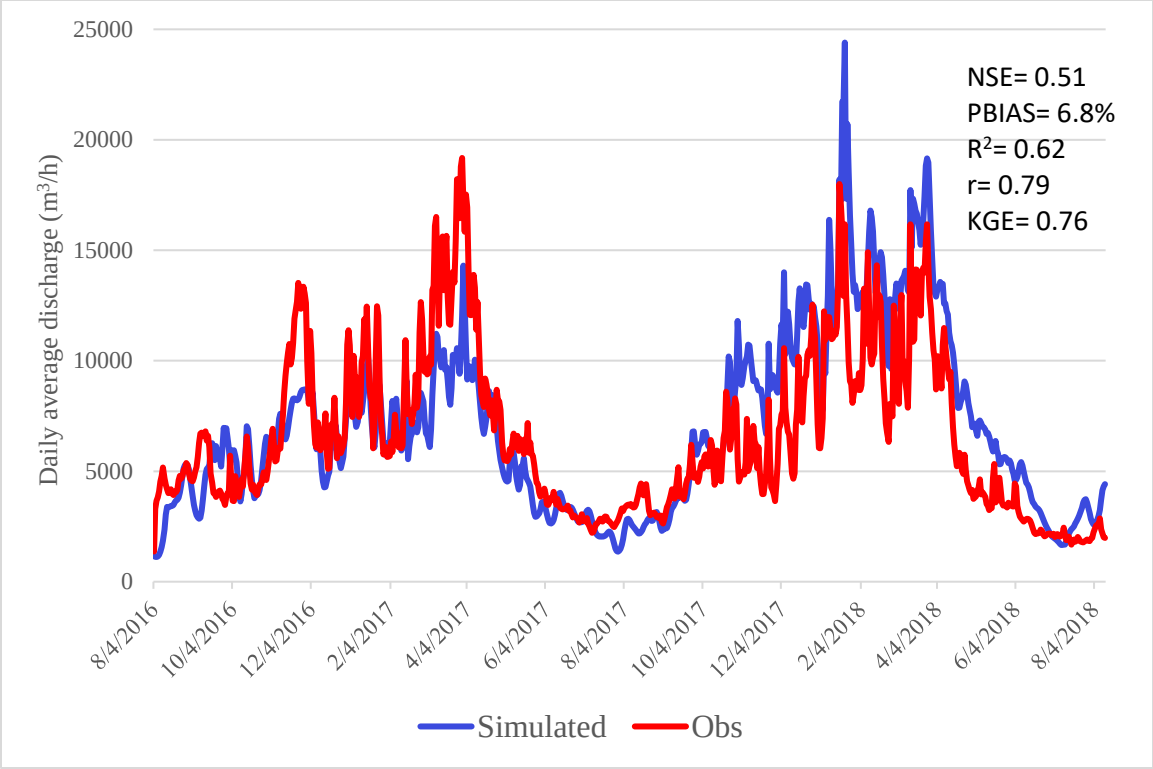


*Figure 12- Casa de Agua streamflow, simulated and observed.*

## 5.2 Groundwater

Groundwater in high mountain basins is poorly understood and receives little scientific attention despite its' major influence on the timing and quantity of downstream water supplies (Somers et al., 2020; Baraer et al., 2015). Based on groundwater storage values calculated by CRHM for each HRU, and adjusted based on area, the total storage value is 0.00174 $km^3$. This value is based on an average of storage values for each HRU from January 1, 2015, to August 12, 2018. These results are smaller than results from Glas et al. (2019) that found the drainable groundwater storage potential for Quilcayhuanca Valley above 3800 m is 0.006 to 0.02 $km^3$. The difference between these estimates could be a result of an underestimated maximum available water holding capacity of the ground water reservoir in the CRHM model. However, Glas et al. (2019) notes that the calculation for storage potential varies greatly with porosity estimates and that further work is required to constrain this value.

### 5.2.1 Groundwater flow

Groundwater accounts for 31.5% of total basin outflow (streamflow + groundwater flow), according to model results for August 4, 2016, to August 12, 2018. This equates to 46% of

streamflow outflow. The percentage of water exiting the valley as groundwater increases in the dry season. For the 2017 dry season (May 1st- Sep 30th), 35% of the total outflow was groundwater, or 53% of the streamflow. Although the total amount of groundwater exiting the basin is greater in the wet season, its proportion to total outflow is reduced. In the 2016/2017 wet season, groundwater is 30% of the total outflow. The proportional increase of groundwater exiting the basin in the dry season is in agreement with many other studies in the region (e.g., Chavez, 2013; Baraer et al., 2015; Gordon et al., 2015; Maharaj, 2011; Glas et al., 2018; Somers et al., 2019). However, most other studies report on groundwater contribution to streamflow, not groundwater exiting the basin outflow point at Casa de Agua as groundwater. This represents a gap in our understanding of the flow pathways of this groundwater past Casa de Agua as we cannot directly measure how much water flows via the subsurface out of the catchment. This is discussed in Section 5.5.

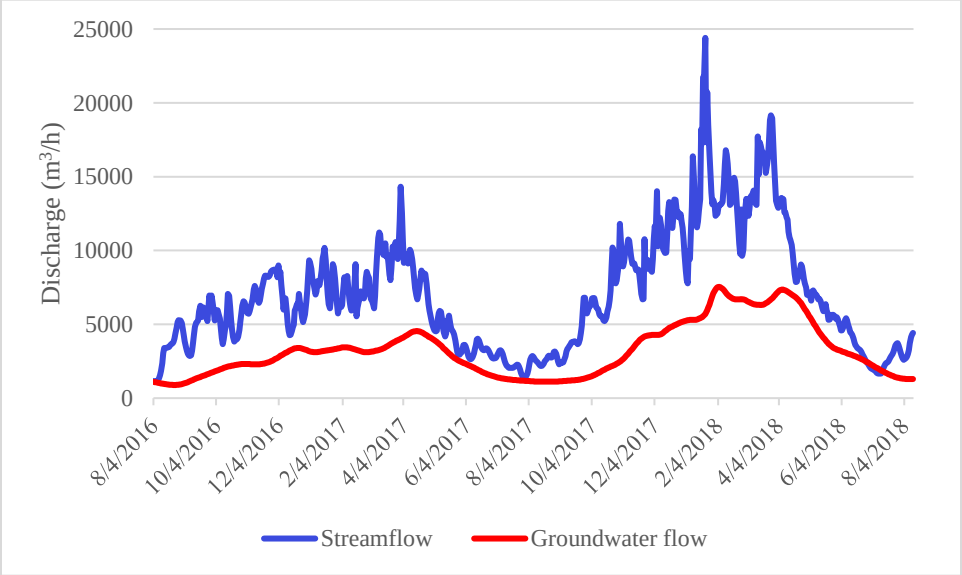


*Figure 13- Simulated total basin outflow separated into streamflow and groundwater flow.*

Groundwater routing with CRHM is a combination of manual calibration and basin conceptualizations of flow pathways based on literature findings (Baraer et al., 2015; Chavez, 2013; Glas et al., 2018; Gordon et al., 2015; Maharaj, 2011; Somers et al., 2019). The simulations allow for the observation of groundwater flowing in and out of the valley bottom (HRU 8). If we calculated the difference of groundwater inflow and outflow from HRU 8, we identify when the groundwater reservoir is being recharged (positive values) and when it is being depleted (negative values).

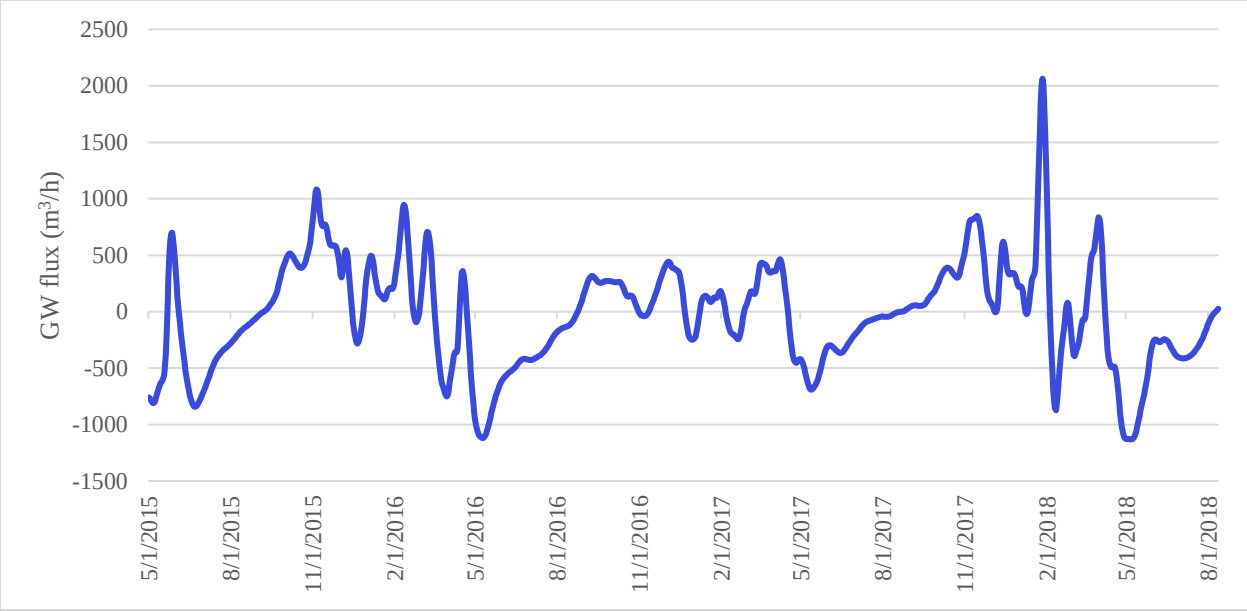


*Figure 14- Net groundwater flow (inflow – outflow) for the valley bottom (HRU 8).*

The daily average groundwater flux is -251 $m^3/h$ for the 2015-2017 dry seasons, and 187 $m^3/h$ for the 2015-2018 wet seasons. As expected, the groundwater reservoir is being recharged in the wet season and depleted in the dry season. In Figure 14 there is a noticeable trough at the end of each wet season in May when the groundwater storage of HRU 8 is gaining water at the highest rates. This likely occurs at the end of the wet season because of the residence time and lagged delay of high groundwater outflow not being recharged by equivalent groundwater inflows. The lag in groundwater flow compared to streamflow can be seen in Figure 13.

### 5.2.2 Groundwater storage

The following section compares the CRHM groundwater storage results value for the valley bottom (HRU 8) to five piezometers for the period of 2016 to 2018. Like many high mountain hydrology studies, the piezometers are positioned in the valley bottom floor (Figure 15) as this area is easily accessible and hydraulic head is more stable (Somers et al., 2020).

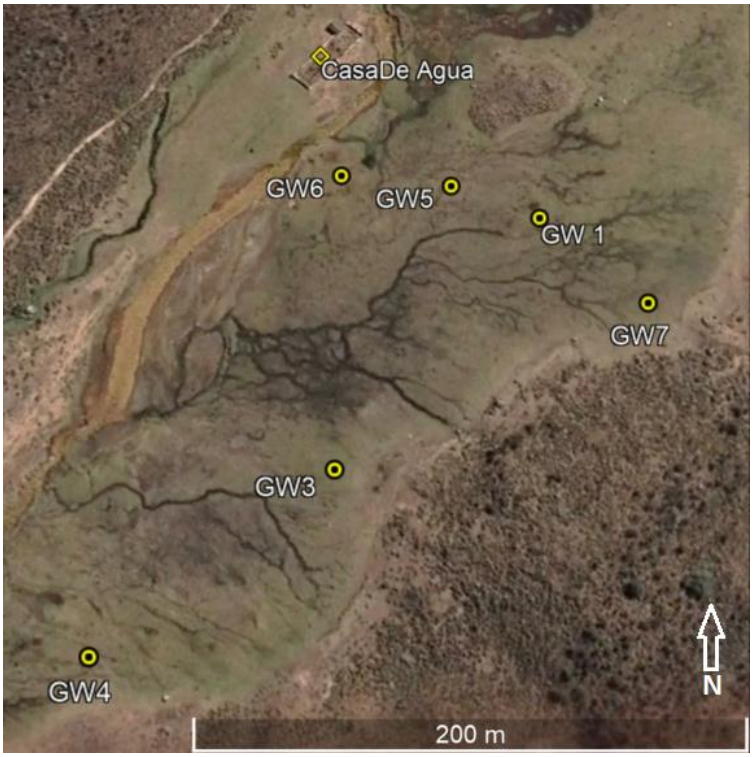


*Figure 15- Google Earth image with piezometer locations and the Casa de Agua meteorological station. Piezometer installation description in Chavez (2013).*

The CRHM groundwater storage value considers the volume of water stored, whereas the loggers measure the height of water; to compare these values an assumed value of porosity is required. Further, the CRHM groundwater storage output value represents the entire valley bottom (HRU 8) and takes into consideration the entire HRU area, whereas the piezometers are point source measurements that can become locally over pressurized. As such, it is not an exact comparison, so the primary focus is on the timing correlation between the CRHM output and the level loggers. All level loggers were adjusted relative to the initial CRHM output value, as the relative changes and timing of groundwater levels are of most interest. Subsurface parameters were estimated based on geophysical studies conducted by Maharaj (2011), Chavez (2013), and Glas et al., (2019) and conceptual models developed by Baraer et al., (2015), Gordon et al, (2015), Somers et al., (2016), and Glas et al., (2018).

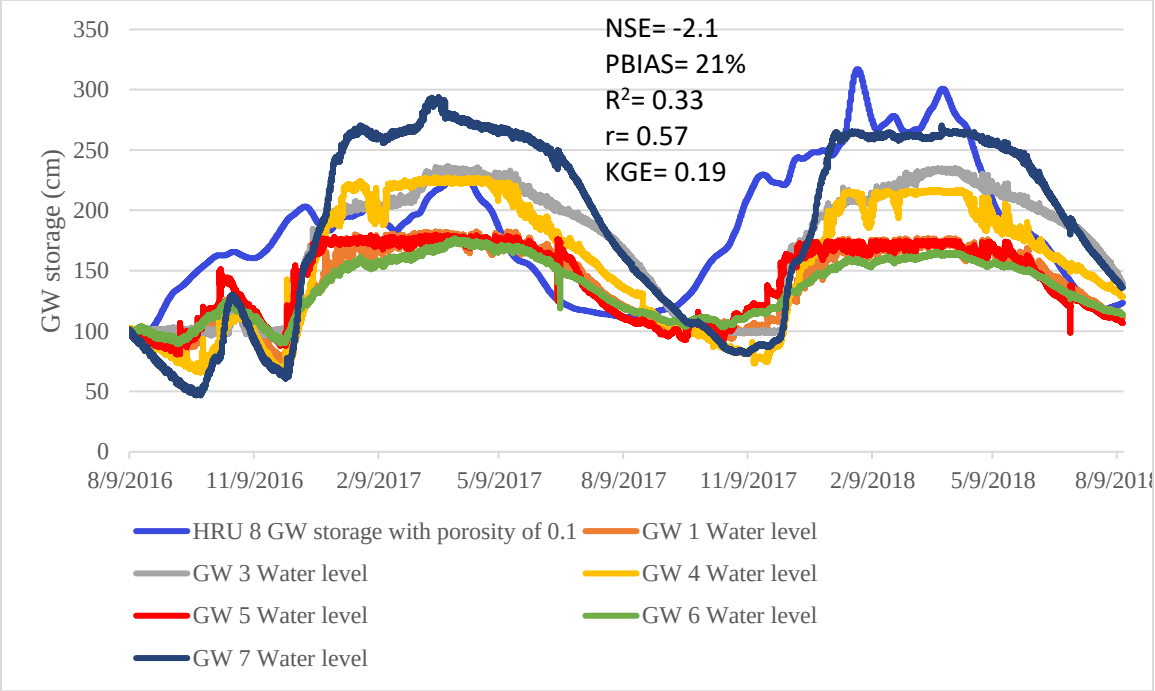


*Figure 16- Comparison of 6 water level data loggers (locations in Figure 15) to the CRHM simulated storage value for the same region (adjusted based on a porosity of 0.1).*

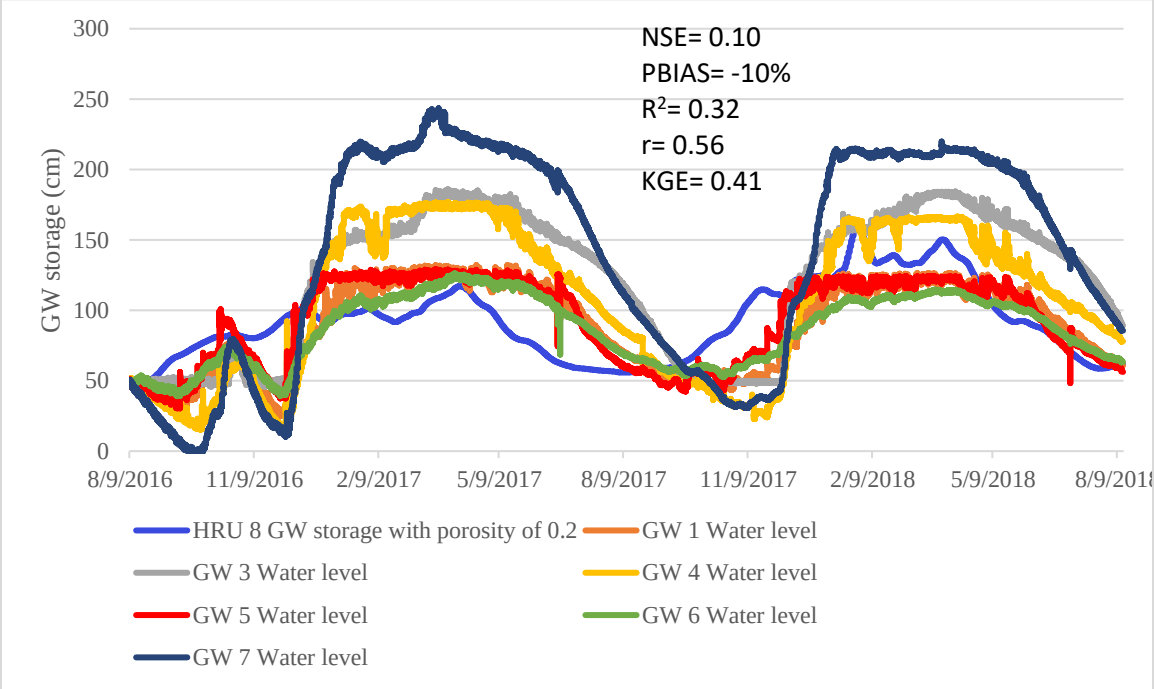


*Figure 17- Comparison of 5 water level data loggers to CRHM storage value (adjusted based on a porosity of 0.2).*

The effect of porosity on the amplitude between dry and wet season water levels can be seen in Figure 16 and 17. The average Pearson product-moment correlation coefficient is highest with a porosity of 0.1 (r=0.57), followed closely by a porosity of 0.2 (r=0.56).

From the above figures, the timing of the peaks (wet season) and troughs (dry season) indicate that the model may have a groundwater storage value that is too small. This was initially run with a groundwater storage value of 10 days. In the following Section, the model is run with a groundwater storage value set to 60 days. If greater than 60 days, the groundwater flow becomes unrealistically dampened compared with the groundwater data accessible.

#### 5.2.2.1 Groundwater storage changed to 60 days

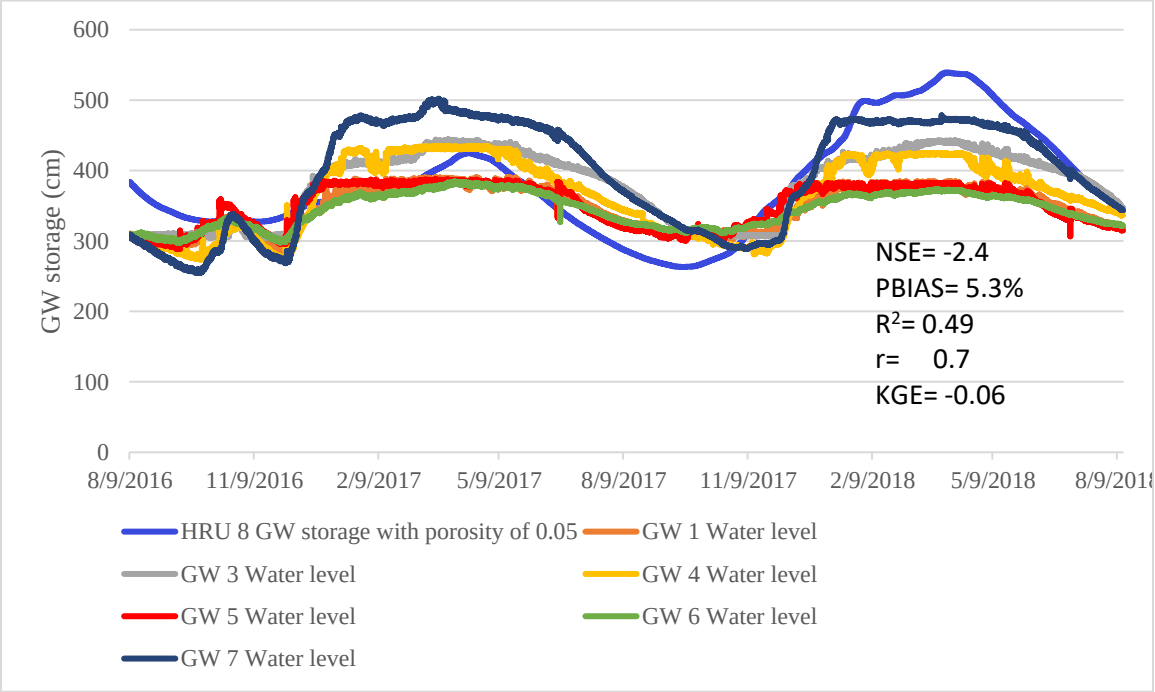


*Figure 18- Comparison of 6 water level data loggers to CRHM storage value (adjusted based on a porosity of 0.05, and GW storage of 60 days). Water level data loggers are initially anchored to 75 cm below initial CRHM storage value for ease of comparison.*

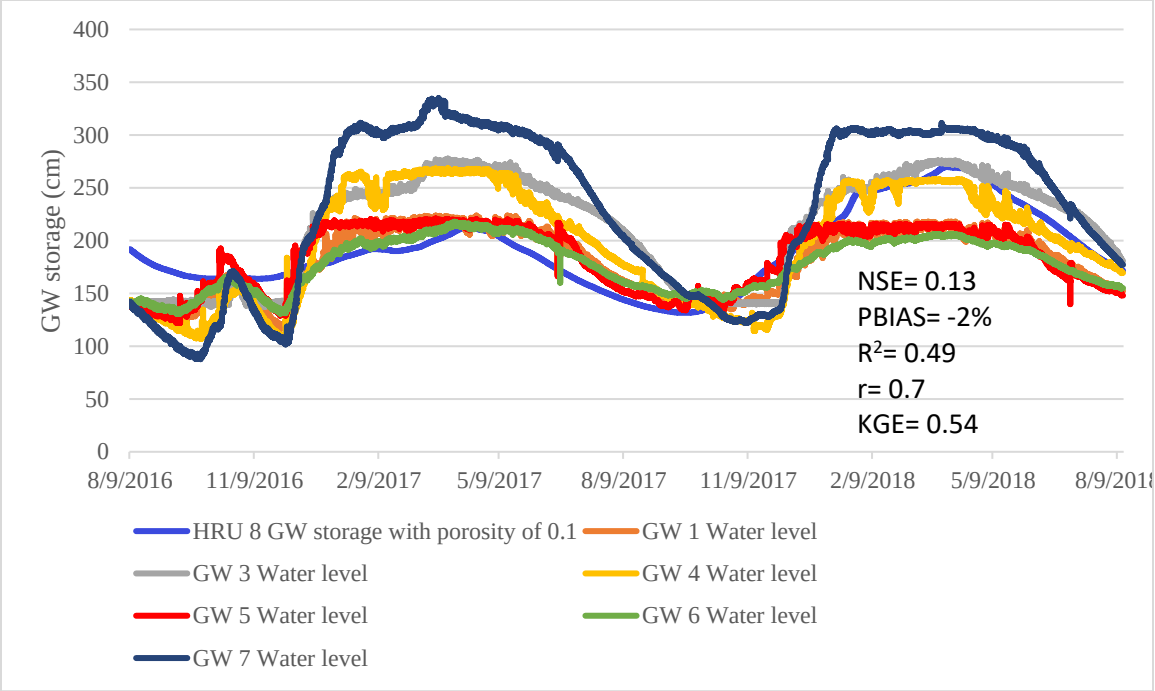


*Figure 19- Comparison of 6 water level data loggers to CRHM storage value (adjusted based on a porosity of 0.1, and GW storage of 60 days). Water level data loggers are initially anchored to 50 cm below initial CRHM storage value for ease of comparison.*

When the groundwater storage value was changed to 60 days, the timing correlation is greatly improved compared to the field data (Figures 18 and 19).

### 5.2.3 Groundwater recharge from soil storage

Findings from Wigmore (2016) for three proglacial valleys in the Cordillera Blanca indicate that evapotranspiration is the primary mechanism through which soil moisture is removed from the system (Mark et al. 2017). Compared with ET fluxes, the fluxes to deeper groundwater reservoirs from subsurface flow and percolation from soils are much smaller (Mark et al. 2017).

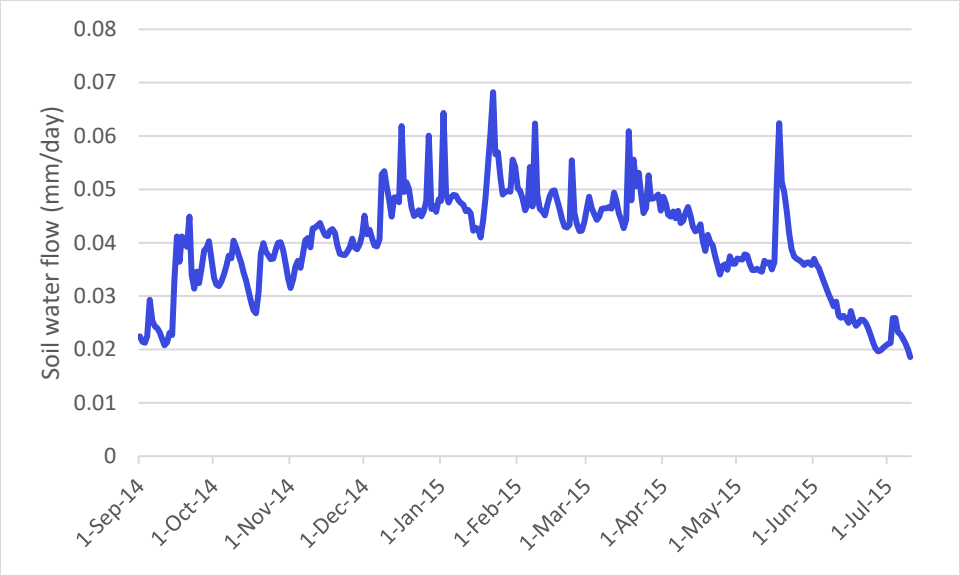


*Figure 20- The maximum amount of the soil water excess for HRU 8 that is routed directly to the associated groundwater reservoir each day.*

CRHM model output in Figure 20 for excess soil water routed to groundwater agrees with Mark et al. (2017); the daily subsurface flow to deeper groundwater reservoirs is two orders of magnitude smaller than evapotranspiration (Figure 26).

## 5.3 Glacial melt

### 5.3.1 Changes in glacier thickness

In the model, there are 5 glaciated HRUs. They were selected based on elevation and aspect. Of the delineated basin area of 67.34 $km^2$, 17.18 $km^2$ is glaciated (25.5% of basin). In the CRHM model the basin area was established on the upstream catchment area from the Casa de Agua station outflow point. Glacier meltwater is directed to the surface of the associated HRU, and then routed either into the associated HRU's subsurface or to the surface water of down slope HRUs.

The initial ice albedo for all HRUs was set to 0.3 and firn albedo was set to 0.5. The initial water equivalent of glacier ice (m w.e.) for all HRUs was set to 70 m, based on thickness estimates from Fyffe et. al. (2021). The actual thickness of glaciers in the basin is highly heterogeneous, but ice thickness for all glaciated HRUs was set to 70 m based on estimated averages across the HRU areas. The thickness of the glacier does not affect the glacial melt values in CRHM, as firn and ice melt are taken from the glacier surface. However, it does affect timing projections for complete deglaciation of the 5 glaciated HRUs.

The 5 glaciated HRUs have significantly different mass balances, driven primarily by their elevation and aspect (Table 1). HRU 6 is the lowest elevation glacier (mean elevation = 4893 m), while HRU 2 is the highest elevation glacier (mean elevation = 5495 m). As seen in Figure 21, HRU 6 glacier thickness decreases by ~25 m w.e. within 4 years, while HRU 2 gains about 1 m w.e. over a 4-year period.

To assess the performane of the glacial melt module, we compare to Fyffe et al. (2021) who applied a physically-based, energy balance melt model at five glacier sites within Peru, including Cuchillacocha Glacier in HRU 3 (Cuchillacocha Low Glacier from Table 1). Cuchillacocha Glacier lies above Lake Cuchillacocha and flanks the south side mount Pucaranra. (The glacier is referred to as both Pucaranra Glacier and Cuchillacocha Glacier in previous literature. Here, it will be referred to as Cuchillacocha Glacier as it lies above Lake Cuchillacocha and matches naming in Fyfee et al., 2021). Specifically, the lower part of Cuchillacocha Glacier (HRU 3) is analyzed, as this is the area modelled in Fyffe et al. (2021). The upper part of Cuchillacocha Glacier is represented by HRU 2 and has a much higher mean elevation than the area modelled by Fyffe et al. (2021). Fyffe et al. (2021) found that the surface height of Cuchillacocha Glacier decreased by ~9 m w.e. from July 2014 to July 2016 (Figure S 6 in summplementary resuls). Over the same time period, the CRHM results indicate a similar surface height decrease of 8.88 m w.e.

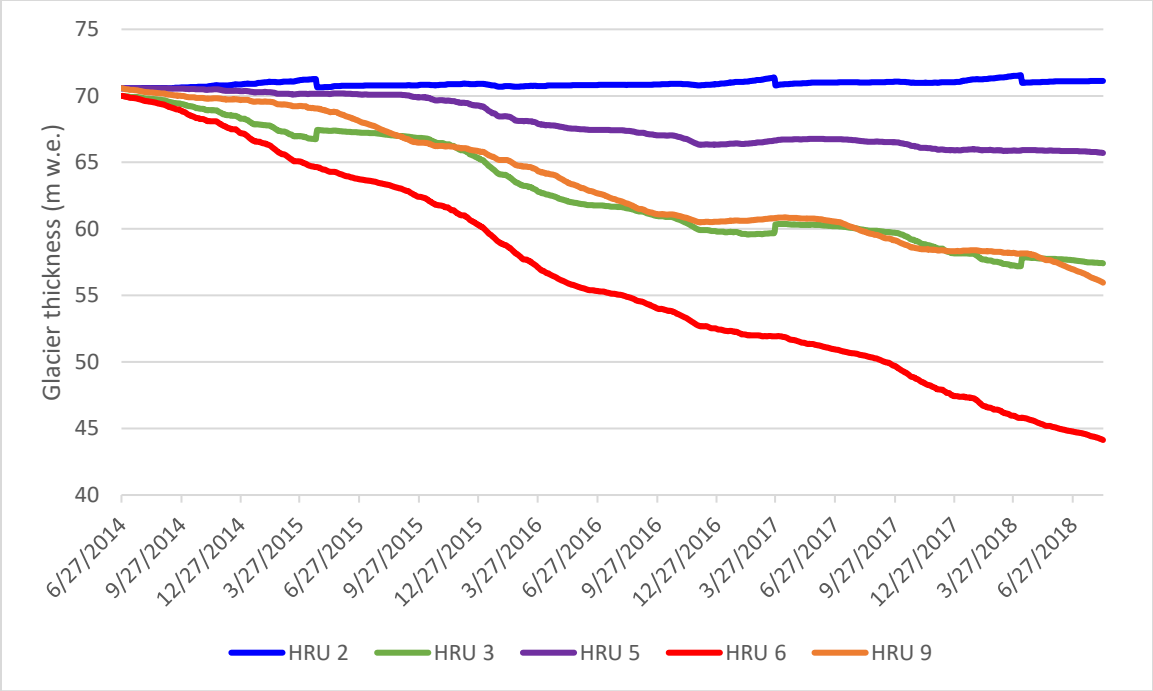


*Figure 21- Glacier thickness (m w.e.) of 5 HRUs. The green line represents the lower part of Cuchillacocha Glacier, which is the location modelled by Fyffe et al. 2021 (at the toe of this glacier). Note that the sudden decreases in HRU 2 (upper Cuchillacocha Glacier) thickness represent avalanching events, increasing the thickness of underlying HRU 3.*

### 5.3.2 Glacier ablation rates

The ablation rates for the five glaciated HRUs and the model results of Fyffe et al. (2021) are shown in Table 2. All ablation rates are higher than the model results of Fyffe et al. (2021), except for the lowest elevation glacier in HRU 6. The mean elevation of HRU 6 is 4893 m, while the elevation set by Fyffe et al. (2021) for their study site on Cuchillacocha Glacier was 4821 m. Fyffe et al. (2021) modelled the glacier melt rate based on a point source measurement near the toe of Cuchillacocha Glacier, whereas this study modelled the glacier ablation rates based on the mean elevation for each HRU. The ablation rates calculated in this study included periods of glacier growth, whereas the melt rate calculated by Fyffe et al. (2021) appears to only consider ablation. (This difference is likely because the Fyffe et al. (2021) study site is near the toe of the glacier and far below the Equilibrium-Line Altitude). The ablation rates calculated in this study are synonomous with mass balance rates; melt rates are only reported when considering only glacier mass loss. The mean elevation for HRU 3 (Cuchillacocha low glacier) is 5021 m. Therefore, the CRHM ablation rates appear comparable to the melt rate indicated by Fyffe et al. (2021), relative to their average elevation. The basin-wide glacier ablation rate normalized for various

HRU areas is -2.51 m w.e. $yr^{-1}$. Although this value appears high, the observable changes to the low elevation glaciers has been dramatic over the past decade (Figures 22 and 23). These findings support the conclusion that the valleys predicted to undergo the most significant changes over the next century are those with high glacier coverage at or below 5,400 m a.s.l. (Rabatel et al., 2013).

*Table 2- Average ablation rates for 2014 to 2018 (mm w.e. $h^{-1}$ and m w.e. $yr^{-1}$) for 5 glaciated HRUs and Fyffe et al (2021) model results. The Fyffe results are for a low elevation site in HRU 3. Note that a negative ablation rate means glacier growth. The mean elevation for the entire basin is normalized based on HRU areas.*

| **Glacier/ HRU #** | **Average ablation rates for 2014 to 2018 (mm w.e. $h^{-1}$)** | **Average ablation rates for 2014 to 2018 (m w.e. $yr^{-1}$)** | **Mean elevation (m a.s.l.)** |
|---|---|---|---|
| 2 | -0.096 | -0.842 | 5495 |
| 3 | 0.283 | 2.48 | 5021 |
| 5 | 0.09 | 0.79 | 5251 |
| 6 | 0.706 | 6.81 | 4893 |
| 9 | 0.368 | 3.219 | 5152 |
| Entire Basin Average | 0.287 | 2.51 | 5150 |
| Fyffe et al. (2021) | 0.616 | 5.396 | 4821 |

The glacier melt model results appear reasonable, although there is a great deal of inherent uncertainty when comparing model to model results. Fyffe et al. (2021) evaluated model performance by comparing modelled melt rates with stake measurements over a 2 week period. Their findings showed an ablation overestimation of the model of 0.05 m w.e. over the 2 week observation period. This equates to 1.3 m w.e. on an annual basis, ignoring seasonal variability. Therefore, it can be assumed that the average melt rate found by Fyffe et al. (2021) is 5.40 +/- 1.3 m w.e. $yr^{-1}$. In the tropical Andes, Rabatel et al. (2013) found that glaciers with a maximum elevation below 5400 m a.s.l. are estimated to be losing mass at a rate (-1.2 m w.e. $yr^{-1}$) double that of glaciers with an elevation above 5400 m a.s.l. The model results displayed here span a much wider range than these values, but the basin-wide mass balance is in line with the value calculated by Rabatel et al. (2013) for the tropical Andes.

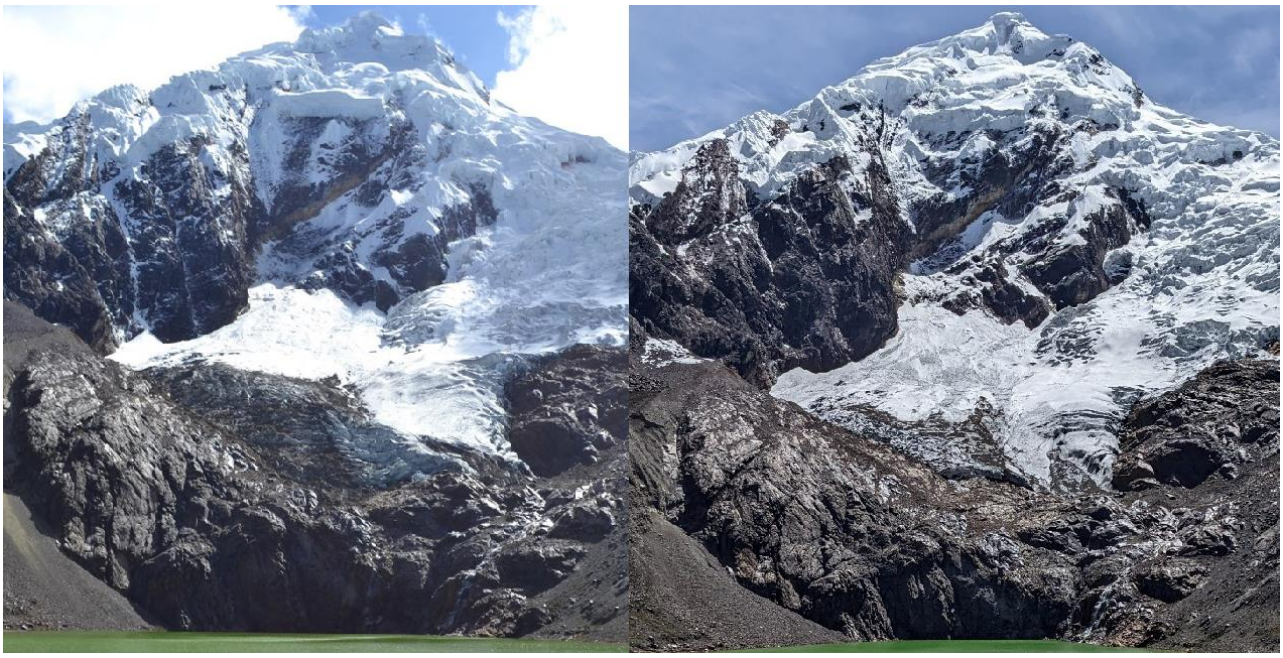

*Figure 22- Mount Pucaranra (June 2014 on left and May 2022 on right) with Lake Cuchillacocha in foreground. The upper section of this glacier is represented by HRU 2 and the lower section by HRU 3. Photos taken by Jeffrey McKenzie (left) and Gavin McNamara (right).*

*Figure 23- Mount Tullparaju (2012 on left and 2022 on right) with Lake Tullparaju in foreground. The upper section of glacier is represented by HRU 5 and 9, while the lower section is represented by HRU 6. Photos by Jeffrey McKenzie.*

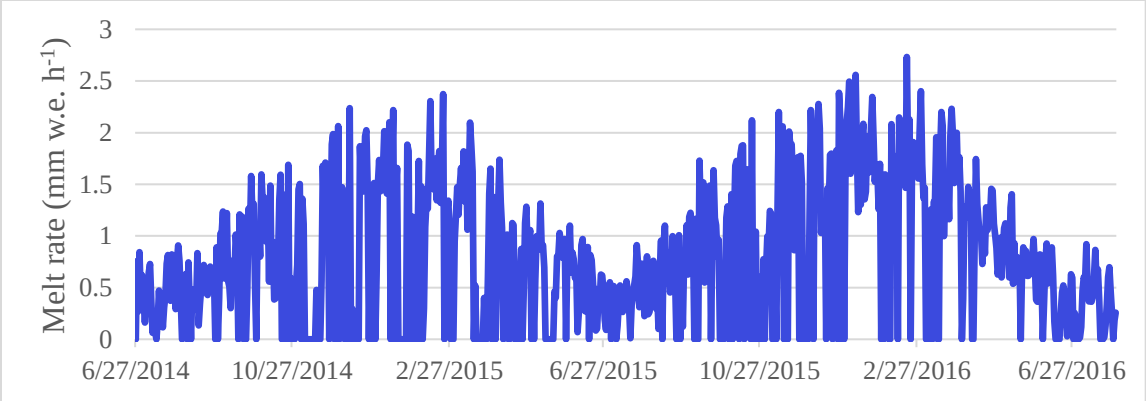


*Figure 24- Melt rate for glaciated HRU 6 displaying the seasonal variation of glacier melt. The melt rate is about twice as high in the peak of the wet season versus the low in the dry season. This pattern is unfortunate for water resources purposes and the buffering effect of glacier melt during the dry season.*

Figure 24 displays the CRHM simulated melt rate for the lowest elevation glacier, HRU 6. Unlike higher latitudes, the energy available for melt is greater in the wet season than the dry season (Kaser, 1999). The results illustrate the compensatory impact of energy loss through increased longwave radiation and latent heat flux (lower relative humidity) offsetting the greater net shortwave radiation in the dry season (Fyffe et al., 2021). The results from CRHM confirm the same glacier melt rate patterns for 4 out of the 5 glaciated HRUs. However, for the low elevation glaciers, the annual melt rates and ablation rates (mass balances) are very similar.

*Table 3-Melt rate seasonality*

| **Glacier/ HRU #** | **Dry season melt rate as a percentage of wet season melt rate (%)** |
|---|---|
| 2 | 32.5 |
| 3 | 27.5 |
| 5 | 47.6 |
| 6 | 70.4 |
| 9 | 295.0 |
| Entire Basin | 90.4 |

The basin-wide average dry-season glacier melt rate is 2.44 m w.e. $yr^{-1}$ for 2014 to 2018, while the wet season melt rate is 2.66 m w.e. $yr^{-1}$ for the same period. The glacier melt rate during

the dry season is 90% of the melt rate during the wet season (Table 3), and the wet season rate is higher as expected (Kaser, 1999). Both the growth rates (Figure 25) and melt rates are higher in the wet season. The melt rates are much higher than the growth rates in the wet season for all HRUs except HRU 2. This glacier grows more in the wet season than it melts, as it has the highest mean elevation (5495 m).

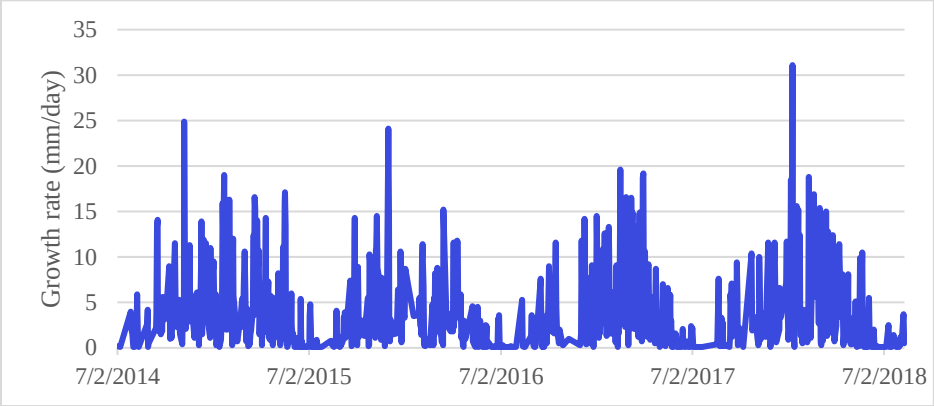


*Figure 25- HRU 2 growth rate. This is the only HRU that advances in the wet season. This is due to its higher growth rates than melt rates.*

The only glacier that does not follow the pattern of higher melt rates in the wet season is HRU 9. A possible explanation for this discrepancy is the different aspect of HRU 9, as it is the only northwest facing glacier. This aspect results in more solar radiation, including a greater flux in the dry season for north facing slopes. A CRHM function corrects shortwave radiation based on slope, and as such the model output supports this theory.

### 5.3.3 Glacier contribution to streamflow

Despite much higher glacier ablation rates in the wet season, the relative glacier contribution to streamflow is much higher in the dry season (Table 4).

*Table 4- Seasonal glacier melt water contribution to groundwater and streamflow.*

| **2017 Dry Season (May 1st to September 30th)** | | |
|---|---|---|
| Glacier contribution to streamflow (%) | Glacier contribution to groundwater flow (%) | Glacier contribution to total outflow (%) |
| 60.0 | 36.6 | 51.9 |
| **2017/18 Wet Season (October 1st to April 30th)** | | |
| Glacier contribution to streamflow (%) | Glacier contribution to groundwater flow (%) | Glacier contribution to total outflow (%) |
| 30.8 | 37.3 | 32.8 |

## 5.4 Evapotranspiration

Evapotranspiration (ET) in Quilcayhuanca Valley is significant, comprising 20% of total hydrological outflows. This is equivalent to 41.6% of the total observed discharge and 31% of precipitation (August 4, 2016, to August 12, 2018). On an annual basis, the total volume of evapotranspiration is $1.6 \times 10^7$ $m^3$.

The daily average evapotranspiration rate for three years (August 4, 2015, to August 8, 2018) is 1.18 mm $d^{-1}$ for HRU 8 (valley bottom). In nearby Llanganuco Valley, Hellstrom et al. (2006) reported a dry season ET of 0.03 mm $d^{-1}$ and a wet season ET of 2.63 mm $d^{-1}$, resulting in an average evapotranspiration rate of 1.33 mm $d^{-1}$. Hellstrom et al. (2006) modelled ET rates using the BROOK90 (v.4.4e) model with meteorological data from June 17 to July 11, 2005, and December 7 to December 31, 2005. CRHM model results for dry and wet season (1.14 mm $d^{-1}$ and 1.20 mm $d^{-1}$, respectively) showed less seasonal variability than those measured by Hellstrom et al. (2006). There are a few potential reasons for this discrepancy. In the CRHM model there could be an overcalculation of the amount of soil moisture available in the dry season (allowing actual ET to be closer to potential ET). It could also be due to the 24-day period Hellstrom et al. (2006) used to extrapolate for the dry and wet seasons or a hydrological difference between the two valleys. On an annual basis, the CRHM model results of ET being 31% of precipitation is slightly lower than estimates of 33% in the dry season and 37% in the wet season from Hellstrom et al. (2006).

Evapotranspiration values calculated by Wigmore (2016) are generally 2 to 3 mm $d^{-1}$, and have similar seasonal variation to CHRM results (Figure 26, 27). This is unsurprising as Wigmore (2016) and the CRHM evaporation module calculate ET using the Penman-Monteith Hourly Interval approach (Allen et al., 1998; Monteith, 1965). Also, Wigmore (2016) calculated ET rates in the Quilcayhuanca Valley at Casa de Agua weather station using the same meteorological data as the input for the CRHM model.

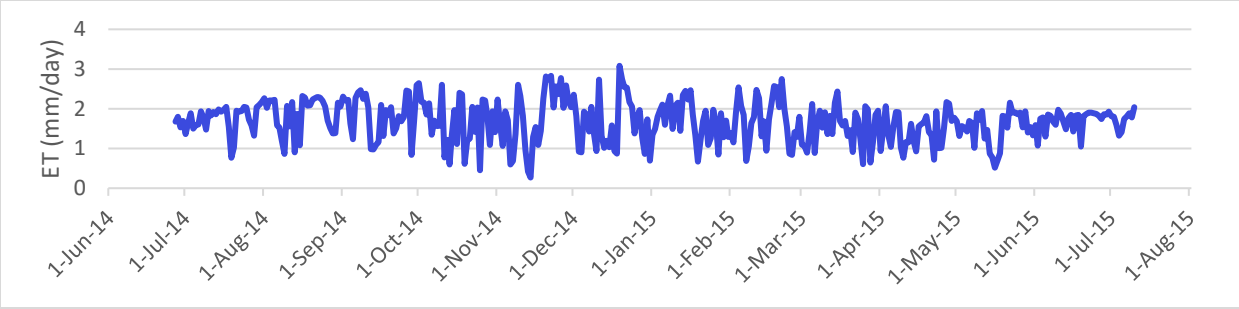


*Figure 26- CRHM output for HRU 8 (valley bottom) evapotranspiration. CRHM module evap_Resist calculates ET using hourly values for snowcover free period. Data presented here is aggregated from hourly data for comparative display.*

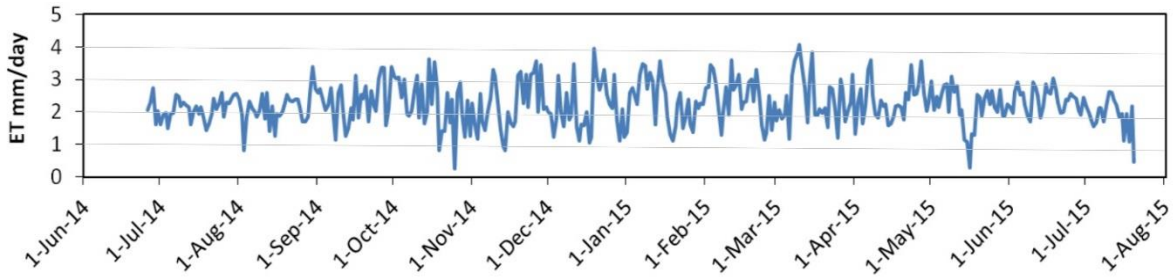


*Figure 27- Modified figure from Wigmore (2016) based on 2014 meteorological data. Calculated evapotranspiration rates at Casa De Agua, Quilcayhuanca Valley.*

## 5.5 Water Balance

A water balance for the entire basin is used to test if total hydrological inputs equaled outputs:

$$Inflows = Outflows \; - \; \Delta S \tag{18}$$

$$\Delta S = \; PPT \; + \; Glacier\; melt \; - \; ET \; - \; Glacier\; gain \; - Q_{SW} - Q_{GW} \tag{19}$$

$$\Delta S = \; -9{,}243{,}695\; m^3\; yr^{-1}\; (-3.6\%) \tag{20}$$

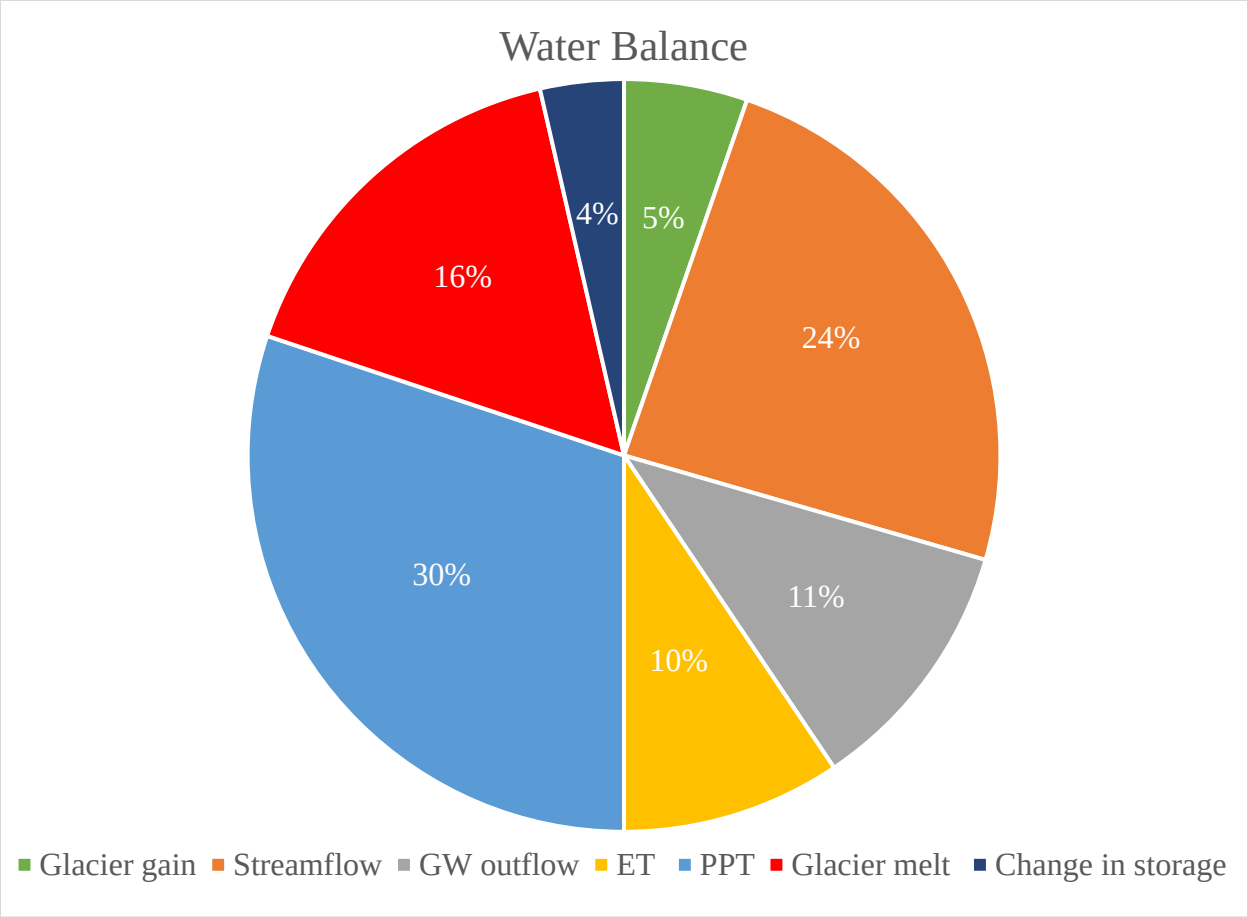


*Figure 28- Water balance component percentages for August 4, 2016, to August 12, 2018, including change in storage. The change in storage may reflect a water storage deficit and/or errors in the model setup and input data.*

The simulation results show that the hydrological inflows from August 2016 to August 2018 equal 46.4% of the total water balance (inflows are 92.8% of outflows). The results show that there is a 3.6% net negative change in storage (Equations 18, 19 and 20). The water balance calculation used the area of each HRU (to normalize values), and associated values calculated by CRHM for evapotranspiration, precipitation, and glacier gain/loss. Groundwater outflow and streamflow are all directed through HRU 8 as the final catchment outflow. The water balance estimation suggests two potentially overlapping factors; the Quilcayhuanca basin is in a water storage deficit over the period of simulation and/or there are errors in the model routing, setup, parameterization, and/or meteorological observations. There is potential for multiple sources of error, and likely a combination led to this small imbalance in water storage. However, the total water balance for the basin is satisfactory.

The water balance demonstrates the importance of groundwater, as 22% of the total outflows are through groundwater. However, the fate of groundwater that outflows from the study catchment beyond Casa de Agua is evaluated. Many studies have addressed groundwater flow pathways and interaction with surface water upstream of Casa de Agua, but groundwater flow pathways between Casa de Agua and the Santa River are relatively unknown (e.g., Chavez, 2013; Baraer et al., 2015; Gordon et al., 2015; Maharaj, 2011; Glas et al., 2018; Somers et al., 2019). Deep fracture flow and mountain system recharge are potential regional groundwater pathways contributing to streamflow beyond the catchment, and these flows may be emerging much further down valley (Somers et al., 2020). Mountain system recharge (MSR) describes the process of mountain-derived groundwater feeding a basin aquifer through the transition zone between mountains and the valley floor (Somers et al., 2020; Wahi et al., 2008). Welch and Allen (2014) employed numerical groundwater models within a defined watershed to investigate groundwater flow pathways and found that 12-15% of total basin recharge became deep mountain system recharge and discharged to higher order streams.

Another noteworthy result of the water balance is the glacier component (Figure 28). On an annual basis, 5% of the total hydrological inputs is glacier mass gain. The difference in glacier gain (5%) from glacier loss (16%) is 11%, a non-renewable loss of “fossil” ice. Thus 11% of the total annual inflows and outflows is from a permanent change in storage. This glacial ice loss is a finite resource and its contribution to the water balance will decrease, assuming glacial peak water has already passed (Baraer et al., 2012). In response, the quantity of groundwater and surface water outflows will decrease.

## 5.6 Parameter sensitivity analysis

To understand the sensitivity and robustness of the CRHM results, a sensitivity analysis of key parameters is used to evaluate the model outcomes. While there are hundreds of parameters in the CRHM structure that have some influence on the hydrology of the basin, based on thousands of model runs the sensitivity analysis focuses on lapse rates, routing structure, and albedo.

### 5.6.1 Lapse rates

Lapse rates are a major source of uncertainty in hydrological modelling. In the Cordillera Blanca, like all high-mountain regions, there is significant spatiotemporal variability in lapse rates

(Hellstrom et al., 2017). Near surface lapse rates are steeper during the dry season compared with the wet season and are steeper at higher altitudes (Hellstrom et al. 2017). Temperature variation with elevation is a complex, dynamic, and spatiotemporally dependent parameter that is often input as a single value for hydrological models (e.g., van Tiel, Stahl et al., 2020). Factors such as aspect, katabatic winds, and insolation can have dramatic effects on local lapse rates (Schauwecker et al., 2017).

Model simulations are run for three lapse rates: -0.44 °C/100 m, -0.64 °C/100 m, and -1.32 °C/100 m, based on literature values. The lapse rate of -0.44 °C/100 m is calculated based on the temperature difference of the two observed weather stations 718 m apart (Casa de Agua, 3924 m, and Cuchillacocha, 4642 m). The lapse rate of -0.64 °C/100 m is selected based on a more thorough lapse rate analysis by Hellstom et al. (2010) in nearby Llanganuco Valley. This rate is similar to the lapse rate of -0.65 °C/100 m assumed by Schauwecker et al. (2017) for the Cordillera Blanca. The lapse rate of -0.64 °C/100 m is used for all other model results in this study. The lapse rate was kept constant throughout the year, as no definitive variation was seen in the Llanganuco Valley (Hellstrom et al., 2010). The lapse rate of -1.32 °C/100 m is selected based on comparisons to a study of the Cuchillacocha Glacier in 2014 (Aubry-Wake et al., 2015). This lapse rate is calculated by comparing 2 weeks of temperature data collected on Cuchillacocha Glacier with the observation station at Cuchillacocha lake. The steeper (greater) lapse rate based on these two weeks of data agrees with findings from Hellstrom et al. (2017) indicating higher lapse rates at higher altitudes.

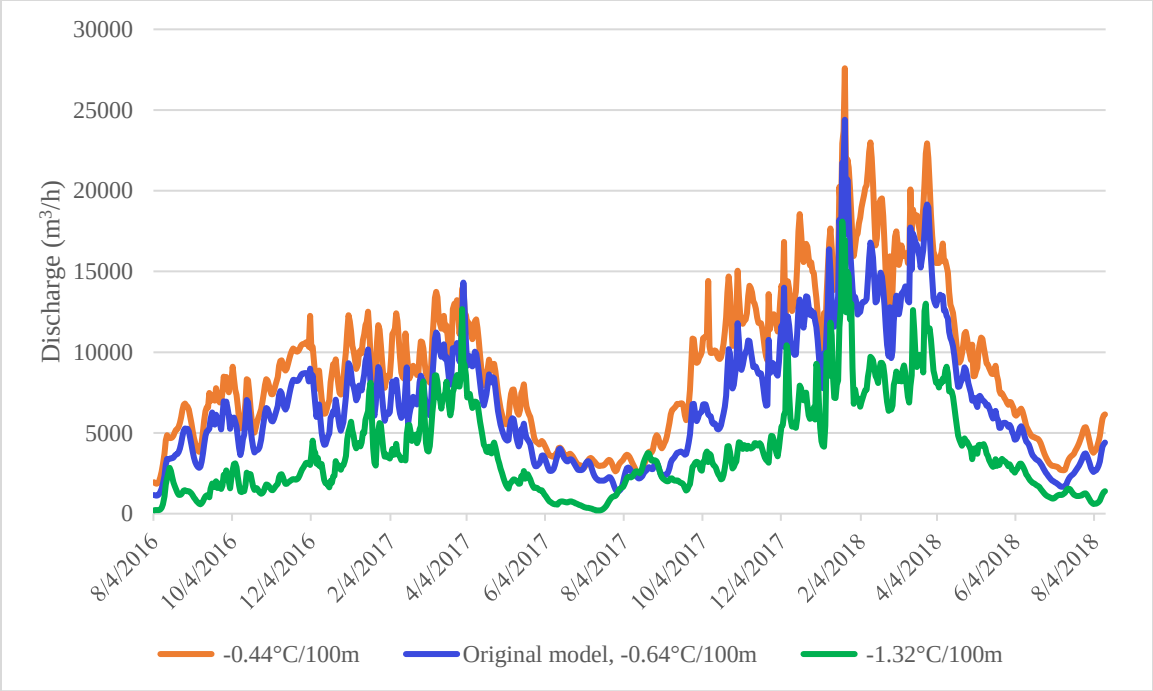


*Figure 29- Effect of various lapse rates on streamflow. Steeper lapse rates lead to more precipitation falling as snow, and an increase in glacier growth.*

Figure 29 displays the significant effect lapse rate estimations have on streamflow calculations. A lapse rate of -0.44 °C/100 m results in a 30% increase in streamflow compared to a lapse rate of -0.64 °C/100 m. A lapse rate of -1.32 °C/100 m results in a 45% reduction in streamflow compared to a lapse rate of -0.64 °C/100 m. Shallow lapse rates lead to faster glacier ablation rates and more precipitation falling as rain versus snow. The steepest lapse rate, -1.32 °C/100 m, leads to high elevation glacier growth with 4 out of 5 glaciated HRUs having glacier growth.

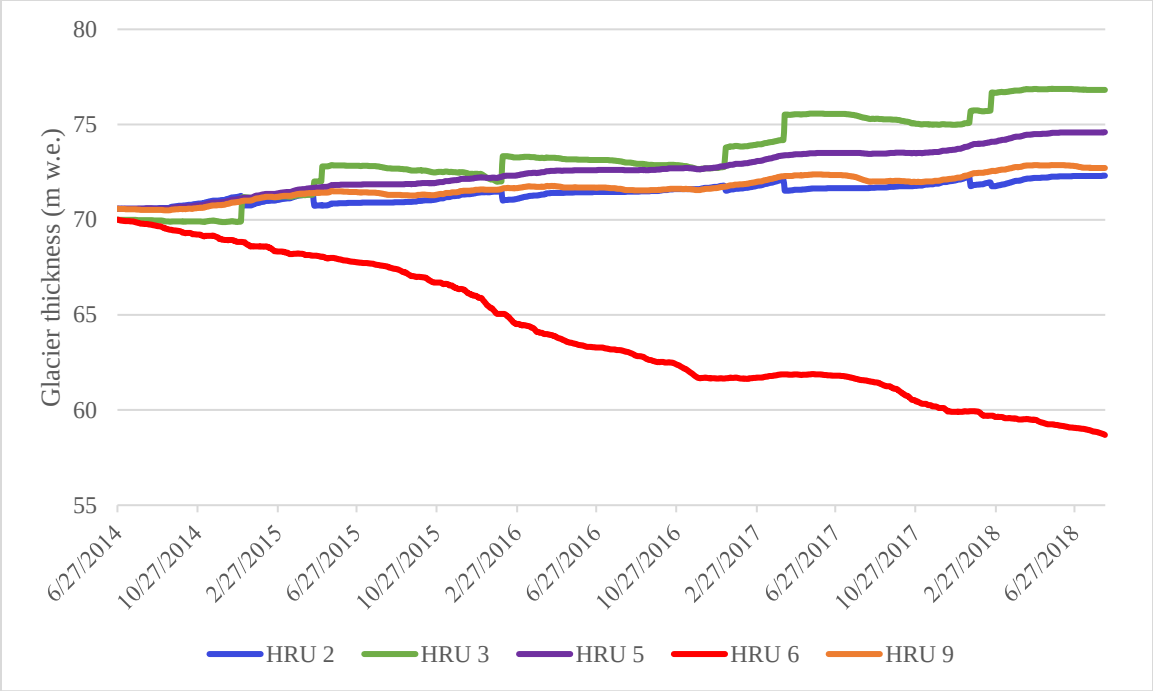


*Figure 30- Effect of -1.32 °C/100m lapse rate on glacier mass balance. Four out of five glaciers are growing with this steep lapse rate, versus four out of five retreating with the selected -0.64 °C/100m lapse rate.*

Interestingly, HRU 3 grows fastest despite not being the highest elevation HRU. This is likely due to an unrealistic amount of snow redistribution via avalanching from the higher, steeper, glacier (HRU 2). Each rapid step up in glacier thickness seen in Figure 30 correlates to an outgoing snow slide transport event from overlying HRU 2. Lapse rates are critical to glacio-hydrological modelling, and thus further research should be made in this area (Hellstrom et al., 2017).

### 5.6.2 Routing

The flow pathways of all surface and subsurface water are a major uncertainty in hydrological modelling. In this study, the flow pathways conceptualized by previous studies was critical to having a semi-realistic routing network (e.g., Chavez, 2013; Baraer et al., 2015; Gordon et al., 2015; Maharaj, 2011; Glas et al., 2018; Somers et al., 2019). Manual calibration for various subsurface parameters that were not explicit in previous literature were also required to match hydrograph flashiness and quantity of streamflow (See Tables A1 and A2 in Appendix). To test the effect of routing on model sensitivity, two extreme scenarios are compared; all groundwater must discharge to the land surface and no groundwater is discharged to the land surface.

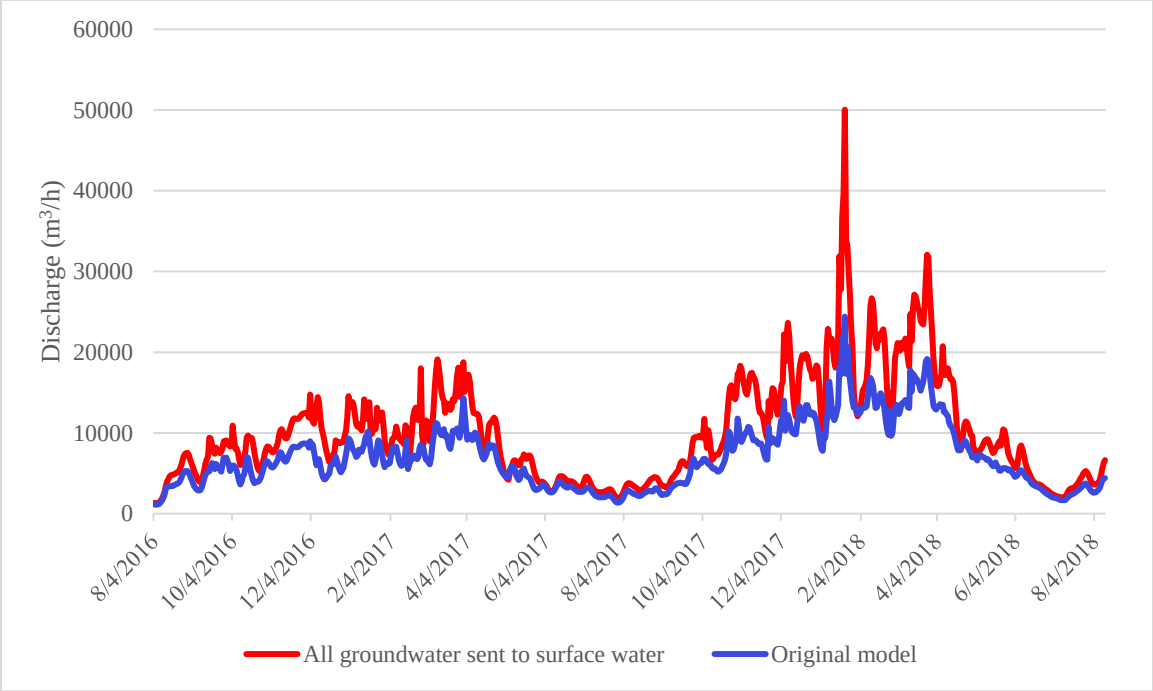


*Figure 31- Effect of subsurface parameterization on basin streamflow. No groundwater transfers between HRUs. All HRU groundwater is sent to down slope HRU surface water, and basin outlet groundwater stores are sent to surface outflow point.*

Figure 31 displays the effect of unrealistic routing of all groundwater being routed to the surface of adjacent down slope HRUs and to the surface at the basin outflow point. This assumes that there is no groundwater transfer between HRUs and all water exiting the basin is via surface water at Casa de Agua. The result of this extreme surface water routing scenario is an overestimation of streamflow. This model setup results in 155% of the total observed discharge for August 4, 2016, to August 12, 2018.

At the other extreme, if all groundwater is continually transferred to adjacent down slope HRUs' groundwater storage, there is an underestimation of streamflow. In this scenario (Figure 32), with no springs for groundwater discharge to the land surface, there is a 29% underestimation of streamflow and 18% more groundwater exiting the basin than surface water.

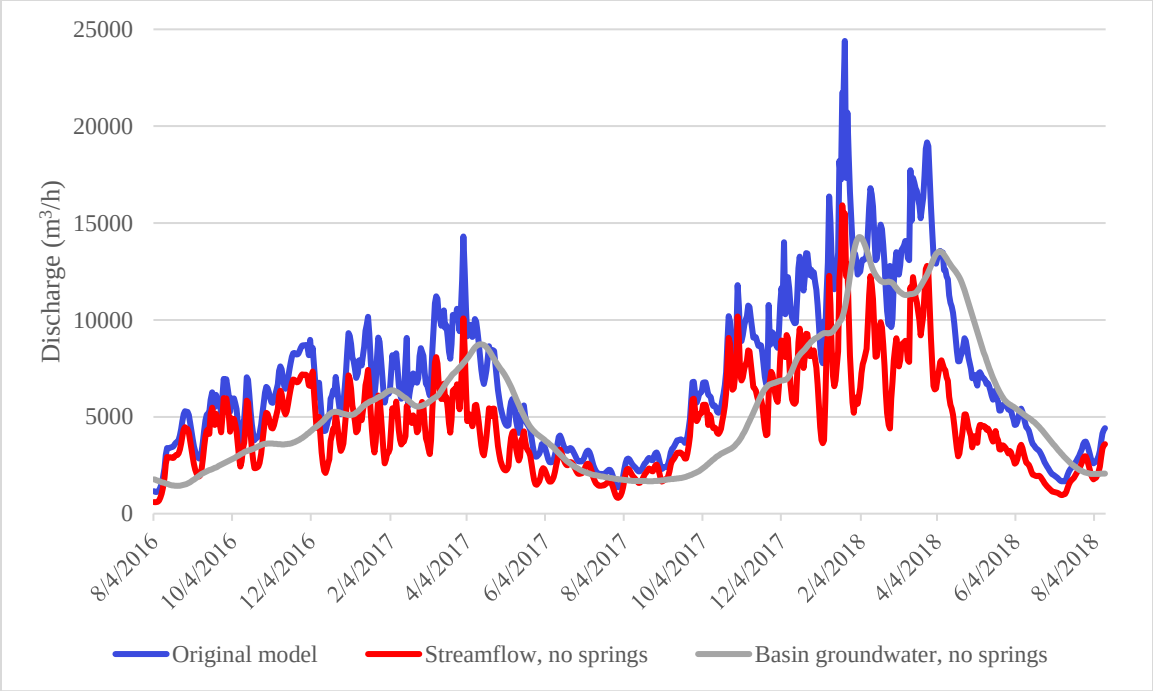


*Figure 32- Effect of subsurface routing on streamflow and groundwater flow. No groundwater exfiltration to land surface.*

### 5.6.3 Albedo

Ice albedo has a significant effect on glacier ablation rates and the resulting basin streamflow. Ice albedo can vary significantly based on age of ice, ashfall from nearby forest fires, etc. (Aubry-Wake et al., 2022a). In the Canadian Rockies, on-ice albedo dropped from a high of 0.29 in 2015 to a low of 0.16 in 2018 following extensive forest fires and subsequent ashfall deposition (Aubry-Wake et al., 2022a). The ablation rates increased by slightly over 10% in years after these fires, but without smoke. The resulting soot deposition had persistent effects on lowering the albedo in 2019 and 2020 (Aubry-Wake et al., 2022a).

In this section, the effects of varying ice albedo on the model results of 2016 to 2018 streamflow and 2014 to 2018 glacier ablation rates were analyzed. The original model, on which the results are based, had an ice albedo set to 0.3. In this section, an ice albedo of 0.2 and 0.4 are used for comparison.

#### 5.6.3.1 Effect of albedo on streamflow

With all glaciated HRUs ice albedo set to 0.2, the total streamflow ($m^3$) for 2016 to 2018 is 10% greater than the model with ice albedo set to 0.3. Net shortwave radiation increases with a decrease in albedo. Based on CRHM output for HRU 3, a decrease in albedo from 0.4 to 0.2 will

result in a 31% net increase in all-wave radiation. The *Netall* module in CRHM simulates net all-wave radiation from the calculated short-wave and long-wave radiation using the Brunt Equation (Granger and Gray, 1990). The subsequent increase in radiation from a decrease in albedo results in significant changes to glacier melt and thus streamflow. As displayed in Figure 33, a change in ice albedo from 0.4 to 0.2 results in a 21% increase in streamflow.

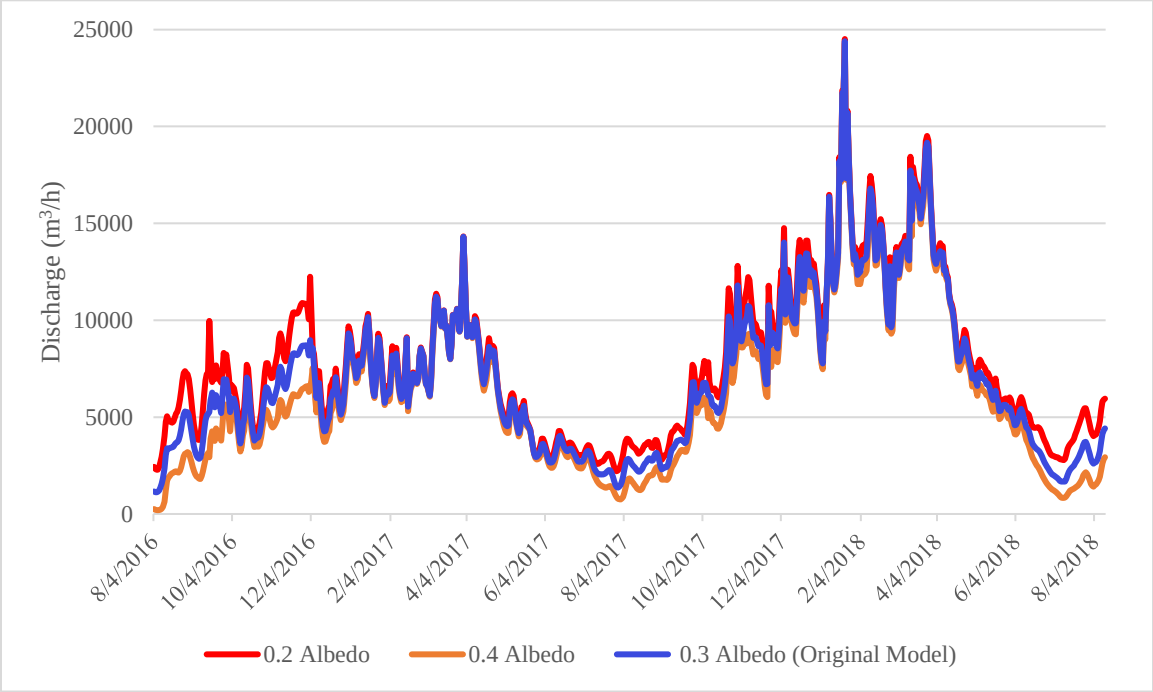


*Figure 33- Effect of ice albedo on streamflow.*

### 5.6.3.2 Effect of albedo on glacier melt

The effect of ice albedo on glacier melt is most pronounced for the lower elevation glaciers. For the lowest elevation glacier (HRU 6, mean elevation = 4893 m), the difference in glacier thickness is 4.47 m w.e. over 4 years for a glacier with ice albedo of 0.2 versus 0.3 (Figure 34). For HRU 6, this results in 18,112,879 $m^3$ w.e. over 4 years. For the largest glaciated HRU (HRU 5), the difference in glacier thickness is about 2.1 m w.e. over 4 years for a glacier with ice albedo set to 0.2 versus 0.4. For this HRU, the result is 15,702,102 $m^3$ w.e. over 4 years.

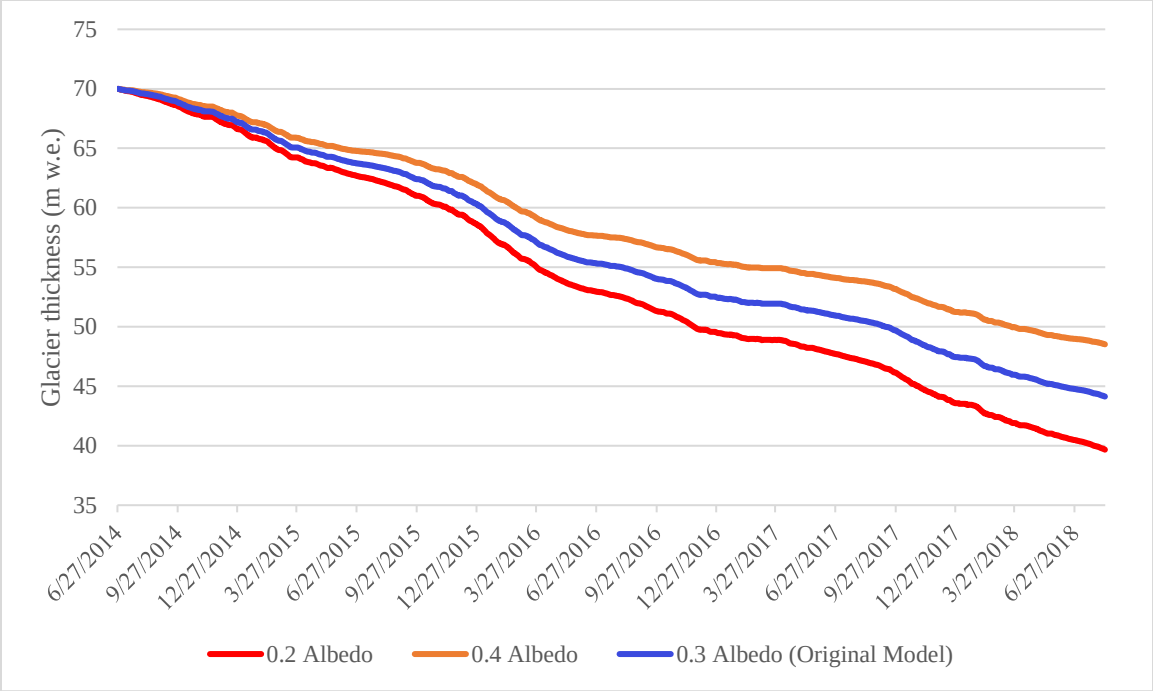


*Figure 34- Effect of ice albedo on ablation of HRU 6*

The basin-wide glacier mass balance changes from -2.5 m w.e. $yr^{-1}$ to -3.1 m w.e. $yr^{-1}$ when the ice albedo of all glaciers is decreased from 0.3 to 0.2.

## 5.7 Climate projections

The strength of the CRHM platform is the ability to modify the meteorological data based on future climate scenarios. Several climate projection simulations are run to illuminate and understand changes in dominant hydrological processes within the basin. In this section, combinations of deglaciation, temperature, and precipitation are analyzed to assess future shifts in hydrology. The date ranges are kept constant as the future projections are made by adjusting the original 2014 to 2018 meteorological data and to aid in comparison with the original model. Temperature or precipitation changes are simply added to or subtracted from each time interval within the four years of meteorological observation data.

### 5.7.1 Deglaciation

Complete deglaciation with no temperature or precipitation pattern changes is an unrealistic projection, but it highlights the importance of glaciers in the Quilcayhuanca basin.

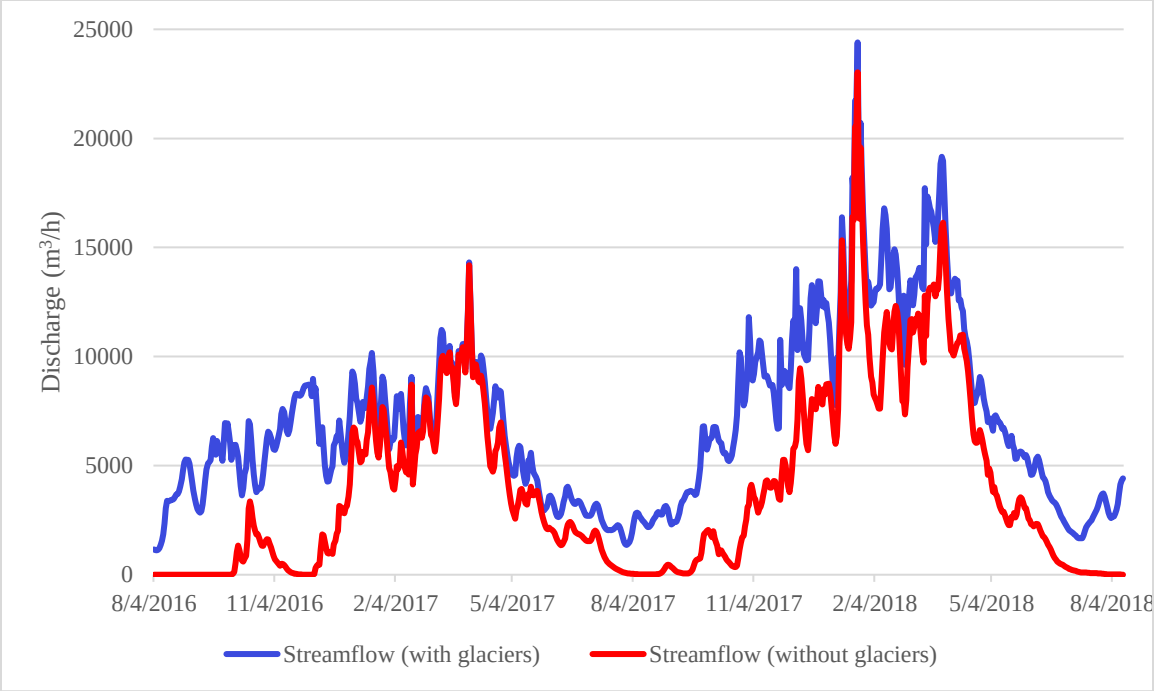


*Figure 35- Streamflow for current basin-wide glaciation and for complete deglaciation.*

In an unglaciated basin scenario, streamflow is reduced by 42% from August 4, 2016, to August 12, 2018 (Figure 35). The most notable change for this scenario is dry season flow, due to the complete loss of buffering capacity of glacier meltwater. With glaciers, the percentage of streamflow that is contributed by glacial meltwater is much higher in the dry season (60% dry season versus 31% wet season; Table 4).

In a deglaciated basin CRHM predicts a 60% streamflow decrease in the 2017 dry season. This prediction is comparable to findings from Baraer et al. (2012), where it was found that complete deglaciation results in dry season discharge decreases of over 60% for Paron and Llanganuco Valleys. The Quilcayhuanca Valley catchment is like Paron and Llanganuco Valleys with respect to glacier coverage and hydrological characteristics. Therefore, the 60% estimated decline in dry season streamflow is reasonable.

Groundwater flow is also heavily buffered by glacier melt in the dry season (Figure 36). There may be deep groundwater reservoirs and flow pathways that are not as affected by seasonal glacier melt, but the semi-shallow (~0.3m to 15m) groundwater reserves modelled in this study are partially recharged by glacier melt. With complete deglaciation, groundwater flow is reduced

by 43% between August 4, 2016, and August 12, 2018. In a deglaciated basin CRHM predicts a 52% loss of total outflow during the 2017 dry season.

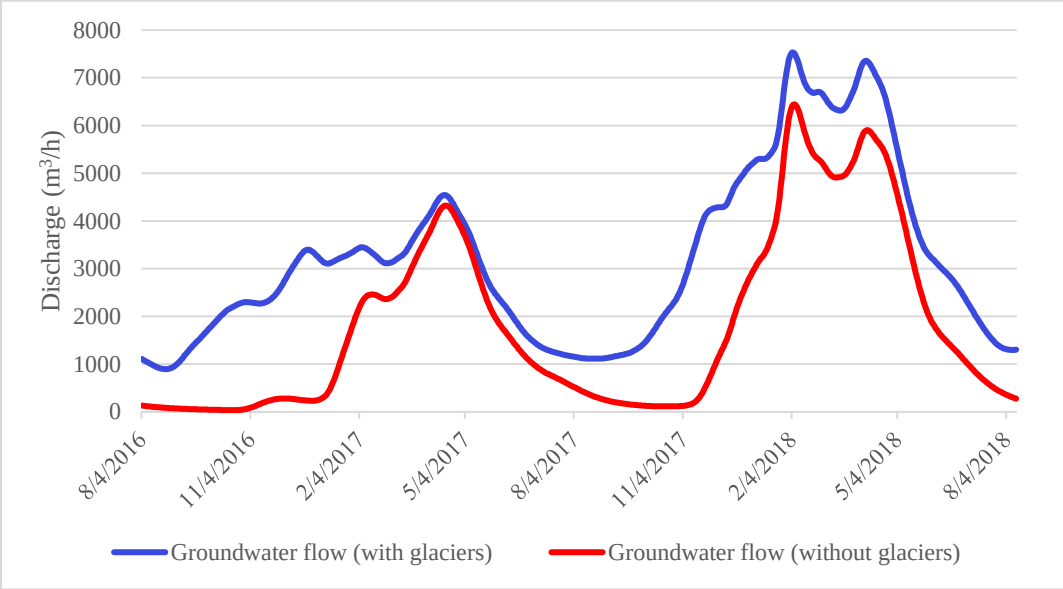


*Figure 36- Groundwater flow for current basin-wide glaciation and for complete deglaciation.*

The model simulation indicates a similar conclusion to the findings from Baraer et al. (2015); the degree of glaciation is inversely proportional to the groundwater contribution amount to basin outflow. However, this is only true in the dry season, as the groundwater percentage of total basin outflow is the same with and without glaciers. In the 2017 dry season, with glaciers, groundwater is 35% of total outflow, but with no glaciers it is 46% total outflow. These results are consistent with results from Somers et al. (2019), whereas glaciers recede, groundwater becomes a larger fraction of streamflow.

### 5.7.2 Temperature increase

A 2 °C or 4 °C warmer scenario with no deglaciation is also unrealistic but illuminates the effect temperature has on glacial ablation rates and contributions to streamflow. Results from Vuille et al. (2008) predict a 4.5 to 5 °C temperature increase for the region by the end of the 21$^{st}$ century under SRES A2 emission scenario. This is in line with findings from Solman (2013) that predict a 4 °C temperature increase over the Andean region by the end of the 21$^{st}$ century.

#### 5.7.2.1 Temperature increase effect on evapotranspiration

In a 4 °C warmer climate, evapotranspiration increases by 20%. This is equivalent to 50% of the total current observed discharge (August 4, 2016, to August 12, 2018).

#### 5.7.2.2 Temperature increase effect on streamflow

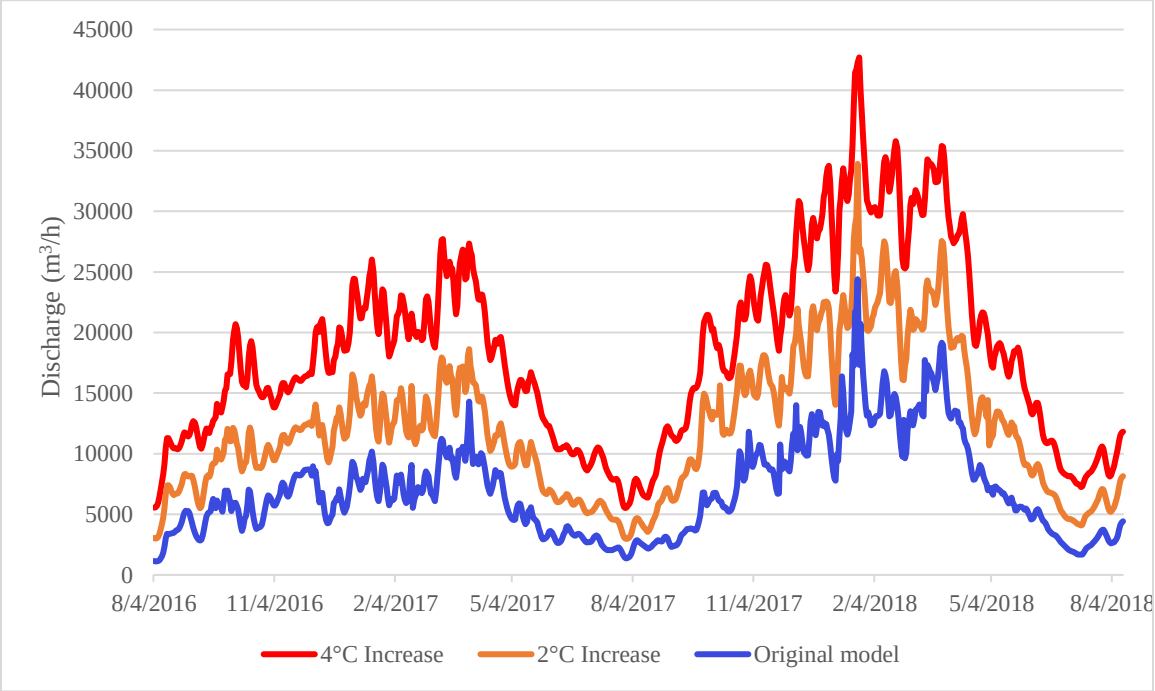


*Figure 37- Streamflow changes with current glaciation and increased temperatures.*

From 2016 to 2018, there is 173% more streamflow in a 2 °C warmer basin, and 263% more streamflow in a 4 °C warmer basin (Figure 37). This is due to the significant increase in glacial ablation rates for both scenarios. The lowest elevation glacier (HRU 6) almost disappears completely in a 4-year span in the 4 °C warmer scenario (Figure 39).

#### 5.7.2.3 Temperature increase effect on glacier melt

There is typically a paradox in basins with fast retreating glaciers; meltwater can become more abundant for a few decades as the increase in glacier ablation rates outpace the corresponding decrease in glacier size. However, many of the basins in the Cordillera Blanca have passed this "glacial peak water" and are now exhibiting consistent declining runoff (Baraer et al., 2012; Huss and Hock, 2018; Huss et al., 2017).

A note on the correlation between increasing glacial melt and streamflow: CRHM does not have explicitly areally retreating glaciers within a given HRU. Melt is taken from the surface of the glacier, until that glacier disappears. Realistically, the glacier is retreating and decreasing its areal coverage while having surface lowering and decreasing its meltwater output. Therefore, the glacial peak water concept is not captured in CRHM. CRHM likely overestimates the increase in

streamflow under these warmer climate scenarios. This compensatory effect is more accurately represented in Section 5.7.3 with smaller glaciers in conjunction with increased temperatures.

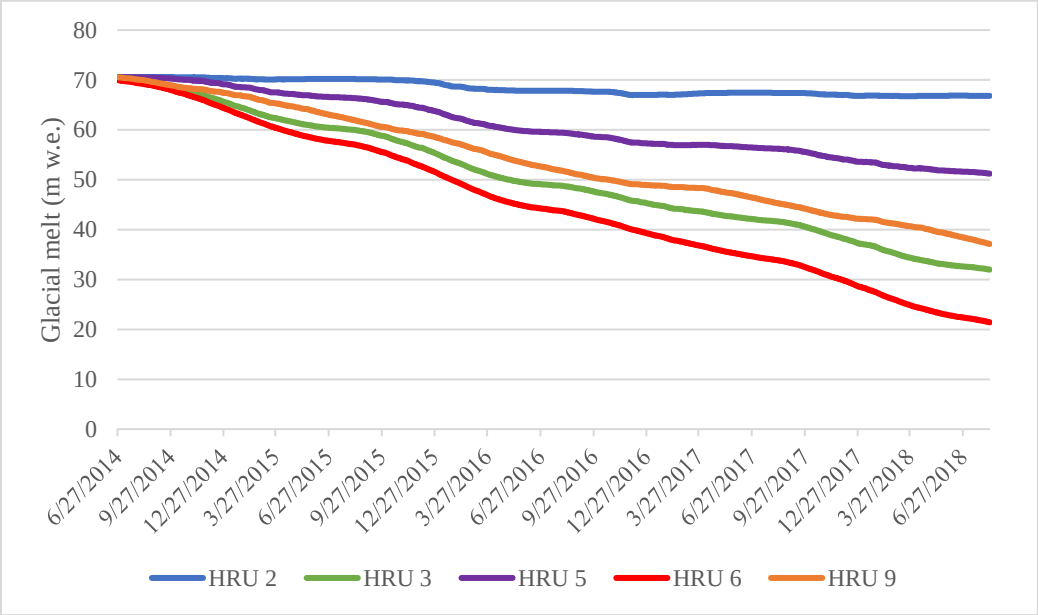


*Figure 38- Effect of a 2 °C temperature increase on glacier melt.*

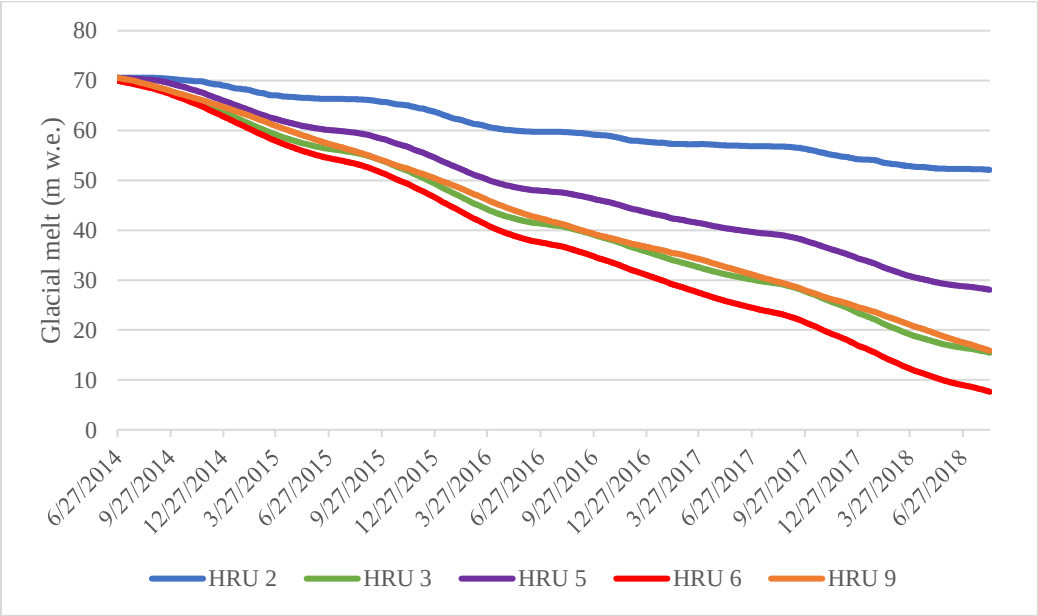


*Figure 39- Effect of a 4 °C temperature increase on glacier melt.*

The basin-wide mass balance is -7.03 m w.e. $yr^{-1}$ for a 2 °C temperature increase and -11.74 m w.e. $yr^{-1}$ for a 4 °C temperature increase. The difference in mass balance between the current actual temperature model and the 2 °C and 4 °C warmer scenarios is -4.52 m w.e. $yr^{-1}$and -9.23 m w.e. $yr^{-1}$, respectively. These differences are very close to the findings of Fyffe et al. (2021) for

Cuchillacocha Glacier, where 2 °C and 4 °C warmer scenarios yielded a specific mass balance change of -4.9 m w.e. $yr^{-1}$and -9.8 m w.e. $yr^{-1}$, respectively. In both the 2 °C and 4 °C warmer scenarios, all 5 glaciated HRUs are retreating. HRU 2 glacier (highest elevation glacier, 5495 m.a.s.l.) is close to being stable in the 2 °C warmer scenario with a mass balance of -0.91 m w.e. $yr^{-1}$ (Figure 38). All glaciated HRUs reach negative mass balance averages at a basin-wide temperature increase of 0.9 °C.

Every 1 °C increase in temperature leads to an increase of -2.3 m w.e. $yr^{-1}$ for the basin-wide glacier melt rates. According to results from Vuille et al. (2008), near-surface air temperatures have increased by 0.1 °C/ decade from 1939 to 2008. Applying this projection, for every decade there will be an increase of ~0.23 m w.e. $yr^{-1}$ in the basin-wide glacier melt rate. Results from Mark (2002) and Mark and Seltzer (2005) indicate a temperature increase of 0.35-0.39 °C $decade^{-1}$ from 1951 to 1999 in central Peru (9-11°S). This would result in an increase of 0.85 m w.e $decade^{-1}$ of glacier melt.

#### 5.7.2.4 Glacier recession and timing

Results from Schauwecker et al. (2017) indicate that by the end of the 21st century the freezing level height (FLH) in the Cordillera Blanca may rise from its current mean annual elevation of 4900 m to 5130 m under RCP2.6 and to 5750 m under RCP8.5. The freezing level height is defined as the lowest level in the free atmosphere where the temperature is 0 °C (Schauwecker et al., 2017). Under RCP 8.5, glaciers may only remain above approximately 5800 m a.s.l. (Schauwecker et al., 2017). In the Cordillera Blanca, the area above the current wet season FLH is 614 $km^2$ (Schauwecker et al., 2017) and only 1% of this area may be above the end-of-century FLH (Schauwecker et al., 2017). Under RCP2.6, approximately 42% of the area will be above the end-of-century FLH (Schauwecker et al., 2017). Based on a warming of 4.5-5 °C by the end of the century found by Vuille et al. (2008) using the SRES A2 scenario (similar radiative forcing to RCP 8.5), and an assumed lapse rate of 0.65 °C/100m, this would correspond to a rise of 690-770 m in the FLH (Schauwecker et al., 2017).

Based on maintaining the current climate (from the 2014 data set), the simulations show that the Quilcayhuanca basin will be completely deglaciated in 28 years. However, this result is based on using the entire basin ablation rate (-2.51 m w.e. $yr^{-1}$). If divided into the 5 glaciated HRUs, some glaciers will disappear sooner, and others will not retreat under the current climate.

The lowest elevation glacier (HRU 6) will disappear in just over 10 years, HRU 9 will disappear after 22 years, HRU 3 has 28 years, HRU 5 has 89 years, and HRU 2 is advancing.

With a temperature increase of 2 °C and the corresponding basin-wide ablation rate (-7.03 m w.e. $yr^{-1}$), the Quilcayhuanca Valley will be completely deglaciated in 10 years. If divided into the 5 glaciated HRUs, the lowest elevation glacier (HRU 6) will disappear in 6 years, HRU 9 will disappear after 9 years, HRU 3 in 8 years, HRU 5 in 15 years, and HRU 2 in 77 years. For comparison, a temperature increase of 4 °C and the associated basin ablation rate (-11.74 m w.e. $yr^{-1}$), the Quilcayhuanca basin will be completely deglaciated in 6 years. If divided into the 5 glaciated HRUs, the lowest elevation glaciers (HRU 3, 6, and 9) will disappear in 5 years, HRU 5 in 7 years, and HRU 2 in 16 years.

Through modifying HRU elevations to find an approximate ELA, under 4 °C warming all glaciers with a mean elevation under 5980 m.a.s.l are retreating. The model results for CRHM glacier melt agree with findings from Schauwecker et al. (2017) that glaciers below 5800 m will not exist in a 4.5 to 5 °C warmer climate. CRHM simulations indicate glacier retreat for all glaciers under 5495 m (mean elevation of HRU 2) at a temperature increase of 0.9 °C. The results demonstrate the highly variable ablation rates that are often oversimplified when considering country wide or even region wide mass balances.

#### 5.7.2.5 Temperature increase effect on precipitation phase

With increased temperatures, a greater proportion of precipitation will fall as rain instead of snow. Not only does this decrease the accumulation rates for glacier growth, but it also decreases the albedo of glacier surfaces and increases net shortwave radiation.

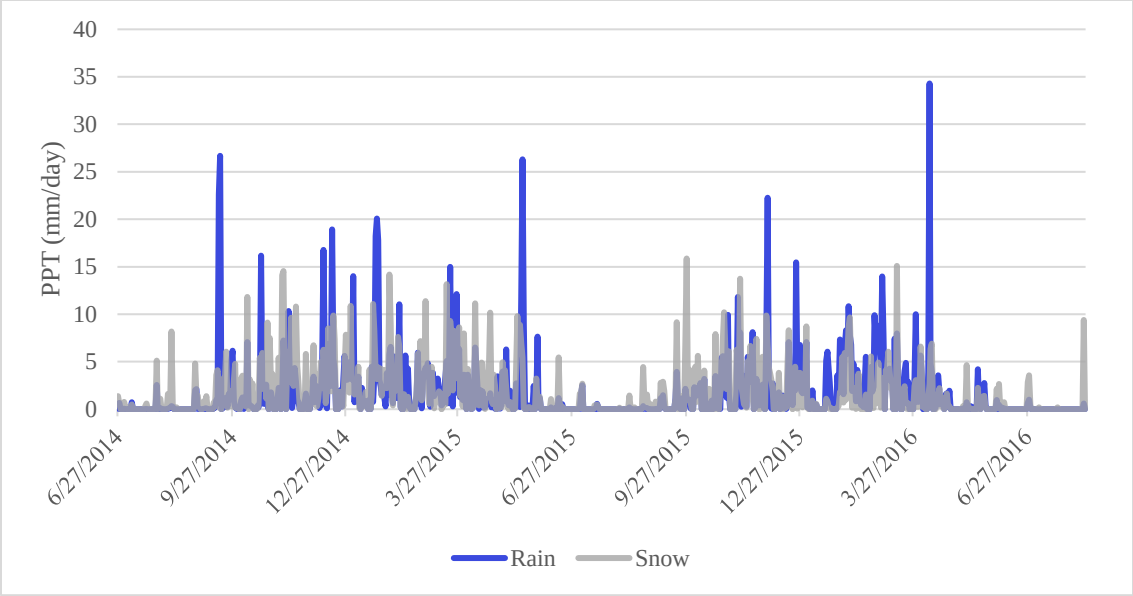


*Figure 40- Current temperature and precipitation phase partitioning onto the lower Cuchillacocha Glacier (HRU 3).*

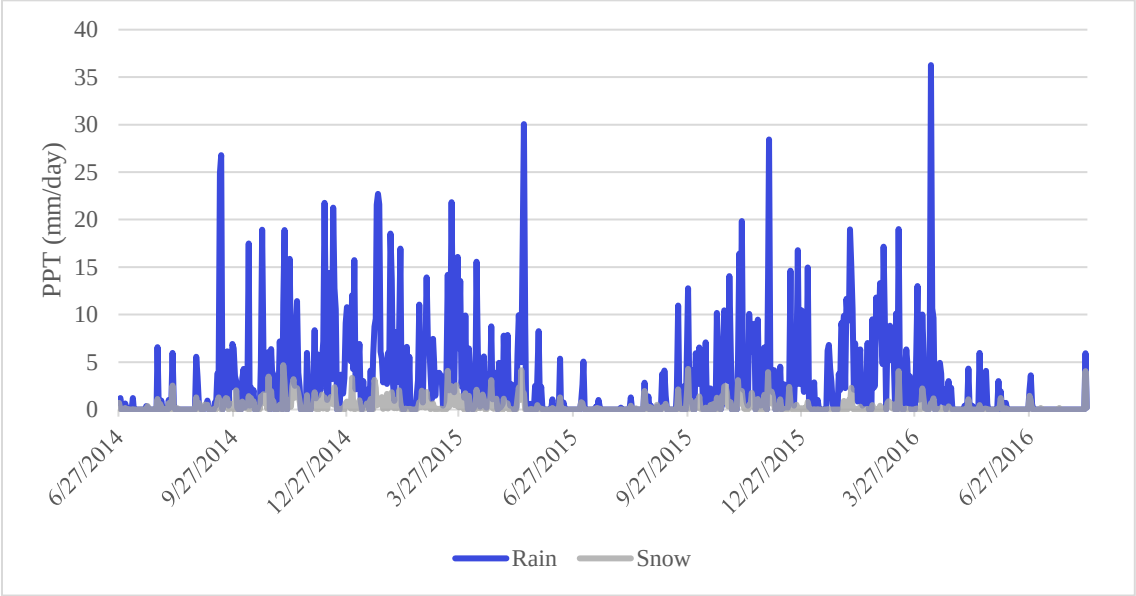


*Figure 41- Precipitation phase partitioning with a 2 °C temperature increase onto the lower Cuchillacocha Glacier (HRU 3).*

For HRU 3 (lower part of Cuchillacocha Glacier), currently 49.5% of precipitation falls as snow (Figure 40). With an air temperature increase of 2 °C the percentage of precipitation falling as snow is 10.4% (Figure 41). This 39.1% decrease in snowfall as a percentage of precipitation is very similar to the amount (41%) found by Fyffe et al. (2021) for Cuchillacocha glacier. Results from Fyffe et al (2021) show that this precipitation phase change leads to a decrease in albedo by 0.11.

### 5.7.2.6 Temperature increase effect on glacier melt components

The components of glacier melt will change drastically as the temperature increases. For the highest elevation glacier, HRU 2, glacier melt becomes dominated by ice melt rather than the current snowmelt dominated glacier runoff (Figures 42 and 43). With an increased percentage of precipitation falling as rain rather than snow on all glaciers, the thin to non-existent snowpack becomes a smaller fraction of glacier melt.

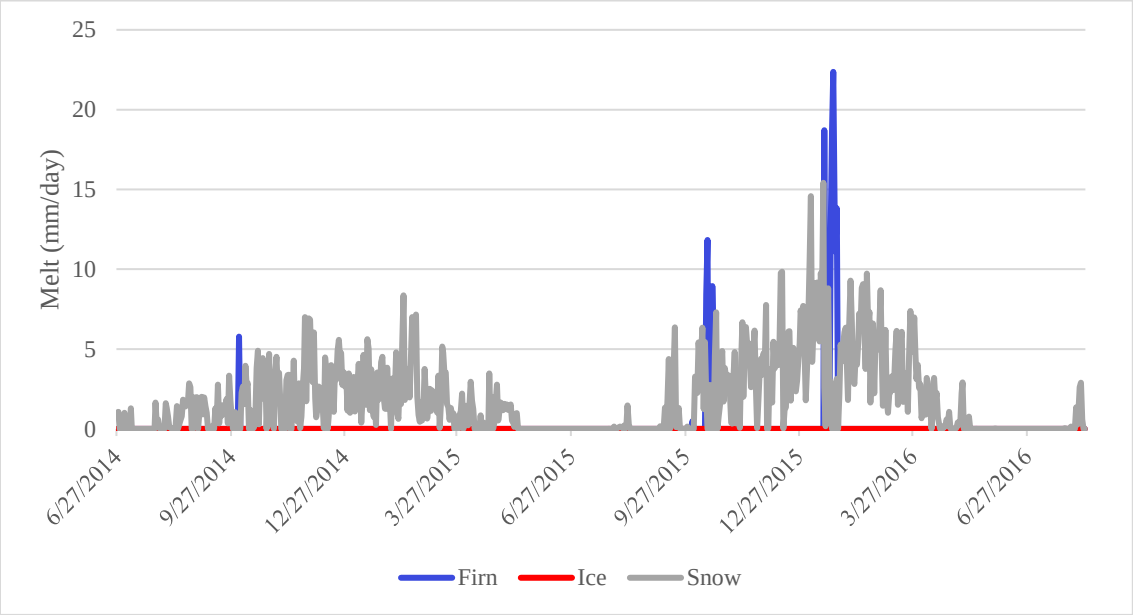


*Figure 42- Glacier melt components, current climate, for HRU 2.*

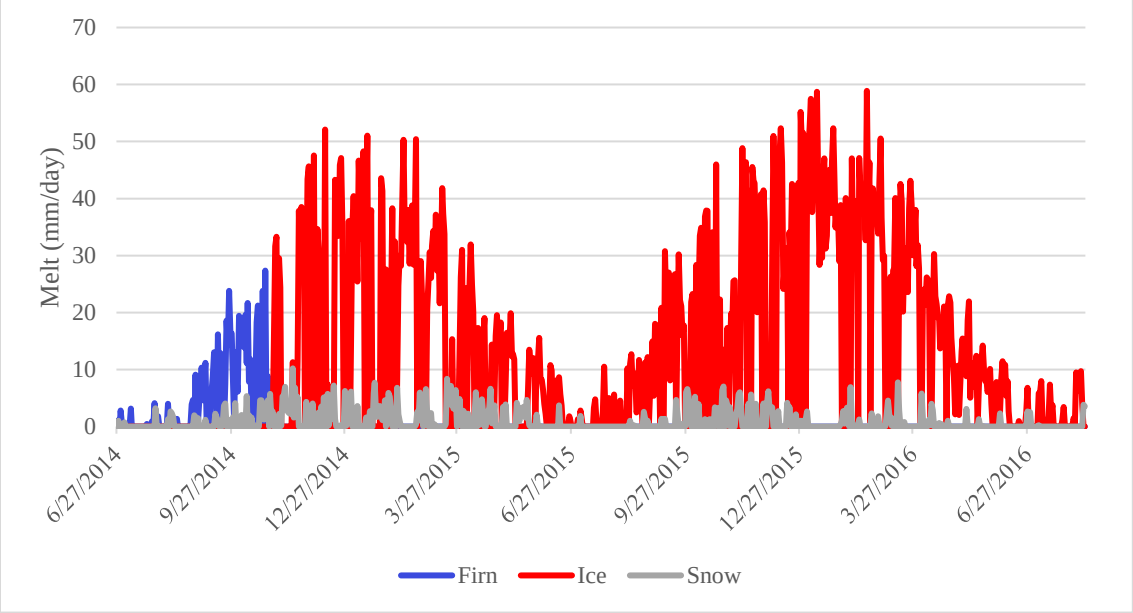


*Figure 43- Glacier melt components, 4 °C warmer climate, for HRU 2.*

### 5.7.3 Possible future scenarios

This section highlights the impact of possible future scenario combinations of temperature increase, precipitation changes, and glacier retreat.

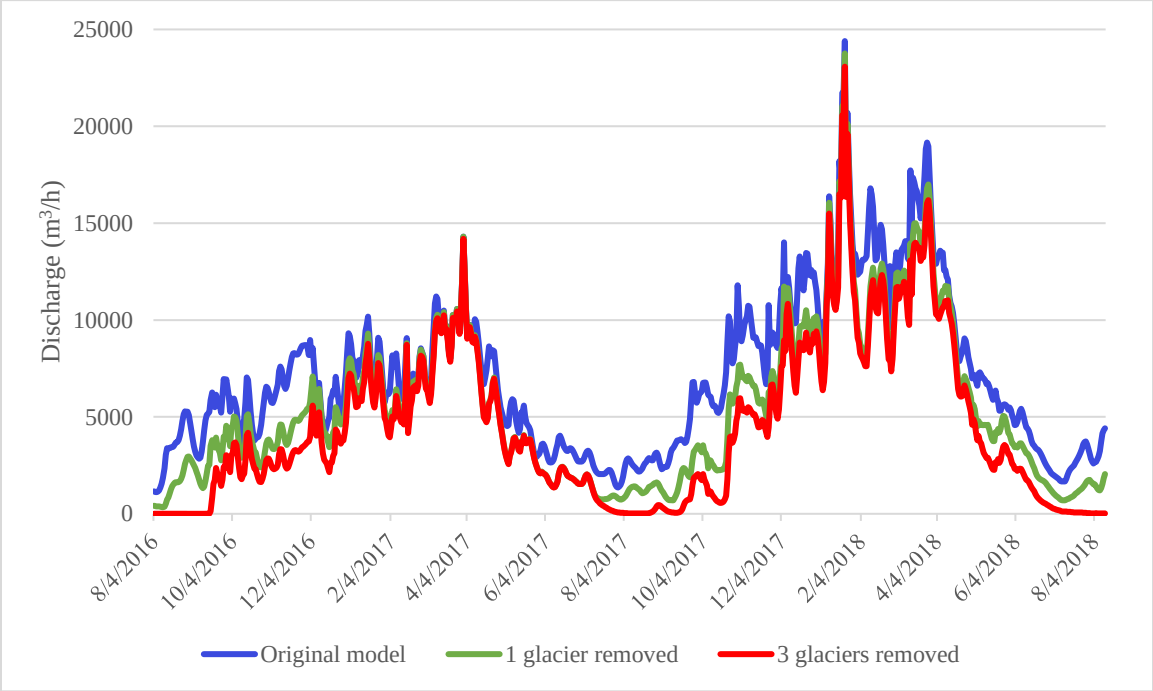


*Figure 44- Future climate scenarios with deglaciation. The blue line is the streamflow of the original model. The green line is for a scenario with 1 glacier removed, and the red line is for a scenario with 3 glaciers removed.*

By virtually removing individual glaciers, it is possible to assess their individual importance to the model outcomes and to assess future warmer scenarios where lower elevation glaciers completely disappear (Figure 44). Unsurprisingly, the outflow streamflow decreases significantly when removing 1 or 3 glaciers. With one glacier removed, the total streamflow for the period is 76% of the original, and for three glaciers removed, the total streamflow is 64% of the original. The most drastic difference in streamflow occurs primarily in the dry season.

One possible future scenario for the region is a warmer, wetter climate. Future precipitation trends are less certain than temperature trends for the Cordillera Blanca, but many model results predict an increase in wet season precipitation (Schauwecker, 2014). There have been precipitation increases observed since the 1990s, correlated with the strengthening of the upper-tropospheric easterly zonal wind component (Schauwecker, 2014). Results from Vuille et al. (2008) indicate an increase in wet season precipitation and a decrease during the dry season.

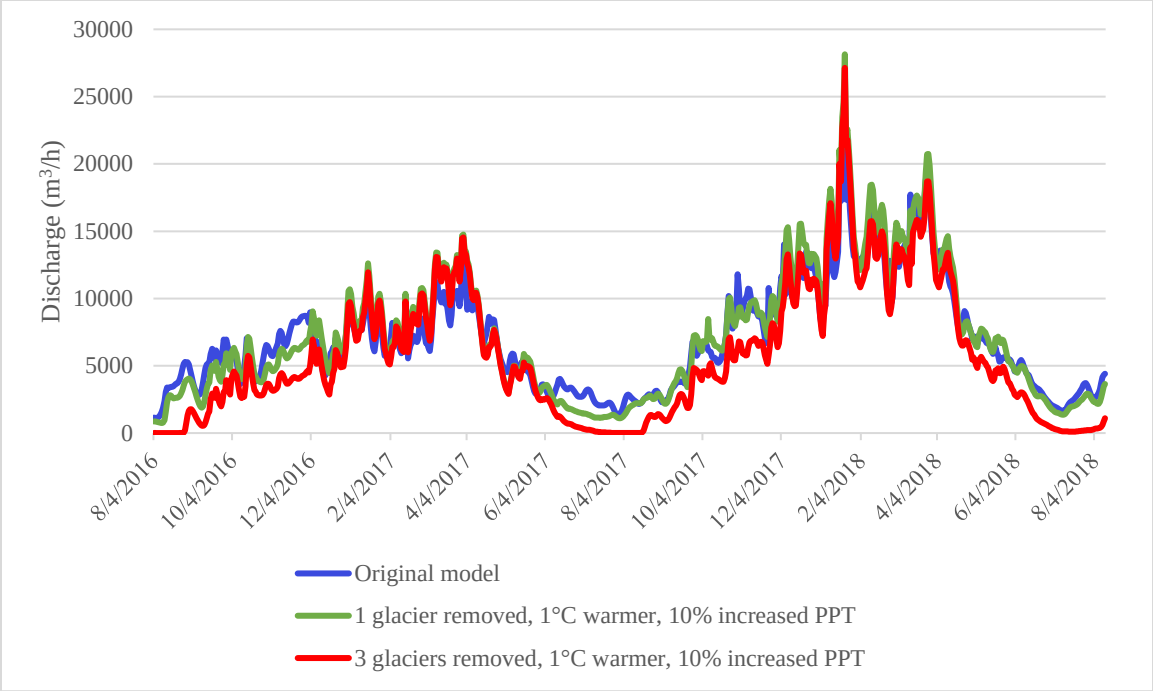


*Figure 45- Future climate scenarios with increased temperatures and precipitation and decreasing glacier coverage. The blue line is the streamflow of the original model. The green line is for a scenario with 1 °C temperature increase, 10% increase in precipitation, and HRU 6 completely deglaciated. The red line is for a scenario with 1 °C temperature increase, 10% increase in precipitation, and 3 lowest elevation glacier HRUs (3, 6, and 9) completely deglaciated.*

Two scenarios are assessed with 1 °C warmer conditions, 10% more precipitation, and 1 or 3 glaciers removed (Figure 45). For 1 glacier removed, the loss of meltwater contributions of the glacier in HRU 6 are mostly offset by the 1 °C warmer basin, which increases the melt rate of the four remaining glaciers, and the 10% increase in precipitation. As displayed in the glacial melt Section 5.3.2, the melt rate is significantly higher in the wet season. In the simulation with 3 glaciers removed, the highs and lows of the wet and dry season are more extreme. The higher temperature and precipitation result in increased wet season streamflow, but the decreased glacier melt is noticeable in the lower dry season flows.

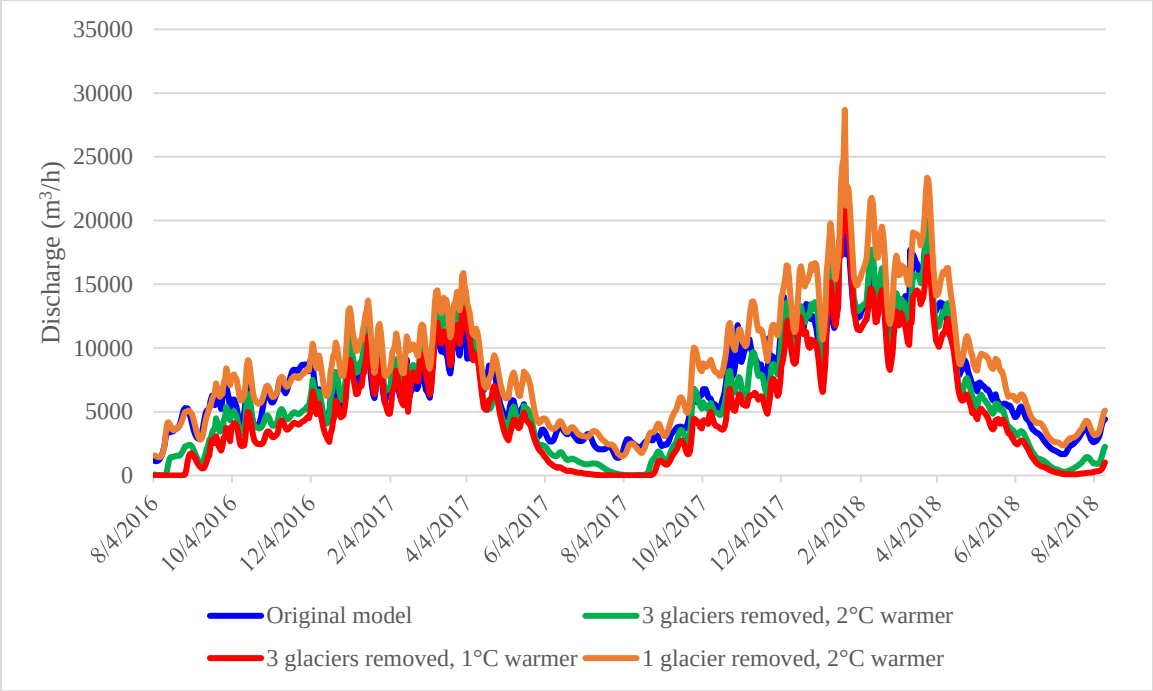


*Figure 46- Future climate scenarios with increased temperatures and deglaciation. The blue line is the streamflow of the original model. The green line is for a scenario with 2 °C temperature increase, and 3 HRUs (3, 6, and 9) completely deglaciated. The red line is for a scenario with 1 °C temperature increase, and 3 HRUs (3, 6, and 9) completely deglaciated. The orange line is for a scenario with 2 °C temperature increase, and HRU 6 completely deglaciated.*

In the simulations for 3 glaciers removed and with 1 or 2 °C warming (Figure 46), dry season flow is most affected by deglaciation. For the dry season streamflow, the proportional increase in dry season melt rates (due to temperature increase) does not compensate for the loss of glaciated area. The orange line (Figure 46) represents a scenario in which "glacial peak water" has not been passed. The increased temperature and relatively little deglaciation results in very high melt rates for the remaining four glaciated HRUs. The quantity of meltwater from the four remaining glaciers is greater than the loss of meltwater from HRU 6. However, other research shows that this area has likely passed glacial peak water, so the scenario is unlikely to occur (Baraer et al., 2012; Huss and Hock, 2018; Huss et al., 2017).

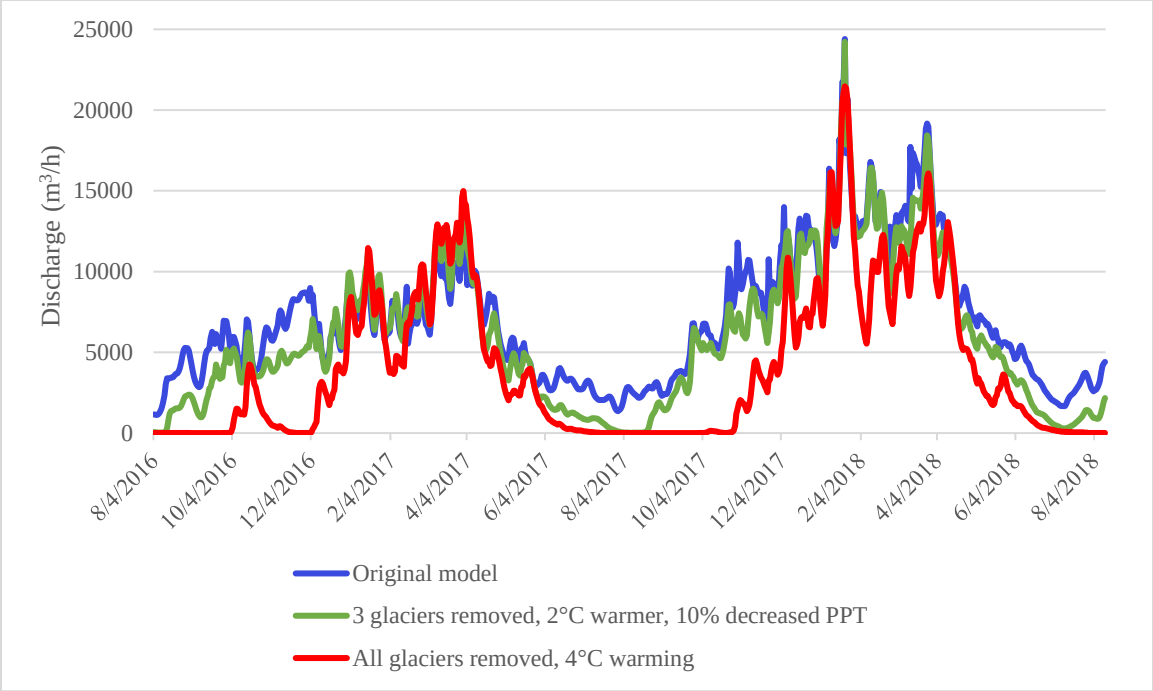


*Figure 47- Future climate scenarios with increased temperatures, decreased precipitation and deglaciation. The blue line is the streamflow of the original model. The green line is for a scenario with 2 °C temperature increase, 10% decrease in precipitation, and 3 HRUs (3, 6, and 9) completely deglaciated. The red line is for a scenario with 4 °C temperature increase, and basin-wide deglaciation.*

A decrease in precipitation is projected in some models under RCP 8.5 (Somers et al., 2019). A simulation with three glaciers removed, and with 2 °C warmer and a 10% decrease of precipitation is used to assess this scenario. For both simulations in Figure 36 the streamflow is reduced all year, but the most pronounced difference is during the dry season. In a completely deglaciated, 4 °C warmer basin, the stream is almost completely dry for August and September, even without decreasing precipitation.

Streamflow decreases in all future scenarios except for those with increased precipitation or minimal deglaciation and very high temperature increases. However, glacial peak water has been reached in this region, and so again these high temperature, high glacial melt scenarios are likely unrealistic (Baraer et al., 2012; Huss and Hock, 2018; Huss et al., 2017).

# 6 Conclusions

Broadly, the thesis evaluates how climate change will impact the hydrology of a glaciated catchment in the tropical Peruvian Andes. The main findings, using a numerical modeling

approach, is that there will be further declines in dry season streamflow for most potential future climate scenarios. The two dominant factors affecting dry season flows are groundwater and glacial melt, but the buffering effect of groundwater with glacier recession is minimal during the dry season for future warmer scenarios. Following is a brief description of the research sub-objectivesand the findings related to them.

The first objective is to test the ability of the Cold Regions Hydrological Model (CRHM) platform to represent hydrological processes in the glaciated tropics. To use CHHM, many in-depth component specific hydrological studies were required for model parameterization (e.g., Aubry-Wake et al., 2015; Baraer et al., 2012, 2015; Chavez 2013; Glas et al., 2018 & 2019; Gordon et al., 2015; Maharaj, 2011; Mark and McKenzie, 2007; Somers et al., 2016, 2019), allowing for a basin-wide understanding of multiple hydrological processes. The results show that the model was capable of simulating streamflow, groundwater flow, evapotranspiration, and glacier melt. Within the model evaluation objective, the knowledge and understanding of dominant hydrological processes was improved and the influence of groundwater on the timing and quantity of downstream water supplies was quantified (Baraer et al., 2015; Somers and McKenzie, 2020). The significant proportion of groundwater exiting the basin (31% from August 4, 2016, to August 12, 2018) is a new insight for the hydrology of the region. As glaciers recede, dry season streamflow declines more than wet season flow. Glacier meltwater no longer buffers the decreased precipitation, leading to groundwater becoming a more important contributor to streamflow. This is most noticeable in the dry season; 46% of the total basin outflow is groundwater in a deglaciated scenario instead of the current 35%.

Glacier melt rates were comparable with findings from Fyffe et al. (2021), and a basin-wide mass balance of -2.51 m w.e. $yr^{-1}$ was calculated. The high variability of individual glacier mass balances presented in this study is often overlooked in regional studies. Despite lower ablation rates in the dry season, the glacier contribution to streamflow is much higher (60% dry season versus 31% wet season). Evapotranspiration values appeared comparable to those measured near Casa de Agua by Wigmore (2016), and in nearby Llanganuco Valley by Hellstrom et al. (2006). The proportional quantity of evapotranspiration in Quilcayhuanca Valley is significant, comprising 20% of total hydrological outflows.

The second objective is to highlight key parameter uncertainties, and to investigate what effect these uncertainties have on basin scale hydrology. The aim of the sensitivity analysis section was to illuminate key gaps in the current understanding of basin scale hydrological processes and to guide future research questions. The results showed that the spatial variability of lapse rates is highly complex yet crucial to accurate glacio-hydrological modelling (Hellstrom et al., 2010). The total streamflow varied from +30% to -45% when switching from a lapse rate of -0.64 °C/100 m to -0.44 °C/100 m and -0.64 °C/100 m to -1.32 °C/100 m, respectively.

Surface and groundwater routing is another challenging parameter within the CRHM platform. If all groundwater is routed to the surface, there is a major overestimation of streamflow. However, if there is no groundwater redirected to the surface as springs, there is a significant underestimation of streamflow. There are many different routing methods, and each yield very different streamflow and groundwater flow results. Investigating these through manual calibration can aid in the conceptualization of the basin flow paths. Further studies in this area of research, including geophysical (Chavez, 2013; Glas et al., 2019) and tracer methods (Baraer et al., 2009, 2015; Gordon et al., 2015; Mark and McKenzie, 2007; Somers et al., 2016), will aid in the parameterization of hydrological models for this region. Surface water losses to groundwater recharge in the dry season is an example of an unknown flow pathway. As stated in previous studies, the simplified groundwater routing module in CRHM has limitations in accurately representing three-dimensional flow pathways and groundwater partitioning, but it does capture seasonality and relative groundwater proportions of basin outflow (Fang et al., 2013).

The third parameter of importance is glacial ice albedo, which can vary based on black carbon content and age of glacial ice (Aubry-Wake et al., 2022a; Carrion et al., 2022). Globally, increases in forest fire occurrence are predicted within a warming climate (Abatzoglou et al., 2019). This, along with anthropogenic pollution, can increase the amount of black carbon on Peruvian glaciers leading to a reduction in albedo (Carrion et al., 2022). A decrease in ice albedo from 0.3 to 0.2 results in a basin-wide glacier mass balance reduction from -2.5 m w.e. $yr^{-1}$ to -3.1 m w.e. $yr^{-1}$. More detailed *in-situ* glacier studies can aid in the parameterization of glaciohydrological models in the Cordillera Blanca.

The third objective is to analyze the hydrological changes that may occur in a changing climate. The simulation results show that with a complete deglaciation scenario with the current

climate, streamflow is reduced by 42% on an annual basis and by 60% in the dry season. Basin-wide mass balances for air temperature increases of 2 °C and 4 °C were -7.03 m w.e. $yr^{-1}$ and -11.74 m w.e. $yr^{-1}$, respectively. All glaciers in the Quilcayhuanca Valley reach annual negative mass balances at a warming of 0.9 °C. Phases of precipitation and components of glacier melt change drastically under a 2 °C and 4 °C warmer climate. For the highest elevation glacier (HRU 2), 92% of the precipitation currently falls as snow, while in a 4 °C warmer climate only 29% of the precipitation falls as snow.

Although CRHM was originally designed for remote and poorly gauged basins, it should be noted that the model performs better in basins that have been studied and previously reported on. Although CRHM does not necessarily require high density hydrometeorological data, there are hundreds of parameters requiring an in-depth knowledge of the routing, vegetation, landcover, soil and subsurface characteristics. For example, CRHM would not have been a good choice for the Quilcayhuanca Study area 10 years ago. This project depended heavily on previous research (Aubry-Wake et al., 2015; Baraer et al., 2012, 2015; Chavez, 2013; Fyffe et al., 2021; Glas et al., 2018; Gordon et al., 2015; Hellstrom et al., 2006, 2010; Maharaj, 2011; Mark and McKenzie, 2007; Mark et al., 2017; Somers et al., 2019, Wigmore, 2016). It would be possible to use CRHM effectively without this depth of prior knowledge but would require multiple field excursions for parameterization data collection. Process and conceptual understanding from field work, along with robust observations and monitoring data are useful precursors to any modelling efforts. Understanding hydrological interaction and compensating behaviour when engaging in model development or various forms of calibration is difficult yet should be strived for.

Glacio-hydrologic modelling is one piece needed to understand the greater basin scale hydrology and climate change challenges in mountainous areas. The social-hydrologic perspective along with transformational adaptation strategies are not examined in this study yet may be more important when considering water use (Carey, 2010; Mark et al., 2017; Drenkhan et al., 2022). However, results of this study may hopefully aid in the conceptualization of the hydro-social risks and in directing future research questions (Mark et al., 2017). Despite the promising results of the present research, CRHM should be applied to other catchments in the tropics to validate its use.

The thesis provides new scientific knowledge to our understanding of tropical Andean glacial hydrology. In particular, the quantity and interaction of all hydrological components, and

how they will interact and be affected by future climate. The thesis is the first study in the Cordillera Blanca to incorporate groundwater in a numerical model throughout the basin, from glacier to outflow. The thesis also provides five new glacier mass balances within the Quilcalhuanca Valley, showing that all glaciers below 5380 m a.s.l. currently have negative annual mass balances. Finally, the results show that every 1 °C increase in air temperature leads to an increase of -2.3 m w.e. $yr^{-1}$ for the basin-wide glacier ablation rates. Hydrological projections with decreased meltwater inputs show a significant decrease in annual surface and groundwater flow, most notably in the dry season.

# 7 References


Abatzoglou, J. T., Williams, A. P., & Barbero, R. (2019). Global emergence of anthropogenic climate change in fire weather indices. *Geophysical Research Letters*, 46(1), 326–336. https://doi.org/10.1029/2018GL080959

Allen RG, Pereira L, Raes D, Smith M (1998) FAO Irrigation and drainage paper No. 56. *Rome: Food and Agriculture Organization of the United Nations*, 56, 97–156.

Anderson, E.A., (1972). Techniques for predicting snow cover runoff. In The role of snow and ice in hydrology, Proceedings of the Banff Symposium 1972, Wallingford*: IAHS Publication* 107, 840–63.

Ångström, A. (1933). On the dependence of ablation on air temperature, radiation and wind. *Geografiska Annaler* 15, 264–71.

Aubry-Wake, C., Bertoncini, A., & Pomeroy, J. W. (2022a). Fire and ice: The impact of wildfire-affected albedo and irradiance on glacier melt. *Earth's Future*, 10, e2022EF002685. https://doi. org/10.1029/2022EF002685

Aubry-Wake C.; Pradhananga D.; Pomeroy J.W., (2022b). Hydrological process controls on streamflow variability in a glacierized headwater basin. *Hydrological Processes*, 36, e14731:e14731, doi: 10.1002/hyp.14731

Aubry-Wake, C., M. Baraer, J. M. McKenzie, B. G. Mark, O. Wigmore, R. Å. Hellström, and L. Lautz (2015). Measuring glacier surface temperatures with ground-based thermal infrared imaging, *Geophysical Research Letters,* 42, 8489–8497, doi:10.1002/ 2015GL065321.

Arias PA, Garreaud R, Poveda G, Espinoza JC, Molina-Carpio J, Masiokas M, Viale M, Scaff L and van Oevelen PJ (2021) Hydroclimate of the Andes Part II: Hydroclimate Variability and Sub- Continental Patterns. *Frontiers in Earth Sciences,* 8:505467. doi: 10.3389/feart.2020.505467

Ayers, H.D. (1959). Influence of soil profile and vegetation characteristics on net rainfall supply to runoff, in: *Proceedings of Hydrology Symposium* No. 1: Spillway Design Floods, National Research Council Canada, Ottawa, 198-205.

Bamber, J. L., Rivera, A. (2007). A review of remote sensing methods for glacier mass balance determination. *Global and Planetary Change*, *59*(1), 138–148.

Baraer, M., McKenzie, J. M., Mark, B. G., Bury, J., and Knox, S. (2009). Characterizing contributions of glacier melt and groundwater during the dry season in a poorly gauged catchment of the Cordillera Blanca (Peru), *Advances in Geosciences*, 22, 41–49, https://doi.org/10.5194/adgeo-22-41-2009, 2009.

Baraer, M.; Mark, B. G.; McKenzie, J. M.; Condom, T.; Bury, J.; Huh, K. I.; Portocarrero, C.; Gomez, J.; Rathay, S. (2012). Glacier recession and water resources in Peru's Cordillera Blanca. *Journal of Glaciology*. 58 (207), 134−150.

Baraer M, McKenzie J, Mark B, Gordon R, Bury J, Condom T, Gomez J, Knox S, Fortner S. (2015). Contribution of groundwater to the outflow from ungauged glacierized catchments: a multi-site study in the tropical Cordillera Blanca, Peru. *Hydrological Processes* 29(11): 2516–2581.

Bernhardt, M. and Schulz, K. (2010). SnowSlide: A simple routine for calculating gravitational snow transport. *Geophysical Research Letters* 37: L11502.

Beven, K. (2009). Environmental Modelling: An Uncertain Future. New York, Routledge.

Bury J, Mark BG, Carey M, Young KR, Mckenzie JM, Baraer M, French A, Polk MH. (2013). New geographies of water and climate change in Peru: coupled natural and social transformations in the Santa River watershed. *Annals of the Association of American Geographers* 103: 363– 374. DOI:10.1080/00045608.2013.754665

Buytaert, W. et al., (2017). Glacier melt content of water use in the tropical Andes. *Environmental Research Letters* 12(11) 114014. doi:10.1088/1748-9326/aa926c

Brock, B., Mihalcea, C., Kirkbride, M., Diolaiuti, G., Cutler, M., and Smiraglia, C. (2010). Meteorology and surface energy fluxes in the 2005–2007 ablation seasons at the Miage debris-covered glacier, Mont Blanc Massif, Italian Alps, *Journal of Geophysical Research*, 115, D09106, https://doi.org/10.1029/2009JD013224.

Carey M, Molden OC, Rasmussen MB, et al. (2017) Impacts of Glacier Recession and Declining Meltwater on Mountain Societies. *Annals of the Association of American Geographers* 107:1–10. https://doi.org/10.1080/24694452.2016.1243039

Caroline Clason, Sally Rangecroft, Gina Kallis, Shaun Lewin & Tom Mullier (2021) GlacierMap: a virtual opportunity to explore the Andes' vanishing glaciers, Geography, 106:3, 148-153, DOI: 10.1080/00167487.2021.1970932

Carrión, Carolina & Schmitt, Carl & Zuñiga Negron, Juan Jose & Jimenez, Wilber & Mamani, Oscar & Enciso, Rosmery & Guevara Sarmiento, Sulema & Rado, Maxwell (2020). Quantitative Estimation of Black Carbon in the Glacier Ampay-Apurimac. *Journal of Sustainable Development of Energy, Water and Environment Systems*. DOI: 10.13044/j.sdewes.d8.0342.

Casassa, G., Haeberli, W., Jones, G., Kaser, G., Ribstein, P., Rivera, A., Schneider, C. (2007). Current status of Andean glaciers. *Global and Planetary Change* 59 (1–4), 1–9.

Chavez D. (2013). Groundwater potential of pampa aquifers in two glacial watersheds, Cordillera Blanca, Peru. *Master's Thesis*, McGill University.

Chow, V.T. (1964). Handbook of Applied Hydrology, *McGraw-Hill, Inc*., New York.

Clark, C.O. (1945). Storage and the unit hydrograph. *Proceedings of the American Society of Civil Engineering* 69: 1419-1447.

Corps of Engineers (1956). *Summary report of the snow investigations, snow hydrology*. Portland, OR: US Army Engineer Division, 437pp

Dos Santos, F.M., de Oliveira, R.P., and Mauad, F.F. (2020). Evaluating a parsimonious watershed model versus SWAT to estimate streamflow, soil loss and river contamination in two case studies in Tietê river basin, São Paulo, Brazil. *Journal of Hydrology: Regional Studies*, 29, 100685.

Drenkhan, F., Buytaert, W., Mackay, J.D. et al. (2022) Looking beyond glaciers to understand mountain water security. *Nature Sustainability*. https://doi.org/10.1038/s41893-022-00996-4

Ellis, C.R., Pomeroy, J.W., Brown, T., MacDonald, J. (2010). Simulation of snow accumulation and melt in needleleaf forest environments. *Hydrology and Earth System Sciences*, 14, 925–940. https://doi.org/10.5194/hess-14-925-2010.

Evans S, Bishop N, Smoll L, Murillo P, Delaney K, Oliver-Smith A (2009) A Re-Examination of the Mechanism and Human Impact of Catastrophic Mass Flows Originating on Nevado Huascarán, Cordillera Blanca, Peru in 1962 and 1970. *Engineering Geology* 108:96–118

Fang, X., Pomeroy, J.W., Ellis, C.R., MacDonald, M.K., DeBeer, C.M., Brown, T. (2013). Multi-variable evaluation of hydrological model predictions for a headwater basin in the Canadian Rocky Mountains. *Hydrology and Earth System Sciences*. 17, 1635–1659. https://doi.org/10.5194/hess-17-1635-2013.

Finsterwalder, S., Schunk, H. (1887). Der Suldenferner. Zeitschrift des Deutschen und Oesterreichischen Alpenvereins 18, 72–89.

Fleming, S. W. (2005). Attenuation of high-frequency interannual streamflow variability by watershed glacial cover. *Journal of Hydraulic Engineering, 131*(7), 615–618.

Föhn, P.M.B. (1973). Short-term snow melt and ablation derived from heat- and mass-balance measurements. *Journal of Glaciology* 12, 275–289.

Fountain, A.G., Tangborn, W.V., (1985). The effect of glaciers on streamflow variations. *Water Resources Research.* 21 (4), 579–586.

Frey, H., Huggel, C., Chisolm, R. E., Baer, P., McArdell, B., Cochachin, A., and Portocarrero, C. (2018): Multi-Source Glacial Lake Outburst Flood Hazard Assessment and Mapping for Huaraz, Cordillera Blanca, Peru, *Frontiers in Earth Sciences*, 6, https://doi.org/10.3389/feart.2018.00210.

Fyffe, C. L., Potter, E., Fugger, S., Orr, A., Fatichi, S., Loarte, E., et al. (2021). The energy and mass balance of Peruvian glaciers. *Journal of Geophysical Research: Atmospheres*, 126, e2021JD034911. https://doi. org/10.1029/2021JD034911

Garnier, B.J. and Ohmura, A. (1970). The evaluation of surface variations in solar radiation income. *Solar Energy* **13**: 21-34.

Garreaud, R. D. (2009). The Andes climate and weather. *Advances in Geosciences*, 22, p.3.

Georges, C. (2004). The 20th century glacier fluctuations in the tropcial Cordillera Blanca, Peru. *Arctic, Antarctic and Alpine Research*, 36(1): 100–107.

Glas, R., Lautz, L., McKenzie, J., Mark, B., Baraer, M., Chavez, D., & Maharaj, L. (2018). A review of the current state of knowledge of proglacial hydrogeology in the cordillera Blanca, Peru. *Wiley Interdisciplinary Reviews: Water*, 5(5), e1299. https://doi.org/10.1002/wat2.1299

Glas, R., Lautz, L., McKenzie, J., Moucha, R., Chavez, D., Mark, B., & Lane, J. (2019). Hydrogeology of an alpine talus aquifer: Cordillera Blanca, Peru. *Hydrogeology Journal*, 27, 2137–2154.

Gordon, R. P., Lautz, L. K., McKenzie, J. M., Mark, B. G., Chavez, D., & Baraer, M. (2015). Sources and pathways of stream generation in tropical proglacial valleys of the Cordillera Blanca, Peru. *Journal of Hydrology*, 522, 628–644. https://doi.org/10.1016/j. jhydrol.2015.01.013

Granger, R.J., Gray, D.M. (1989). Evaporation from natural nonsaturated surfaces. *Journal of Hydrology*. 111, 21–29. https://doi.org/10.1016/0022-1694(89)90249-7.

Granger, R.J. and Gray, D.M. (1990). A net radiation model for calculating daily snowmelt in open environments. *Nordic Hydrology* 21: 217-234.

Granger, R.J., Pomeroy, J.W. (1997). Sustainability of the western Canadian boreal forest under changing hydrological conditions. II. Summer energy and water use, in: Rosjberg, D., Boutayeb, N., Gustard, A., Kundzewicz, Z., Rasmussen, P. (Eds.), *Sustainability of Water Resources under Increasing Uncertainty*. IAHS Publ. No. 240, pp. 243–249.

Gray DM, Landine PG. (1987). Albedo model for shallow prairie snowcovers. *Canadian Journal of Earth Sciences* 24(9): 1760–1768.

Gray, D.M., Landine, P.G. (1988). An energy-budget snowmelt model for the Canadian Prairies. *Canadian Journal of Earth Sciences*. 25, 1292–1303. https://doi.org/10.1139/e88-124

Gupta, H. V., Kling, H., Yilmaz, K. K., & Martinez, G. F. (2009). Decomposition of the mean squared error and NSE performance criteria: Implications for improving hydrological modelling. *Journal of Hydrology*, 377(1–2), 80–91. https://doi.org/10.1016/j.jhydrol.2009.08.003

Hellström, R. Å. and Mark, B. G.: An embedded sensor network for measuring hydrometeorological variability within a tropical alpine valley, *Proceedings of the 63rd*

*Eastern Snow Conference*, U. Delaware, Newark, DE, USA, 22, https://www.easternsnow. org/esc-2006 (last access: 15 January 2022), 2006.

Hellström, R. Å., Higgins, A., Ferris, D., Mark, B. G., and Levia, D. F.: Impacts of complex terrain on evapotranspiration within a tropical alpine valley in the Peruvian Andes, *Proceedings of the 67th Eastern Snow Conference*, Jiminy Peak Mountain Resort, Hancock, MA, USA, 13, https://www.easternsnow.org/esc-2010 (last access: 15 January 2022), 2010.

Hellström, R. Å., Fernandez, A., Mark, B. G., Covert, J. M., Cochachin, A., Gomez, J.: Incorporating autonomous sensors and climate modeling to gain insight into seasonal hydrometeorological processes within a tropical glacierized valley, *Annals of the American Association of Geography*, 107, 260–273, https://doi.org/10.1080/24694452.2016.1232615, 2017.

Hess, H. (1904). Die Gletscher. Braunschweig: Druck und Verlag von Friedrich Vieweg und Sohn, 426 pp.

Hock R. (2005). Glacier melt: a review of processes and their modelling. *Progress in Physical Geography: Earth and Environment*. 2005;29(3):362-391.

Hock, R., Jansson, P. (2006). Modeling Glacier Hydrology. *Encyclopedia of Hydrological Sciences* 10.1002/0470848944.hsa176.

Hock, R., Noetzli, C. (1997). Areal melt and discharge modelling of storglaciären, sweden. *Annals of Glaciology*, *24*, 211–216.

Hock, R. (2003). Temperature index melt modelling in mountain areas. *Journal of Hydrology*, *282*(1), 104–115. https://doi.org/10.1016/S0022-1694(03)00257-9

Hoinkes, H.C., Steinacker, H. (1975). Hydrometeorological implications of the mass balance of Hintereisferner, 1952–53 to 1968–69. *In Proceedings of the Snow and Ice Symposium,* Moscow 1971, Wallingford: IAHS Publication 104, 144–49.

Hopkinson, C., Young, G.J., (1998). The effect of glacier wastage on the flow of the Bow River at Banff, Alberta, 1951–1993. *Hydrology Processes*. 12 (10/11), 1745–1762.

Hsi-Kai Chou, Boris F. Ochoa-Tocachi, Simon Moulds & Wouter Buytaert (2022) Parameterizing the JULES land surface model for different land covers in the tropical Andes, *Hydrological Sciences Journal*, 67:10, 1516-1526, DOI: 10.1080/02626667.2022.2094709

IPCC, (1996). In: Houghton, J.T., Jenkins, G.J., Ephraums, J.J. (Eds.), Climate Change 1995: The Science of Climate Change, Cambridge University Press, Cambridge.

IPCC, (2001). Climate change 2001. The Scientific basis. Houghton, J.T., Ding, Y., Griggs, D.J., Nogyer, M., Van der Linden, P.J., Xiaosu, D. (Eds.), Cambridge: Cambridge University Press 944 pp.

IPCC (2019) Summary for policymakers. In: Pörtner H- O, Roberts DC, Masson-Delmotte V, Zhai P, Tignor M, Poloczanska E, Mintenbeck K, Nicolai M, Okem A, Petzold J, Rama B, Weyer N (eds) IPCC special report on the ocean and cryosphere in a changing climate. (In press)

Jansson, P., Hock, R., & Schneider, T. (2003). The concept of glacier storage: a review. *Journal of Hydrology*, *282*(1), 116–129.

J.W. Pomeroy, T. Brown, X. Fang, K.R. Shook, D. Pradhananga, R. Armstrong, P. Harder, C. Marsh, D. Costa, S.A. Krogh, C. Aubry-Wake, H. Annand, P. Lawford, Z. He, M. Kompanizare, J.I. Lopez Moreno (2022). The cold regions hydrological modelling platform for hydrological diagnosis and prediction based on process understanding, *Journal of Hydrology*, Volume 615, Part A, 128711, ISSN 0022-1694, https://doi.org/10.1016/j.jhydrol.2022.128711.

Kaser, G., Ames, A., and Zamora, M. (1990). Glacier fluctuations and climate in the Cordillera Blanca, Peru, *Annals of Glaciology*, 14, 136–140.

Kaser G. (1999). A review of the modern fuctuations of tropical glaciers. *Global Planet Change* 22(1–4):93–103. https://doi.org/10. 1016/S0921-8181(99)00028-4

King, J. C., Pomeroy, J. W., Gray, D. M., Fierz, C., Paul, M. B. F., Harding, R. J., Jordan, R. E., Martin, E., & Pluss, C. (2008). Snow – atmosphere energy and mass balance. In *Snow and Climate: Physical Processes, Surface Energy Exchange and Modeling*.

Knoben, W. J. M., Freer, J. E., & Woods, R. A. (2019). Technical note: Inherent benchmark or not? Comparing Nash-Sutcliffe and KlingGupta efficiency scores. *Hydrology and Earth System Sciences*, 23(10), 4323–4331. https://doi.org/10.5194/hess-23-4323-2019

Maharaj L (2011) Investigating proglacial groundwater systems in the Quilcayhuanca and Yanamarey Pampas, Cordillera Blanca, Peru. *Master's Thesis*, McGill University.

Mark, B. G., McKenzie, J. M., and Gomez, J. (2005). Hydrochemical evaluation of changing glacier meltwater contribution to stream discharge: Callejon de Huaylas, Peru, *Hydrology Sciences Journal*, 50, 975– 98.

Mark, B. G., J. M. McKenzie, (2007), Tracing Increasing Tropical Andean Glacier Melt with stable 40 Isotopes in Water: Callejon de Huaylas, Peru, *Environmental Science and Technology*, 41(20): 6955-6960.

Marks, D., Kimball, J., Tingey, D., and Link, T. (1998). The sensitivity of snowmelt processes to climate conditions and forest-cover during rain-on-snow: A study of the 1996 Pacific Northwest Flood. *Hydrological Processes* 12: 1569-1587.

Mason, P.J. and Sykes, R.I. (1979). Flow over an isolated hill of moderate slope. Quarterly *Journal of the Royal Meteorological Society* 105: 383-395.

Mateo, Emilio & Mark, Bryan & Hellstrom, Rob & Baraer, Michel & Mckenzie, Jeff & Condom, Thomas & Cochachin, Alejo & Gonzales, Gilber & Gómez, Joe & Encarnación, Rolando. (2021). High temporal resolution hydrometeorological data collected in the tropical Cordillera Blanca, Peru (2004–2020). 10.5194/essd-2021-215.

Monteith, J.L. (1965). Evaporation and environment. In State and movement of water in living organisms. 19th Symposium of the Society for Experimental Biology. *Cambridge University Press*: Cambridge, 205-234.

Morris, E. M. (1989). Turbulent transfer over snow and ice. *Journal of Hydrology*, **105**, 205–223.

Munro, D. S. (2004). Revisiting bulk heat transfer on Peyto Glacier, Alberta, Canada, in light of the OG parameterization. Journal of Glaciology, 50(171), 590–600. https://doi.org/10.3189/172756504781829819

Nash, J. E. and Sutcliffe, J. V. (1970). River flow forecasting through conceptual models, Part I – A discussion of principles, *Journal of Hydrology*, 10, 282–290.

Oerlemans, J., & Grisogono, B. (2002). Glacier winds and parameterisation of the related surface heat fluxes. Tellus, Series A: Dynamic Meteorology and Oceanography, 54(5), 440–452. https://doi.org/10.1034/j.1600-0870.2002.201398.x

Oestrem, G., Brugman, M. (1991). Glacier Mass-Balance Measurements. National Hydrology Research Institute, *Environment Canada*. 15-16.

Paterson, W.S.B. (1994). The physics of glaciers (third edition). Oxford: Pergamon Press, 480 pp.

Pepin, N. et al (2015). Elevation-dependent warming in mountain regions of the world. *Nature Climate Change,* 5(5), p. 424.

Pomeroy, J.W. and Li, L. (2000). Prairie and Arctic areal snow cover mass balance using a blowing snow model. *Journal of Geophysical Research* 105: 26619-26634.

Pomeroy J., Gray D., Brown T., Hedstrom N., Quinton W., Granger R., Carey S., (2007). The cold regions hydrological model: A platform for basing process representation and model structure on physical evidence. *Hydrological Processes*. 21, 2650-2667.

Pradhananga, D., Pomeroy, J.W. (2022). Diagnosing changes in glacier hydrology from physical principles, using a hydrological model with snow redistribution, sublimation, firnification and energy balance ablation algorithms. *Journal of Hydrology.* 608, 127545 https://doi.org/10.1016/j.jhydrol.2022.127545.

Priestley, C.H.B. and Taylor, R.J. (1972). On the assessment of surface heat flux and evaporation using large-scale parameters. *Monthly Weather Review* 100: 81-92.

QGIS Development Team (2021). QGIS Geographic Information System. Open Source Geospatial Foundation Project. http://qgis.osgeo.org

Rabatel, A., Francou, B., Soruco, A., Gomez, J., Cáceres, B., Ceballos, J. L., et al. (2013). Current State of Glaciers in the Tropical Andes: a Multi-century Perspective on Glacier Evolution and Climate Change. *The Cryosphere* 7 (1), 81–102. doi:10.5194/tc-7-81-2013

Schauwecker, S., M. Rohrer, C. Huggel, J. Endries, N. Montoya, R. Neukom, B. Perry, N. Salzmann, M. Schwarb, and W. Suarez (2017), The freezing level in the tropical Andes, Peru: An indicator for present and future glacier extents, *Journal of Geophysical Research: Atmospheres*., 122, 5172-5189, doi:10.1002/2016JD025943

Sicart, J.E., Pomeroy, J.W., Essery, R.L.H., Bewley, D. (2006). Incoming longwave radiation to melting snow: Observations, sensitivity and estimation in northern environments. *Hydrological Processes* 20: 3697-3708.

Sicart, J. E., Hock, R., Six, D. (2008). Glacier melt, air temperature, and energy balance in different climates: the bolivian tropics, the french alps, and northern sweden. *Journal of Geophysical Research: Atmospheres*, 113(D24).

Singh, P. and Kumar, N. (1996). Determination of snowmelt factor in the Himalayan region. *Hydrological Sciences Journal*. 41, 301–10.

Somers, L. D., Gordon, R. P., McKenzie, J. M., Lautz, L. K., Wigmore, O., Glose, A. M., … Condom, T. (2016). Quantifying groundwater–surface water interactions in a proglacial valley, cordillera Blanca, Peru. *Hydrological Processes*, 30(17), 2915–2929. https://doi.org/10.1002/hyp.10912

Somers, L. D., McKenzie, J. M., Mark, B. G., Lagos, P., Ng, G. C., Wickert, A. D., … Silva, Y. (2019). Groundwater buffers decreasing glacier melt in an Andean watershed—But not forever. *Geophysical Research Letters*, 46, 13016–13026. https://doi.org/10.1029/2019GL084730

Somers, L. D., McKenzie, J. M., Zipper, S. C., Mark, B. G., Lagos, P., & Baraer, M. (2018). Does hillslope trenching enhance groundwater recharge and baseflow in the Peruvian Andes? *Hydrological Processes*, 32(3), 318–331. https://doi.org/10.1002/hyp.11423

Somers LD, McKenzie JM. (2020). A review of groundwater in high mountain environments. *WIREs Water* 7:e1475. https://doi.org/10.1002/wat2.1475.

Solman SA (2013) Regional climate modeling over South America: a review. *Advances in Meteorology*. 18:1–13. https://doi.org/10.1155/2013/ 504357

Studies of longitudinal stream profiles in Virginia and Maryland (1957), US Geological Survey Professional Paper, 294- B.

Sverdrup, H.U. (1935). Scientific results of the Norwegian-Swedish Spitzbergen Expedition in 1934. Part IV. The ablation on Isachsen's plateau and on the Fourteenth of July Glacier in relation to radiation and meteorological conditions. *Geografiska Annaler* 17, 145–66.

Sverdrup, H.U. (1936). The eddy conductivity of the air over a smooth snow field. *Geofysiske Publikasjoner* 11, 5–69.

Taylor, L. S., Quincey, D. J., Smith, M. W., Potter, E. R., Castro, J., & Fyffe, C. L. (2022). Multi-decadal Glacier area and mass balance change in the southern Peruvian Andes. *Frontiers*. Doi: 10.3389/feart.2022.863933

Toledo, O., Palazzi, E., Cely Toro, I. M., & Mortarini, L. (2021). Comparison of elevation-dependent warming and its drivers in the tropical and subtropical Andes. *Climate Dynamics, 58*(11-12), 3057–3074. https://doi.org/10.1007/s00382-021-06081-4

Urrutia, R., and Vuille, M. (2009). Climate change projections for the tropical Andes using a regional climate model: Temperature and precipitation simulations for the end of the 21st century. *Journal of Geophysical Research,* 114, D02108, doi:10.1029/2008JD011021.

van Tiel, M., Stahl, K., Freudiger, D., & Seibert, J. (2020). Glaciohydrological model calibration and evaluation. *Wiley Interdisciplinary Reviews: Water*, 7(6), 1-51. https://doi.org/10.1002/wat2.1483

Verseghy, D.L. (1991). CLASS - A Canadian Land Surface Scheme for GCMS. I. Soil Model. *International Journal of Climatology*. 11, 111–133. https://doi.org/10.1002/joc.3370110202.

Viviroli D, Kummu M, Meybeck M, et al (2020) Increasing dependence of lowland populations on mountain water resources. *Nature Sustainability*. 3:917–928. https://doi.org/10.1038/s41893-020-0559-9

Wahi, A. K., Hogan, J. F., Ekwurzel, B., Baillie, M. N., & Eastoe, C. J. (2008). Geochemical quantification of semiarid mountain recharge. *Ground Water*, 46(3), 414–425. https://doi.org/10.1111/j.1745-6584.2007.00413.x

Walcher, J. (1773). Nachrichten von den Eisbergen in Tyrol. Wien, 99 pp.

Walmsley, J.L., Taylor, P.A. and Salmon, J.R. (1989). Simple guidelines for estimating windspeed variations due to small-scale topographic features – an update. *Climatological Bulletin* 23: 3-14.

Warren, S.G. (1982). Optical properties of snow. *Reviews of Geophysics and Space Physics* 20, 67–89.

Wigmore, Wigmore, O. H. (2016). Assessing Spatiotemporal Variability in Glacial Watershed Hydrology: Integrating Unmanned Aerial Vehicles and Field Hydrology, Cordillera Blanca, Peru. [Doctoral dissertation, Ohio State University]. OhioLINK Electronic Theses and Dissertations Center. http://rave.ohiolink.edu/etdc/view?acc_num=osu1471854919

# 8 Appendix

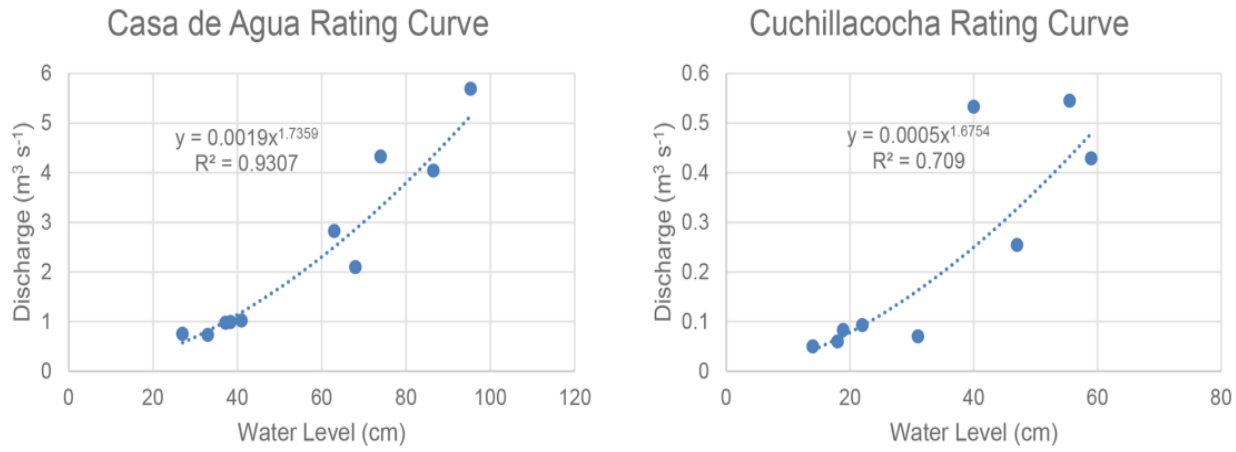


*Figure A1- Rating curves for Casa de Agua and Cuchillacocha. Figure from Mateo et al., 2021*

*Table A1- Parameterization for 19 HRUs and 17 modules*

| **Shared** | **albedo_Richard** | **Ayers** | **basin** | **CanopyClearing** | **evap_Resist** | **glacier** |
|---|---|---|---|---|---|---|
| Area, aspect, elevation, slope, and latitude all changed based on mean value calculated by ArcGIS | Changed smin (Minimum snowfall to refresh albedo) to 1 mm/h, because no trees (no interception) | Groundcover and texture changed based on estimated infiltration values from field work and literature. | HRU names changed | All set to 1 for clearing. Passed along to next module. | HRU 1-17 evaporation type changed to Penman Monteith to include plants ET. Lakes (HRU 18 and 19) switched to Priestley Taylor for potential evap calculation based on net radiation. | Elev_Adj_glacier_surf changed to 1 (glacier depth plus land elevation) |
| Ht changed based on vegetation estimates (from field observations) for alpine to valley bottom. | | | | | Htmax for veg. height same as shared module | firn storage changed to 9.9 for high glacier (based on Logan's value for Peyto glacier). Low glacier is not in accumulation zone so there is no firn. |
| Sdmax (Max depression storage) changed for HRU 18 and 19. Set to 1 m for lake spill over | | | | | LAI changed to 1 and 0.75, based on rough estimates taken from Kenneth Byrne et al 2005 paper | ice albedo changed to 0.3. firn 0.5. |

| | | | | | | |
|---|---|---|---|---|---|---|
| | | | | | rcs (minimum stomatal resistance, s/m) changed to 25 for glacier and lakes and 50 for all others. | firn densities changed for glacier HRUs, based on Caroline recommendations |
| Soil_moist_max and soil_rechr_max changed based on field observations/ Caroline and Logan recommendations | | | | | soil depth changed based on estimates from field work and literature | firn_h_init (initial depths of firn densification layers) changed to 0.3 m for high glacier HRUs based on Caroline's recommendation |
| Zwind (wind measurement height) changed to 2 m. | | | | | soil type changed based on estimates from field work and literature | icestorage changed to 0.5 (based on Fang et al. (2013) value for Peyto glacier) |
| | | | | | | ice_init to 0 for all non-glaciated HRU. 70 m for glaciers based on Fyffe at al., 2021 and photos |
| | | | | | | katabatic lapse rate changed to 0.02 from Caroline Aubry-Wake. Tested at Peyto Glacier by Munro (2004). |
| | | | | | | SWE storage changed to 2 (based on Logan's value for Peyto glacier) |
| | | | | | | SWE to firn Julian changed to 274 (October 1st), end of dry season |
| | | | | | | SWE lag change to 1 hour based on John Pomeroy's recommendation |

*Table A2- Continued parameterization for 19 HRUs and 17 modules*

| global | K_Estimate | longVt | Netroute_M_D | obs | pbsmSnobal | SnobalCRHM | Soil | SWESlope | walmsley_wind |
|---|---|---|---|---|---|---|---|---|---|
| Time offset changed to -0.067 (4mins) | Changed saturated hydraulic conductivities for various layers to 0.001 m/s (Bear, 1972), 2.1E-5 m/s and 1E-7 m/s (based on Chavez, 2013 and Fetter, 2001) for valley bottom, 1E-4 m/s for steep valley sides (talus value from Chavez, 2013, noting that exposed talus slope should have higher conductivity than buried talus). | Vt (terrain view factor) changed to 0.2 for glacier and alpine. 0.3 for all other HRUs | Channel shape changed to 1 (parabolic) | ElevChng_flag (elevation change control) changed to 1 to keep Vp within Vsat maximum. | A_S (stalk diameter) changed to 0.05 m for vegetated HRUs and changed to 0.01 for non vegetated HRUs (based on field observations) | hru_F_g (ground flux when observation F_g not available) set to 5 based on Caroline recommendation | cov_type (vegetation evaporation type) changed to 2 for all vegetated HRUs (all water taken from all water column). | Glaciated HRUs routed down elevation | walmsley height changed to 0 for no change of wind speed |
| | | | Estimated distrib_Route flow direction, based on ArcGIS, field work, and literature | HRU_obs changed to 1 or 2 depending on which observation station was closer in elevation | Distribution fractions set to -1 in HRU 4, 6, and 8. This is to have fractions of total flow to check/compare in upper basin. | T_g or G_flux changed to 1 (use ground flux value) for all HRU based on Caroline recommendation | gw_init (initial value of available water in ground water reservoir) set to 400mm for alpine, glacier, and lake HRUs. Set to 800 mm for vegetated HRUs. Calibrated, yet constrained from literature. | Hd_min (minimum SWE holding depth changed to 50 mm) | |
| | | | GwKStorage changed to 10 days based on alpine hydrogeology conptualization (Hayashi, 2020) and calibration (manually calibrated, | obs_elev changed based on Casa de Agua (2) or Cuchillacocha (1) | N_S (vegetation number density, 1/m2) changed to 50 for all HRU except for valley bottom | z_u (height of wind measurement) changed to 2m | gw_max (maximum available water holding capacity of ground water reservoir) value changed to 500mm for alpine, | | |

| | | | | | | | | | |
|---|---|---|---|---|---|---|---|---|---|
| | | | matching flashiness of streamflow) | | (set to 100) | | glacier, and lake HRUs. Set to 1000mm for vegetated HRUs | | |
| | | | gwwhereto sent to downstream HRUs. Valley side talus slopes groundwater directed as springs to surface water of valley bottom HRU based on literature and basin conceptualization. HRU 8 gw sent out of basin as GW | Temperature lapse rate changed to 0.64 °C/100m based on Hellstrom et al. 2010. | | | Sdinit (Initial depression storage) set to 900mm for lakes | | |
| | | | Upper valley side talus slopes (HRU 11 and 16) surface runoff directed to lower HRUs groundwater. Based on literature and conceptual model | Precip_elev_adj (precipitation lapse rate) changed to 0.01 based on calculation between 2 observation stations over 4 year period. | | | Soil_moist_init (initial value of available water in soil profile) changed to = soil moist max (SHARED module) x soil moisture (0.3, estimated) | | |
| | | | Hack's law used for route_L (routing length) | snow rain determination changed to Harder (Based on Harder & Pomeroy, 2013). | | | soil_rechr_init (initial value of available water for soil recharge zone) = soil_rechr_max (SHARED module) x soil_moisture (0.3, estimated) | | |
| | | | route_n (Manning roughness coefficient) set to 0.025 based on various literature for similar streams | | | | soil_ssr_runoff changed to 0 for ALL (soil column excess sent to interflow) | | |

| | | | | | | | | | |
|---|---|---|---|---|---|---|---|---|---|
| | | | route_R (hydraulic radius) changed to 0.15 m for all HRU except valley bottom (0.3m). Based on field observations. | | | | soil withdrawal [1] changed to 4 (organics) for all, and 3 (clay) for lower layer [2] | | |
| | | | route_So (longitudinal channel slope) changed to tan(HRU_GSL) for rise/run | | | | | | |
| | | | runKstorage (runoff storage constant) changed to 0.1 days for all HRU. Partially calibrated but constrained based on field observations and literature. | | | | | | |
| | | | soil_rechr_bypass changed to 0 | | | | | | |
| | | | ssrKstorage (subsurface runoff storage constant) changed to 1 day. Partially calibrated but constrained based on field observations and literature. | | | | | | |

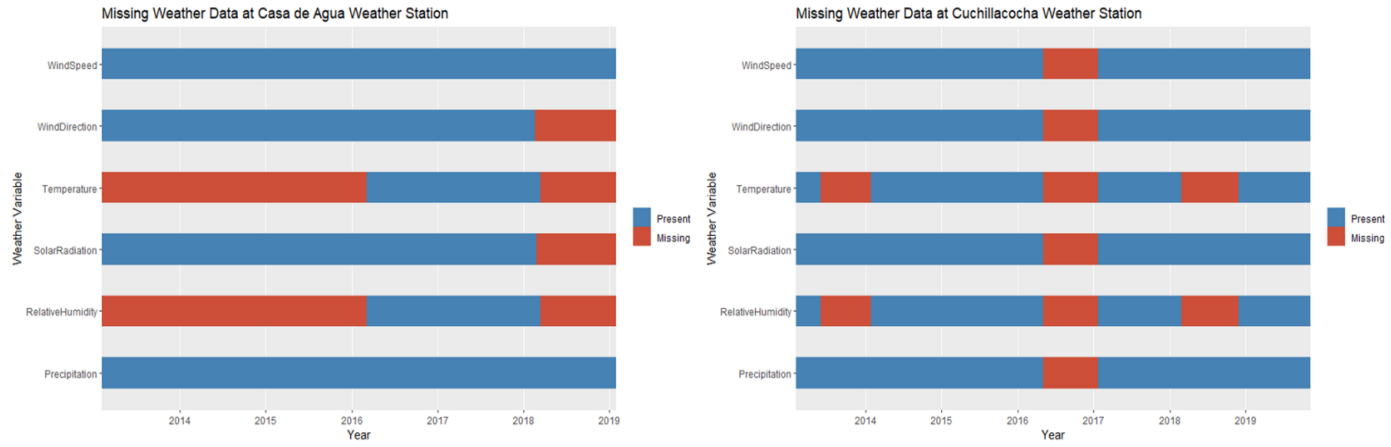


*Figure A2- Missing meteorological data figure from Mateo et al., 2021*

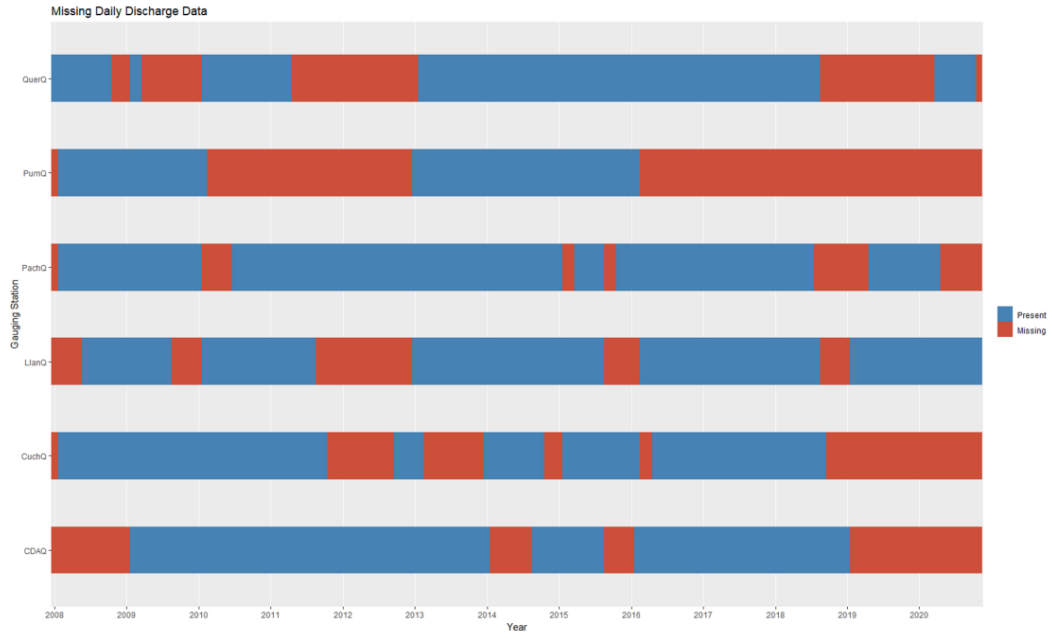


*Figure A3- Missing stream gauging data figure from Mateo et al., 2021*